Molecular basis for the regulation of phosphoinositide 3-kinase γ (PI3Kγ)

by

Manoj Kumar Rathinaswamy
BTech, Anna University, 2015

A Dissertation Submitted in Partial Fulfillment
of the Requirements for the Degree of

DOCTOR OF PHILOSOPHY

in the Department of Biochemistry and Microbiology

Supervisory Committee

Molecular basis for the regulation of phosphoinositide 3-kinase γ (PI3Kγ)

by

Manoj Kumar Rathinaswamy
BTech, Anna University, 2015

Supervisory Committee

Dr. John E. Burke, Department of Biochemistry and Microbiology
Supervisor

Dr. Perry L. Howard, Department of Biochemistry and Microbiology
Departmental Member

Dr. Alisdair B. Boraston, Department of Biochemistry and Microbiology
Departmental Member

Dr. J. Scott McIndoe, Department of Chemistry
Outside Member

Abstract

Cells transduce signals from the external environment to the inside through phosphatidylinositol-3,4,5-phosphate (PIP_3), a major signaling lipid on the plasma membrane. PIP_3 is generated by the action of a family of lipid kinases called Class I phosphoinositide 3-kinases (PI3Ks) and controls an array of essential cellular functions including growth, proliferation, survival, metabolism and cytoskeletal architecture. PI3Ks are large heterodimeric complexes composed of a catalytic p110 subunit and a regulatory subunit. Crucial to healthy PIP_3 production is the interpretation of diverse activating inputs arising from signaling proteins on the membrane by these subunits. A member of the PI3K family, PI3Kγ is a master regulator of immune functions with therapeutic implications in cancer immunity and inflammatory disease. PI3Kγ is distinct from other well studied PI3Ks due to the presence of unique regulatory mechanisms that control its ability to integrate signals from G-protein coupled receptors, small GTPases, immunoglobulin receptors and toll-like receptors. However, unlike the other well characterized PI3Ks, there are significant gaps in understanding of the molecular details of these mechanisms and how regulatory processes are translated into functions elicited by PI3Kγ in its unique milieu within the immune system.

To understand PI3Kγ regulation, I utilized a synergy of cutting-edge approaches including protein biochemistry, X-ray crystallography, cryo-electron microscopy and hydrogen-deuterium exchange mass spectrometry to elucidate the unique regulatory features within its catalytic and regulatory subunits and how these features are disrupted in disease. These studies significantly advanced our understanding of how this enzyme functions and provided novel avenues for potentially targeting the enzyme better in therapy. This dissertation will consist of an introduction chapter summarizing PI3Kγ regulation and its role in disease, followed by three data chapters investigating previously uncharacterized regulatory mechanisms that control its function and how these mechanisms are implicated in disease. These data chapters are followed by a final chapter describing conclusions and future directions.

In summary, the work presented in this thesis provides novel insights into the unique regulatory features in the catalytic and regulatory subunits of PI3Kγ that mediate its stimulation by upstream activating partners and the mechanisms by which these features are disrupted in disease. Further, these studies have facilitated the effective characterization of potent molecules that can specifically target PI3Kγ in disease. Altogether, the findings of this dissertation constitute a major advancement in our understanding of PI3K regulation.

Table of Contents

List of Figures

List of Abbreviations

β-AR	β adrenergic receptor
aa	Amino acid
ABD	Adaptor binding domain
ADP	Adenosine diphosphate
ARAP	Activation-dependent raft-recruited ADAP-like phosphoprotein
ATP	Adenosine triphosphate
BLI	Biolayer interferometry
bMe	Beta mercaptoethanol
CHAPS	3-[(3-Cholamidopropyl)dimethylammonio]-1-propanesulfonate
Cryo-EM	Cryogenic electron microscopy
CSF	Colony stimulating factor
DMSO	Dimethyl sulfoxide
DNA	Deoxyribonucleic acid
EM	Electron Microscopy
EMDB	Electron microscopy data bank
EtOH	Ethanol
FBS	Foetal Bovine Serum
GBD	Gβγ binding domain
GDP	Guanosine diphosphate
GFB	Gel filtration buffer
GPCR	G-protein coupled receptor
GSK3β	Glycogen synthase kinase 3β
GTP	Guanosine triphosphate
HDX-MS	Hydrogen deuterium exchange mass spectrometry
IgE	Immunoglobulin E
IL	Interleukin
kDa	Kilo dalton
mTOR	Mammalian target of rapamycin
MS	Mass spectrometry
MS/MS	Tandem mass spectrometry
MWCO	Molecular weight cut off
Ni-NTA	Nickel nitrotriacetic acid
NB	Nanobody
PBD	p110γ binding domain

PBS	Phosphate buffer saline
PC	Phosphatidylcholine
PCR	Polymerase chain reaction
PDB	Protein data bank
PDE3B	Phosphodiesterase 3B
PDGFR	Platelet derived growth factor receptor
PDK1	Phosphoinositide dependent kinase 1
PE	Phosphatidylethanolamine
PH	Pleckstrin homology
PI	Phosphoinositide
PI3K	Phosphoinositide 3-kinase
PIP_2	Phosphatidylinositol-4,5-bisphophate
PIP_3	Phosphatidylinositol-3,4,5-trisphosphate
PM	Plasma membrane
PKA	Protein kinase A
PKC	Protein kinase C
PS	Phosphatidylserine
PTEN	Phosphatase and tensin homolog
pY	Phosphorylated tyrosine
RBD	Ras binding domain
RTK	Receptor tyrosine kinase
SDS-PAGE	Sodium dodecyl sulphate polyacrylamide gel electrophoresis
Sf9	*Spodoptera frugiperda 9*
SH2	Src homology 2
SM	Sphingomyelin
Strep	Streptavidin
TAM	Tumor-associated macrophage
TCEP	Tris(2-carboxyethyl)phosphine
TIRF	Total internal reflection fluorescence
TNF	Tumor necrosis factor
TLR	Toll-like receptor
TOF	Time of flight
TSC2	Tuberous sclerosis complex 2
VEGF	Vascular endothelial growth factor
WAVE2	WASp family verprolin-homologous protein 2
WT	Wild type

Acknowledgements

I am immensely grateful to the many amazing individuals who have mentored me and supported my research career so far. Like many graduate students, my journey in science has been one of numerous trials and tribulations and I cannot begin to imagine how it would have been without these people.

First, I must thank my wonderful supervisor, Dr. John Burke. I came into his lab without a smidge of experience in membrane or structural biology. I am glad he believed in me and provided me with the opportunity to work in his awesome lab. He has been an excellent mentor with a great sense of focussing research in the right direction and finding efficient ways to solve scientific problems. He has been very patient, providing me with ample time to grow, collaborate and succeed as a graduate student. Beyond research, I am also grateful for his efforts in helping me communicate my science better and network. I want to extend my gratitude to all members of the Burke Lab, past and present- Gill, Meredith, Jacob, Braden, Reece, Jordan, David, Emily, Kaelin, Noah, Eleanor, Ed, Harish and Matt. The fun times playing volleyball/soccer/abysmal basketball and the nights out drinking have definitely helped me endure the hard times. Special thanks to Kaelin, Noah and Jordan for making important contributions to this dissertation.

Outside my lab, I would like to acknowledge my committee members, Dr. Perry Howard, Dr. Scott McIndoe and Dr. Al Boraston for their valuable advice on improving my research. I want to also thank the folks at the Biotechnical Support Centre for their help in keeping the equipment running smoothly. Outside UVic, I am immensely thankful to the many great collaborations I have been lucky to be a part of. My PhD would not have been as successful without the work of these collaborators - Udit Dalwadi, Dr. Scott Hansen, Dr. Zied Gaieb, Carson Adams, Dr. Chiara Borsari, Dr. Els Pardon and the llama B-cell that made NB1-PIK3R5. I also want to thank my many mentors from before grad school- Dr. Tamil Selvan (Anna University), Dr. Sweta Srivastava (NCBS), Dr. Andrea Musacchio (MPI Dortmund), Dr. Christian Haering (EMBL) and Dr. Thomas Jenuwein (MPI Freiburg), who have helped me realize my scientific interests.

I am incredibly grateful for the support of my family and friends without which this journey would not have been possible. My regular interactions with Muthu (my friend of 14 years), Rama (prospective #1 synthetic biologist) and Vijay (distributor of dank memes) have definitely helped keep my sanity. Finally, I want to thank Mom, Dad, Madhu and Pooja for putting up with me and being pillars of support throughout the many highs and lows.

Dedication

I dedicate this dissertation to my father Rathinaswamy, who first pushed me to explore science and to my mother Vasanthi, my first teacher.

Chapter 1: Phosphoinositide-3-kinase γ (PI3Kγ) in signaling and disease

Partially adapted from:

Rathinaswamy, M.K. and Burke, J.E. (2020). Class I phosphoinositide-3-kinase (PI3K) regulatory subunits and their roles in signaling and disease. Advances in Biological Regulation 75, 100657.

1.1 Abstract

Phosphoinositide-3-kinase γ (PI3Kγ) is a master regulator of immune function with major therapeutic implications in inflammation, immunodeficiency and tumor immunity. PI3Kγ belongs to a family of heterodimeric lipid kinases called class I phosphoinositide-3-kinases (PI3Ks) which regulate crucial physiological processes including proliferation, growth, metabolism, survival, immunity and cytoskeletal architecture. Critical to PI3K function is the ability of all members to be activated by diverse stimulatory signals originating from major receptors and membrane-localized signaling proteins. PI3Kγ is uniquely positioned in the family due to the presence of regulatory mechanisms that are distinct from other class I PI3K members. These mechanisms confer upon PI3Kγ, the ability to receive signals from activators such as G-protein coupled receptors (GPCRs) and control immune cell migration and produce inflammatory signals. However, unlike other class I PI3K members, the regulatory features of PI3Kγ are poorly understood. Mutations disrupting these features are seen in diseases including cancer and immunodeficiency. Therefore, understanding PI3Kγ regulation is essential in deciphering its roles in cellular function and disease.

1.2 Phosphatidylinositol-3,4,5-trisphophosphate (PIP_3) as a signaling molecule

A cell's growth and survival is dependent on cues received from its environment. These cues are received by molecules on the plasma membrane (PM) and are transduced inwards to elicit the necessary responses. Lipids in the PM are essential members of this process owing to their location at the interface between the cytoplasm and the external environment. One such molecule is the phospholipid, phosphatidylinositol-3,4,5-trisphosphate (PIP_3). PIP_3 belongs to a family of lipids called phosphoinositides (PIs) which contain an inositol head group and a diacylglycerol tail bridged by a phosphodiester linkage (Figure 1.1A) (1). The inositol can be phosphorylated at the

3', 4' and 5' positions, leading to the production of seven distinct phosphoinositide species. These lipids line various cellular compartments and control a multitude of physiological processes including growth, metabolism and membrane trafficking. Phosphoinositides are able to perform these functions by recruiting proteins containing domains that recognize these lipids, eventually leading to their activation and transduction of signals.

Extracellular signals received by receptors such as Receptor Tyrosine Kinases (RTKs) and G-Protein coupled receptors (GPCRs) lead to the production of PIP_3 which controls cell division, growth, metabolism, motility and the cytoskeleton. PIP_3 was first identified in neutrophils activated by formyl peptide and leukotriene B4 (2). This resulted in actin polymerization, increase in intracellular calcium and production of reactive oxides independent of the then canonical protein kinase C (PKC) pathway. Chromatographic analysis showed a transient increase in a novel phospholipid which was identified to be PIP_3. Concurrently, a PI-kinase was found to phosphorylate the inositol head group at the third position in fibroblasts stimulated by platelet-derived growth factor (PDGF) or transformed with the polyomavirus middle T antigen and was later found to produce PIP_3 (3,4). In response to PDGF receptor activation, a burst of PIP_3 production was observed in neutrophils immediately followed by the removal of phosphates and return to negligible basal levels. This showed that kinases and phosphatases work in concert to keep PIP_3 levels under tight control to ensure proper signaling. The most well studied of the PIP_3 phosphatases is the tumor suppressor PTEN which hydrolyzes the 3' phosphate giving rise to phosphatidylinositol-4,5-bisphosphate or PIP_2 (Figure 1.1A). PIP_3 can also be converted to phosphatidylinositol-3,4-bisphosphate by the action of 5' phosphatases, SHIP/INPP5 (5,6).

PIP_3 generated at the plasma membrane serves as a docking point for numerous downstream effectors (Figure 1.1B) (7). The most well studied of the PIP_3 effectors is protein kinase Akt, which recognizes PIP_3 through its pleckstrin homology (PH) domain. Akt is locked in an autoinhibited state by contacts between the PH and kinase domains. The binding of the PH domain to PIP_3 and phosphorylation of the kinase domain by phosphoinositide dependent kinase 1 (PDK1) and mammalian target of rapamycin (mTOR) complex 2 relieves the inhibition and activates Akt (8–10). Additionally, PDK1 also contains a PH domain and is recruited to the membrane by PIP_3 serving as a coincidence signal in the activation of the Akt pathway. Akt phosphorylates numerous targets including mTOR complex 1 inhibiting tuberous sclerosis complex 2 (TSC2), glycogen synthase kinase 3β (GSK3β) and FOXO family transcription factors, which control cellular processes associated with growth, survival and

metabolism. Other PIP_3 effectors are Guanine Nucleotide Exchange factors (P-Rex1, Vav), GTPase activating proteins (ARAP3) and cytoskeletal proteins (WAVE2) which regulate movement and structural integrity (1,11).

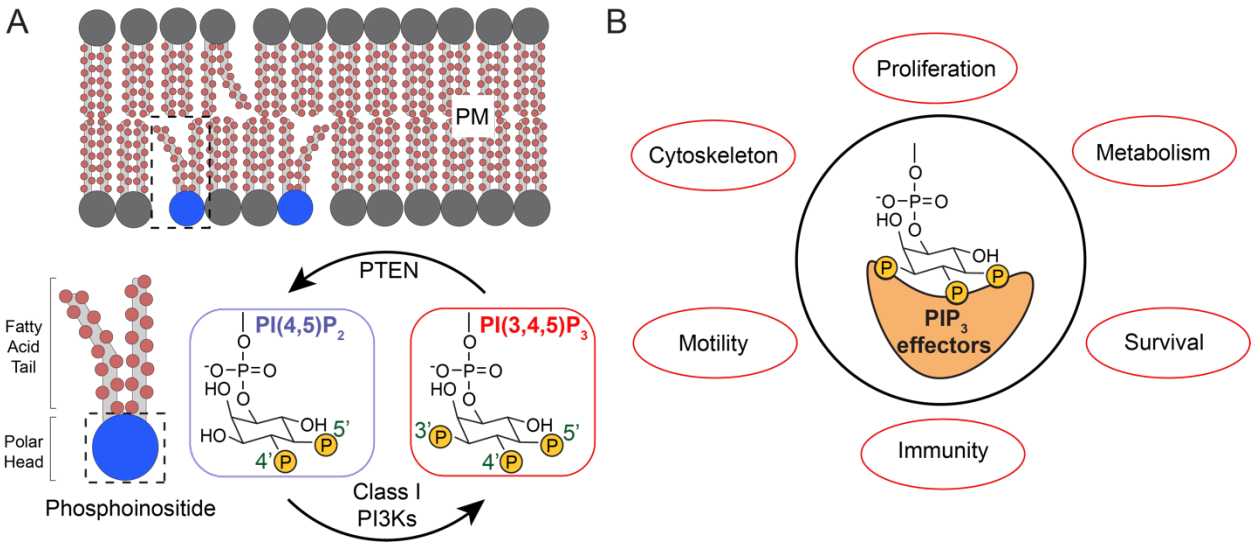

Figure 1.1. Class I PI3Ks generate PIP3 which controls essential cellular functions (A) Class I PI3Ks generate the signaling lipid PIP_3 at the plasma membrane (PM) by phosphorylating the 3' position on the inositol ring in the head group of PIP_2. PIP_3 is converted back to PIP_2 by the action of phosphatase PTEN. **(B)** PIP_3 activates downstream effectors by recruiting them to the plasma membrane. These effectors elicit numerous essential physiological functions.

1.3 Class I Phosphoinositide-3-Kinases (PI3Ks)

PIP_3 is generated by the phosphorylation of the 3' hydroxyl group on the inositol head group of phosphatidylinositol-4,5-bisphosphate (PIP_2) through the action of enzymes called class I phosphoinositide-3 kinases (PI3Ks) (Figure 1.1A). Class I PI3Ks are heterodimeric protein complexes composed of a catalytic p110 subunit and a regulatory subunit. Most multicellular animals possess four p110 isoforms, p110α, p110β, p110γ and p110δ encoded by the PIK3CA, PIK3CB, PIK3CG and PIK3CD genes, respectively (12). These isoforms assemble with different regulatory subunits which subdivides the family into two groups- Class IA and Class IB PI3Ks (Figure 1.2). The Class IA p110 isoforms, p110α, p110β and p110δ interact with a p85 or p85-like regulatory subunit (encoded by the PIK3R1, PIK3R2 and PIK3R3 genes) while the Class IB p110 isoform, p110γ binds to one of two regulatory subunits-p101 (encoded by the PIK3R5 gene) or p84/p87 (encoded by the PIK3R6 gene). All p110s share a common organization composed of four well characterized domains- Ras binding domain (RBD), C2 domain, helical domain and a bilobal kinase domain which is homologous to that of other lipid kinases (Figure

1.2A+C) (13,14). The class IA p110s also possess a ubiquitin-like adaptor binding domain (ABD) at the N-terminus. The different p110 isoforms have quite distinct expression patterns in human cells and tissues. While p110α and p110β are ubiquitously expressed, p110δ and p110γ are highly expressed in immune cells and a few select tissues such as neurons and the heart (15–18).

The regulation of PI3K activity and subsequent PIP_3 production is driven by the interplay between two phenomena- signals arising from upstream activating stimuli and the interpretation of these signals by the PI3K catalytic and regulatory components. PI3Ks are recruited to the membrane directly by inputs from three major families of signaling proteins- Ras superfamily of small GTPases, GPCRs and RTKs (Figure 1.2B+D) (19,20). Activated small GTPases bind to the Ras-binding domain of all p110s and enhances membrane recruitment (21–24). The p110α, p110δ, and p110γ isoforms are activated by Ras subfamily proteins while p110β is activated by members of the Rho GTPase subfamily (25). GPCR activation of PI3K is mediated by the Gβγ subunits which can bind and activate both p110β and p110γ (26,27). All class IA PI3Ks are able to be recruited and activated at the membrane by phosphorylated tyrosines on RTKs and their adaptor proteins (28). This diversity in the ability of various PI3K isoforms to differentially sense signaling inputs is key to their broad and physiologically crucial roles.

In mammals, the class IA catalytic subunits p110α, p110β, p110δ interact with five regulatory proteins which are encoded by three genes, PIK3R1, PIK3R2 and PIK3R3, broadly classified as p85s. PIK3R1 can give rise to p85α and two splice variants- p50α and p55α, while PIK3R2 and PIK3R3 encode p85β and p55γ respectively. All five p85 family proteins contain two Src homology domains (called nSH2 and cSH2) separated by a coiled-coil inter-SH2 domain (iSH2) (Figure 1.2A). The p85α and p85β proteins have two additional domains at the N-terminus of the SH2 domains- an SH3 domain and a Bcr Homology (BH) domain. The complex between the p110 subunits of class IA PI3Ks and regulatory subunits is mediated by the extremely tight interaction between the ABD domain of p110 and the iSH2 coiled coil of the regulatory subunits. The interaction with regulatory subunits mediates three key functions, stabilizing p110 subunits, inhibiting activity, and allowing for activation downstream of phosphorylated receptors and adaptors (29,30). Mediating the activation downstream of RTKs are the two SH2 domains, which are binders of phosphorylated tyrosine (pYXXM) motifs. Such motifs exist on membrane receptors (Insulin receptor, Platelet-derived growth factor receptor, etc.) and their adaptors (Insulin Receptor Substrate 1). The SH2 domains mediate the inhibition of p110 through a number of reversible inhibitory interactions. These interactions exist between the nSH2 and C2 and the helical and kinase domains of all class IA p110s and between

the cSH2 and the C-lobe of the kinase domains of p110β and p110δ (31–33). The cSH2 does not bind to p110α due to a loop extension that disrupts this interface. The iSH2 also forms inhibitory contacts with C2 domains of all p110 subunits, with this interface proposed to be slightly weaker for the p110β isoform (34). The binding of nSH2 and cSH2 domains to the phosphotyrosines on RTKs and RTK adaptors relieves these reversible inhibitory contacts and leads to PI3K activation (35).

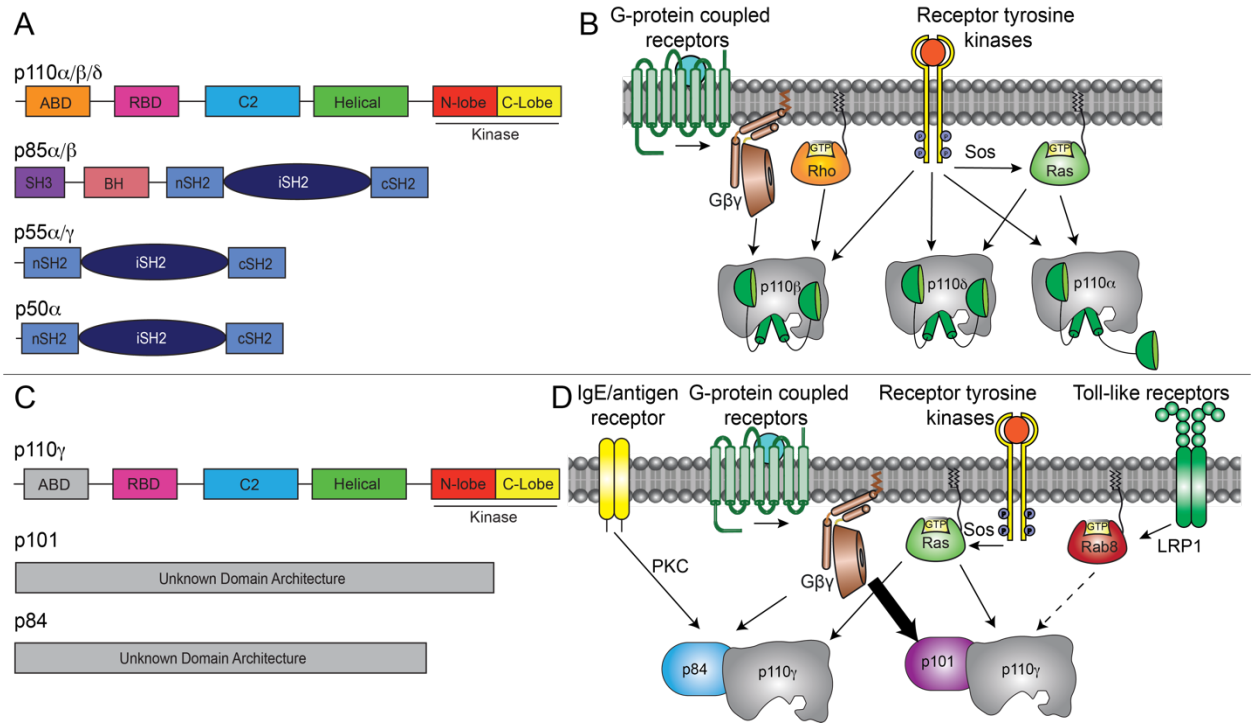

Figure 1.2. Class I PI3Ks are heterodimeric complexes that integrate diverse signaling inputs (A) Domain architecture of class IA catalytic and regulatory subunits **(B)** Schematic showing activating inputs into class IA PI3Ks. All class IA PI3Ks are activated by RTKs and Ras. PI3Kβ is also activated by GPCR subunit, Gβγ **(C)** Domain architecture of class IB catalytic and regulatory subunits **(D)** Schematic showing activating inputs into class IB PI3Ks. Both PI3Kγ complexes are activated by Ras and Gβγ. p110γ/p101 is more sensitive to Gβγ over p110γ/p84. p110γ/p84 is selectively activated by PKC while p110γ/p101 is activated by Rab8 downstream of TLRs by an unknown mechanism.

1.4 Phosphoinositide-3-Kinase γ (PI3Kγ)

The primary focus of this thesis, the class IB PI3K PI3Kγ, is a group of two heterodimeric complexes formed by the catalytic p110γ subunit and one of either p101 or p84 regulatory subunits. p110γ was first identified in myeloid cells and platelets as a GPCR activated PI3K that did not bind p85 (27,36,37). p110γ is encoded by the

PIK3CG gene found on chromosome 7 in humans. The structure of a p110γ fragment showed that it possessed a similar domain organization to class IA p110s composed of the RBD, C2, helical and kinase domains (Figure 1.2C) (14). From sequence analysis, the N-terminus of p110γ appears to possess a domain similar to the ABD but with limited conservation (13-16% identity). PIP_3 generated by p110γ plays important roles in the functioning of immune cells of both the myeloid (macrophages, mast cells and neutrophils) and lymphoid (T cells, B cells and Natural Killer cells) lineages. Critical to p110γ functioning is the ability of the enzyme to be activated by numerous stimulating partners including Ras, GPCRs, RTKs, IgE/Antigen receptors and Toll-like receptors (TLRs).

Ras is a group of membrane localized proteins that cycles between an active GTP bound form and an inactive GDP bound form. In its active form, the switch I and switch II domains of Ras become ordered by GTP and it is able to activate a number of downstream effectors including Raf kinase and class I PI3Ks which are essential in cell growth, survival and proliferation. Consequently, genes encoding the Ras family proteins are the most frequent sites of oncogenic mutations. Similar to other class I p110s, the RBD of p110γ mediates activation by the small GTPase Ras (Figure 1.2D). A crystal structure of the p110γ fragment with Ras-GTP provided the first insight into molecular details of the Ras-RBD interaction. This study showed that Ras uniquely contacts PI3Ks through its switch II unlike its interactions with other effectors which are mediated by the switch I. Corroborating this are covalent Ras inhibitors targeting switch II which inhibit PI3K activation without affecting Raf binding (38). From the crystal structure, it was initially proposed that Ras could induce conformational changes in the kinase domain. However, hydrogen deuterium exchange and single molecule studies have since shown that it activates PI3Ks by enhancing membrane recruitment, consistent with the inability of soluble Ras to mediate activation (21,24). Mice with knock-in mutations in the RBD ($p110\gamma^{DASAA}$) that render p110γ insensitive to Ras activation showed diminished reactive oxide production from neutrophils highlighting the importance of Ras in p110γ function *in vivo* (39,40). In addition to Ras, the RBD of p110γ has been proposed to mediate activation by another small GTPase Rab8a, downstream of the TLR4 receptors in macrophages (41).

Concurrently with Ras, p110γ is also capable of directly interacting with the Gβγ subunit of GPCRs (Figure 1.2D). GPCRs are a large family of membrane receptors which control an array of important cellular roles including sensory perception, circulation, immunity and hormonal response. The binding of a GPCR agonist to the receptor results in the activation of the associated Gα GTPase which breaks its interaction with the Gβγ subunit (42). Gβγ is a

heterodimeric complex comprised of β-propeller Gβ subunit and a lipidated small helical Gγ subunit. It can activate p110γ and p110β by recruiting these PI3Ks to the membrane. Hydrogen-deuterium exchange mass spectrometry (HDX-MS) studies have shown that the binding of Gβγ to p110γ is dependent on the orientation of the linker connecting the C2 and helical domains (43). Mutations in basic residues at the end of the linker (RK552DD) diminished p110γ activation substantially when neutrophils were stimulated by GPCR agonists (44). In addition to the Gβγ binding site on p110γ, activation by GPCRs *in vivo* is highly dependent on the association of the catalytic subunit with regulatory subunits. p110γ associates with one of two class IB adaptor subunits, p101 or p84/p87 (referred to as p84 for the rest of the text). These regulatory subunits are thought to arise from a gene duplication event in jawed vertebrates (12). Among the class IB PI3Ks, p84 has a more widespread expression while that of p101 is restricted to myeloid cells (45). The highest expression of PI3Kγ is observed in immune tissues and cardiac muscle where the two regulatory subunits exhibit varying degrees of redundancy. The p101 and p84 proteins exhibit a sequence similarity of ~40% and their domain architecture is unknown. Unlike p85 which inhibits the class IA PI3Ks in the absence of RTK activation, the regulatory partners of p110γ do not inhibit kinase activity but instead potentiate activating signals.

p101

p101 (*PIK3R5*) was discovered in porcine neutrophils where it was found that the activation of p110γ by GPCR subunit Gβγ was increased by more than 100-fold by association with a 101 kDa protein (46). Biochemical experiments have shown that downstream of GPCRs, the class IB heterodimer comprising p101 is significantly more activated by Gβγ subunits than that containing p84 (Figure 1.2D) (43). HDX-MS experiments have indicated that the C-terminus of p101 provides an additional Gβγ site, driving the enhanced stimulation of p110γ/p101 by GPCRs. It is unknown if one Gβγ is able to engage both binding sites or if each site binds to a Gβγ molecule.

The physiological role of p101 was best characterized in neutrophils where it is highly expressed, with mouse neutrophils lacking p101 exhibiting a 50% reduction in PIP_3 accumulation in response to the GPCR agonist fMLP (39). These neutrophils exhibit reduced chemotaxis in response to accumulation which was attributed to defects in F-actin polymerization. In macrophages, knockdown of p101 results in reduced V-CAM1 mediated adhesion in response to GPCR activating chemokines IL-8 and SDF-1α (47). Stimulation by these chemokines resulted in increased membrane translocation of p110γ/p101 but not p110γ/p84 further providing evidence for the role of p101 in

stimulation of PI3Kγ downstream of GPCRs. There is also evidence that the p110γ/p101 complex is preferentially activated by Rab8a downstream of toll like receptors (TLR) through an unknown mechanism (41,48).

p84

p84 (encoded by *PIK3R6*) was first identified in the mouse genome by sequence similarity to p101, on chromosome 11 in mouse just downstream of PIK3R5 (49) . The p84 regulatory subunit is considered to be a part of a constitutively expressed form of PI3Kγ with high levels of expression in leukocytes, endothelial cells and the heart (45). HDX-MS experiments indicated that the primary interface of p84 on p110γ is the C2-helical linker and helical domain (50). The p84 subunit still facilitates stimulation by GPCRs, but to a much lower extent than p101 (Figure 1.2D) (51). Studies in HEK cells expressing p110γ/p84 showed that Ras is necessary for complete activation of the complex by fMLP (51). Macrophages require p84 for proper adhesion when stimulated by agonists of RTKs such as IL-1β, IL-6, CSF-1, VEGF-A and TNFα. This is thought to happen through the activation of Ras by RTKs and subsequent activation of p110γ/p84 (47).

In neutrophils, p84 has been shown to mediate reactive oxide production in response to fMLP, C5a and LTB_4 (39). Mast cells require p84 for antigen- and IgE induced degranulation mediated by adenosine, a GPCR agonist (52). Interestingly, it was later found that GPCRs do not stimulate a considerable portion of this degranulation response. Instead, the influx of calcium ions and the subsequent activation of PKCβ has been shown to stimulate p110γ. PKCβ phosphorylates p110γ on S582, and this is thought to displace the p84 from the complex activating p110γ by a mechanism that is not entirely clear (50). In cardiomyocytes, p84 has been shown to mediate contractility downstream of the β-adrenergic receptor (β-AR). This is reported to happen through binding of p84 to protein kinase A which phosphorylates T1024 on p110γ. This inhibitory modification subsequently reduces p110γ activity which serves to downregulate the internalization of β-AR (18). p110γ/p84 has also been proposed to control PKA activation through an interaction with phosphodiesterase 3B (PDE3B) which lowers cyclic AMP levels in cardiac muscle cells (53). p84 knockout mice subjected to transverse aortic constriction exhibited higher rates of cardiac failure and cardiac function improved upon inhibition of PI3Kγ (18).

Despite this wealth of research on PI3Kγ, key fundamental questions still remain. Why does p110γ require activating signals despite the lack of inhibitory regulatory subunits? How do p101 and p84 stimulate GPCR activation of p110γ? Biochemical and structural studies answering these questions are required to better understand PI3Kγ functioning *in vivo*. Further underscoring the need for such studies on PI3Kγ is its emergence as a therapeutic target in disease.

1.5 PI3Kγ in disease

Given the essential cellular roles of PIP_3, it is no surprise that all class I PI3Ks are implicated in human disease. This is most evident by the high frequency of hotspot somatic activating mutations found in PIK3CA (encoding for p110α) in multiple human cancers. p110γ is also involved in cancers with overexpression of PIK3CG emerging as a driving feature in pancreatic ductal adenocarcinoma (PDAC) (54–56). Downregulation of p110γ was found to arrest proliferation of hepatocellular carcinoma (57), while increased expression of p110γ was found to promote metastasis in triple negative breast cancer (58). In addition to p110γ overexpression, mutations in PIK3CG have also been found in numerous cancers (59–61), albeit to a lesser extent compared to p110α (1739 for PIK3CG versus 17359 for PIK3CA on the COSMIC database). A PIK3CG mutation was found to be one of the top drivers of cancer progression in a study annotating somatic mutations in pancreatic cancer (62). These oncogenic mutations are found throughout the primary sequence of p110γ and their effects on kinase activity and regulation cannot be ascertained from the existing structure of the catalytic subunit fragment. The mechanisms by which PI3Kγ promotes proliferation and cancer progression are not entirely clear. There is evidence for p110γ acting as a suppressor of cancer immune response in tumor associated macrophages (TAMs) (Figure 1.3A) (63). p110γ was found to be highly expressed in metastatic breast cancer cells but not in the adjacent benign cells. These benign cells underwent metastatic transformation when the enzyme was overexpressed indicating a potential role for PI3Kγ in cancer cell migration (64). Additionally, PI3Kγ has been found to be a key player in endothelial cell migration (65) and could hence potentially promote angiogenesis at the tumor site.

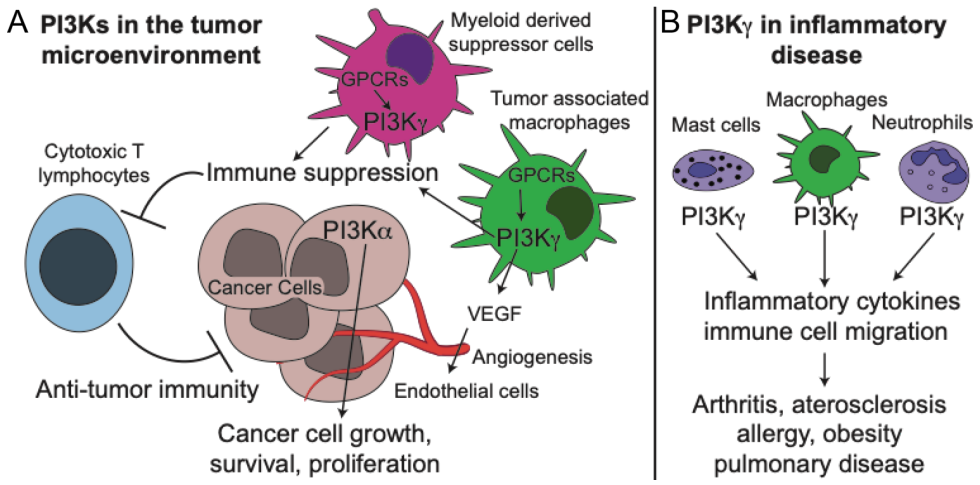

Figure 1.3. PI3Kγ is involved in cancer and inflammatory disease (A) PI3Kγ activity in tumor associated macrophages and myeloid cells blocks recruitment of cytotoxic T lymphocytes to the tumor site. PI3Kγ can also influence tumor angiogenesis by promoting endothelial cell migration. **(B)** P3Kγ is involved in inflammation by promoting cytokine production from immune cells.

In addition to cancer, PI3Kγ is also an important player in inflammatory disease, owing to its ability to promote immune cell migration and cytokine production (Figure 1.3B). Knockout of p110γ was found to be protective in mice models of rheumatoid arthritis (66). p110$\gamma^{-/-}$ mice are protected from obesity-related adipose tissue inflammation and development of insulin resistance (67). p110γ inhibition extended life span of mice with lupus (68). Targeting p110γ has also been shown to reduce mast cell recruitment and degranulation, protecting against allergy and anaphylaxis (69). p110γ inhibition is also proposed to be beneficial in asthma, pulmonary fibrosis, cystic fibrosis and respiratory infection (70). Finally, mutations inactivating p110γ kinase activity have been shown to protect mice against cardiac muscle damage (71).

Given the toxicity of pan-PI3K ATP competitive inhibitors, the limited expression profile of PI3Kγ makes it an attractive target in therapy particularly in cancer, leading to a push for development of p110γ-specific inhibitors. IPI-549, a recently developed inhibitor with >100-fold selectivity for p110γ over other p110 isoforms is currently in clinical trials in solid tumors for use as an immune modulator in conjunction with checkpoint inhibitors (72). IPI-145, a dual p110γ/δ-specific inhibitor has been shown to improve antitumor efficacy of adoptively transferred T-cells (73). Dual γ/δ inhibitors are also in clinical development for asthma and chronic obstructive pulmonary disease (COPD) (70). Targeting p110γ is not without its adverse effects as p110γ ablation in certain dietary settings can induce hepatic damage (56). Bi-allelic mutations that inactivate p110γ kinase activity have been

shown to cause immunodeficiency (74). p110γ inhibitors do not discriminate between the PI3Kγ complexes. Hence, studies on the regulatory subunits could potentially uncover novel strategies for targeting specific PI3Kγ complexes in therapy and prevent these adverse effects.

1.6 Research Objectives

PI3Kγ is a major regulator of immune function with clinical implications in cancer and inflammatory disease. Our understanding of its functional roles in both normal and disease states have been hampered by the lack of information on the regulatory features that control the activity of the p110γ kinase. Defining these features will bridge the knowledge gap between regulation and cellular function and will expand our understanding of how disease-linked mutations alter PI3Kγ activity. These studies can also potentially uncover novel ways to target specific PI3Kγ complexes in disease, bypassing the adverse effects of ATP-competitive p110γ inhibitors. In line with this, this thesis aims to address the following questions:

1. **What is molecular basis for the regulation of p110γ by the regulatory C-terminal motif and how do disease related mutations disrupt this motif?**
2. **How can we target the activation of specific PI3Kγ complexes by nanobodies?**
3. **How does the p101 regulatory subunit assemble with p110γ and regulate activation downstream of GPCRs?**

To answer these questions, a synergy of cutting edge biochemical, biophysical and structural tools including HDX-MS, X-ray crystallography, cryo-electron microscopy (cryoEM) and single molecule microscopy was employed to study the regulation of PI3Kγ. The data presented in this thesis has provided valuable insight into the regulation of p110γ and the molecular basis for regulation by p101 in addition to developing tools for studying the activation of specific PI3Kγ complexes *in vivo*. Notably, this work resulted in the first structural characterization of a heterodimeric PI3Kγ complex. Overall, the studies presented in this thesis provide fundamental insights into how PI3Kγ elicits its cellular roles besides offering novel avenues to inhibit the enzyme in disease.

Chapter 2: The regulatory C-terminal motif in p110γ and its implications in disease and inhibition

Adapted from:

Rathinaswamy, M.K., Gaieb, Z., Fleming, K.D., Borsari, C., Harris, N.J., Moeller, B.J., Wymann, M.P., Amaro, R.E., and Burke, J.E. (2021). Disease related mutations in PI3Kγ disrupt regulatory C-terminal dynamics and reveal a path to selective inhibitors. Elife 10.

Contributions:

Myself: Cloning, expression and purification of all proteins, kinase assays, HDX-MS and crystallography. **Kaelin Fleming/Brandon Moeller**: Assistance with HDX-MS. **Noah Harris**: Assistance with crystallography.

2.1 Abstract

Class I Phosphoinositide 3-kinases (PI3Ks) are master regulators of cellular functions, with the class IB PI3K catalytic subunit (p110γ) playing key roles in immune signaling. p110γ is a key factor in inflammatory diseases, and has been identified as a therapeutic target for cancers due to its immunomodulatory role. Using a combined biochemical/biophysical approach, we have revealed insight into regulation of kinase activity, specifically defining how immunodeficiency and oncogenic mutations of R1021 in the C-terminus can inactivate or activate enzyme activity. Screening of inhibitors using HDX-MS revealed that activation loop-binding inhibitors induce allosteric conformational changes that mimic those in the R1021C mutant. Structural analysis of advanced PI3K inhibitors in clinical development revealed novel binding pockets that can be exploited for further therapeutic development. Overall, this work provides unique insights into regulatory mechanisms that control PI3Kγ kinase activity, and shows a framework for the design of PI3K isoform and mutant selective inhibitors.

2.2 Introduction

The class IB p110γ isoform encoded by *PIK3CG* is a master regulator of immune cell function. It carries out almost all of its physiological functions in the cell when bound to regulatory subunits, with these complexes frequently referred to as PI3Kγ (which can be either p110γ/p101 or p110γ/p84). PI3Kγ plays important roles in the regulation of myeloid (macrophages, mast cells, neutrophils) and lymphoid (T cells, B cells, and Natural Killer cells) -derived immune cells (66,71,75). It regulates immune cell chemotaxis (75–77), cytokine release (69,78), and generation of reactive oxygen species (75), which are important processes in both the innate and adaptive immune systems. The ability of PI3Kγ to mediate multiple immune cell functions is controlled by its activation downstream of numerous cell surface receptors, including G-protein coupled receptors (GPCRs) (79), the IgE/Antigen receptor (78), receptor tyrosine kinases (RTKs) (80), and the Toll-like receptors (TLRs) (81,82). Activation of PI3Kγ downstream of these stimuli are potentiated by their p84 and p101 regulatory subunits (82–86). In mouse models, loss of PI3Kγ either genetically or pharmacologically is protective in multiple inflammatory diseases including cardiovascular disease (71), arthritis (66), Lupus (68), asthma (69), pulmonary inflammation and fibrosis (87,88), and metabolic syndrome (67). PI3Kγ is also a driver of pancreatic ductal adenocarcinoma progression through immunomodulatory effects (89), and targeting PI3Kγ in the immune system in combination with checkpoint inhibitors has shown promise in experimental cancer therapy (63,90).

Extensive biophysical and biochemical assays have identified many of the molecular mechanisms underlying PI3Kγ regulation. The p110γ enzyme is composed of five domains, a putative uncharacterized adaptor binding domain (ABD), a Ras binding domain (RBD), a C2 domain, a helical domain, and a bi-lobal lipid kinase domain (91) (Figure 2.1A). PI3Kγ activation is primarily mediated by Gβγ subunits downstream of GPCR signaling, through a direct interaction of Gβγ with the C2-helical linker of p110γ (86). Activation of PI3Kγ by Gβγ requires a secondary interaction between Gβγ and regulatory subunits for physiologically relevant activation (85), with the free p110γ subunit having no detectable activation downstream of GPCR activation in cells (92). In addition, PI3Kγ activation can be facilitated by Ras GTPases interacting with the RBD of p110γ (93), with the same interface also putatively mediating activation by Rab8 (81). Experiments exploring a novel type II-like kinase inhibitor that targets an active conformation of PI3Kγ revealed novel molecular aspects of regulation involving the C-terminal regulatory motif of the kinase domain, which is composed of the kα7, 8, 9, 10, 11, 12 helices that surround the activation loop, and keep

the enzyme in an inhibited state (94) (Figure 2.1B). The kα10, kα11, and kα12 helices are sometimes referred to as the regulatory arch (95). Inhibition mediated by the C-terminal regulatory motif is conserved through all class I PI3Ks, although for all other isoforms, this inhibited conformation requires interactions with a p85 regulatory subunit (Figure 2.1E+F) (96). The activation of all class I PI3Ks is proposed to require a conformational change in the regulatory motif leading to a reorientation of the C-terminus to a conformation that is compatible with membrane binding (Figure 2.1G). The p110γ catalytic subunit is unique in that it maintains an inactive conformation in the absence of regulatory subunits. This conformation is proposed to be maintained by a Tryptophan lock, where W1080 maintains a closed conformation of the membrane binding C-terminal kα12 helix, leading to an inactive conformation of the activation loop (94) (Figure 2.1B+D).

Disruption of PI3K signaling by either activating or inactivating mutations and deletions are involved in multiple human diseases. Overexpression of any activated class I PI3K isoform can lead to oncogenic transformation (97), although p110α is the most frequently mutated in human disease. Activating p110α mutations are linked to both cancer (98,99) and overgrowth disorders (100), while activating p110δ mutations are linked to primary immuno-deficiencies (101–103). A high proportion of these activating mutations cluster to the C-terminal regulatory motif of the p110 catalytic subunits. Multiple p110γ mutations have been identified in cancer patients (104–106), although at a lower frequency than p110α mutations. It would be expected that these mutations are activating, although this has not been fully explored. Intriguingly, p110γ loss of function mutations in the C-terminal regulatory motif (R1021P, N1085S) have been identified in patients with immunodeficiencies (106,107) (Figure 2.1B). PI3K mediated diseases being caused by both activating and inactivating mutations highlights the critical role of maintaining appropriate PIP_3 levels for human health.

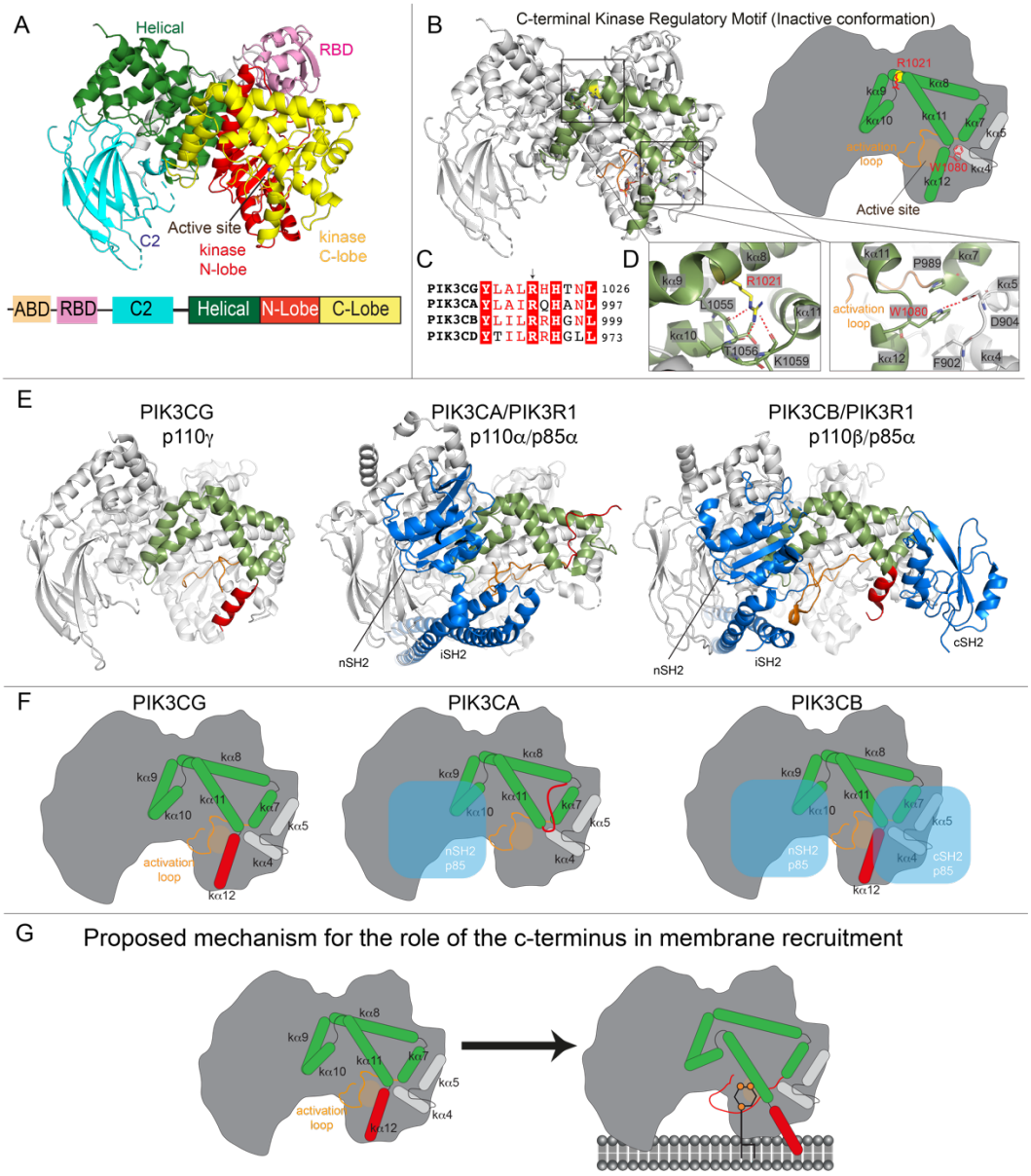

Figure 2.1. PI3Kγ contains a C-terminal regulatory motif which is reorganized upon membrane binding. (**A)** Domain architecture of p110γ (PDB ID: 6AUD) (108), with the domain schematic shown beneath. **(B)** Model of the C-terminal regulatory motif of the kinase domain of p110γ. The helices that make up the regulatory motif, which includes the regulatory arch (kα10, 11,12) and those that pack against them (kα7, 8, 9) are highlighted in green both in the structural model and cartoon schematic. **(C)** Alignment of residues around R1021 in p110γ with class IA p110 isoforms. (**D)** A close up of the W1080 'Tryptophan lock' interaction with kα7 and the kα4-kα5 loop which maintains an inhibited conformation is shown, as well as the interaction of the R1021 residue with residues on the kα10-kα11 loop. **(E)** A structural model comparing the architecture of the C-terminal regulatory motif in PIK3CG (PI3Kγ, PDB: 6AUD (108)), PIK3CA (PI3Kα, PDB: 4JPS (109)), PIK3CB (PI3Kβ, PDB: 2Y3A (110)). The activation loop is shown in orange, with the kα12 helix shown in red (not a helix in PI3Kα). The p85 regulatory subunits interacting with the motif in PI3Kα and PI3Kβ are shown in blue, with the domains of the nSH2, iSH2, and cSH2 annotated on the structure. **(F)** Cartoon model shown in the same format as in Figure 1, highlighting the regulatory motif and its interaction with regulatory subunits. **(G)** Cartoon model highlighting putative conformational changes in the regulatory motif required for membrane binding.

The involvement of activated PI3K signaling in multiple diseases has motivated class I PI3K inhibitor development. There are, however, toxicity effects associated with compounds that target all PI3K isoforms by mechanism-based adverse side effects (111), driving the development of isoform selective inhibitors. These efforts have led to multiple clinically approved inhibitors of PI3Kα and PI3Kδ (112–114). The critical role of PI3Kγ in inflammation and the tumor microenvironment has stimulated development of PI3Kγ specific inhibitors. Two main strategies for generating p110γ selective ATP-competitive inhibitors have been established: i) targeting p110γ specific pockets in and around the ATP binding site which are not conserved among p110 isoforms (72,115), and ii) targeting selective p110γ conformational changes (94). Intriguingly, the conformational selective p110γ inhibitors appear to target its putatively activated conformation.

The parallel discovery of disease linked mutations in the C-terminal regulatory motif, and conformational selective p110γ inhibitors that cause altered dynamics of the C-terminus led us to investigate the underlying molecular mechanisms. Using a combined biochemical and biophysical approach, we characterized the dynamic conformational changes caused by the loss of function R1021P p110γ mutation, as well as a putative oncogenic R1021C p110γ mutation identified in the Catalogue of Somatic Mutations in Cancer database [COSMIC (106)]. We found that the R1021P mutant leads to greatly decreased protein stability, while the activating R1021C mutation leads to localised conformational disruption of the regulatory motif at the c-terminus. A screen of a number of PI3Kγ selective and pan-PI3K inhibitors revealed that many of these molecules induced allosteric conformational changes in p110γ. A combined X-ray crystallography and hydrogen deuterium exchange mass spectrometry (HDX-MS) approach showed that inhibitor interactions with the activation loop mediates the allosteric conformational changes. Intriguingly, similar conformational changes occurred with the R1021C mutant. The R1021C mutant was also found to be more sensitive to inhibition by kinase inhibitors that cause allosteric conformational changes. Overall, this work provides a unique insight into how mutations alter PI3Kγ regulation, and paves the way to novel strategies for isoform and mutant selective PI3K inhibitors.

2.3 Materials and Methods

Expression and Purification of PI3Kγ constructs:

Full length monomeric p110γ (WT, R1021C) and p110γ/p101 complex (WT, R1021C, R1021P) were expressed in Sf9 insect cells using the baculovirus expression system. For the complex, the subunits were co-expressed from a MultiBac vector (116). Following 55 hours of expression, cells were harvested by centrifuging at 1680 RCF (Eppendorf Centrifuge 5810 R) and the pellets were snap-frozen in liquid nitrogen. Both the monomer and the complex were purified identically through a combination of nickel affinity, streptavidin affinity and size exclusion chromatographic techniques.

Frozen insect cell pellets were resuspended in lysis buffer (20 mM Tris pH 8.0, 100 mM NaCl, 10 mM imidazole pH 8.0, 5% glycerol (v/v), 2 mM beta-mercaptoethanol (βME), protease inhibitor (Protease Inhibitor Cocktail Set III, Sigma)) and sonicated for 2 minutes (15s on, 15s off, level 4.0, Misonix sonicator 3000). Triton-X was added to the lysate to a final concentration of 0.1% and clarified by spinning at 15,000 g for 45 minutes (Beckman Coulter JA-20 rotor). The supernatant was loaded onto a 5 mL HisTrap™ FF crude column (GE Healthcare) equilibrated in NiNTA A buffer (20 mM Tris pH 8.0, 100 mM NaCl, 20 mM imidazole pH 8.0, 5% (v/v) glycerol, 2 mM βME). The column was washed with high salt NiNTA A buffer (20 mM Tris pH 8.0, 1 M NaCl, 20 mM imidazole pH 8.0, 5% (v/v) glycerol, 2 mM βME), NiNTA A buffer, 6% NiNTA B buffer (20 mM Tris pH 8.0, 100 mM NaCl, 250 mM imidazole pH 8.0, 5% (v/v) glycerol, 2 mM βME) and the protein was eluted with 100% NiNTA B. The eluent was loaded onto a 5 mL StrepTrap™ HP column (GE Healthcare) equilibrated in gel filtration buffer (20mM Tris pH 8.5, 100 mM NaCl, 50 mM Ammonium Sulfate and 0.5 mM tris(2-carboxyethyl) phosphine (TCEP)). The column was washed with the same buffer and loaded with tobacco etch virus protease. After cleavage on the column overnight, the protein was eluted in gel filtration buffer. The eluent was concentrated in a 50,000 MWCO Amicon Concentrator (Millipore) to <1 mL and injected onto a Superdex™ 200 10/300 GL Increase size-exclusion column (GE Healthcare) equilibrated in gel filtration buffer. After size exclusion, the protein was concentrated, aliquoted, frozen and stored at -80^{o}C.

For crystallography, p110γ (aas 144-1102) was expressed in Sf9 insect cells for 72 hours. The cell pellet was lysed and the lysate was subjected to nickel affinity purification as described above. The eluent was loaded onto HiTrap^{TM} Heparin HP cation exchange column equilibrated in Hep A buffer (20 mM Tris pH 8.0, 100 mM NaCl, 5%

glycerol and 2 mM βME). A gradient was started with Hep B buffer (20 mM Tris pH 8.0, 1 M NaCl, 5% glycerol and 2 mM βME) and the fractions containing the peak were pooled. This was then loaded onto HiTrap™ Q HP anion exchange column equilibrated with Hep A and again subjected to a gradient with Hep B. The peak fractions were pooled, concentrated on a 50,000 MWCO Amicon Concentrator (Millipore) to <1 mL and injected onto a Superdex™ 200 10/300 GL Increase size-exclusion column (GE Healthcare) equilibrated in gel filtration buffer (20 mM Tris pH 7.2, 0.5 mM $(NH_4)_2SO_4$, 1% ethylene glycol, 0.02% CHAPS and 5 mM DTT). Protein from size exclusion was concentrated to >5 mg/mL, aliquoted, frozen and stored at -80°C.

Expression and Purification of lipidated Gβγ:

Full length, lipidated Gβγ was expressed in Sf9 insect cells and purified as described previously (117). After 65 hours of expression, cells were harvested and the pellets were frozen as described above. Pellets were resuspended in lysis buffer (20 mM HEPES pH 7.7, 100 mM NaCl, 10 mM βME, protease inhibitor (Protease Inhibitor Cocktail Set III, Sigma)) and sonicated for 2 minutes (15s on, 15s off, level 4.0, Misonix sonicator 3000). The lysate was spun at 500 RCF (Eppendorf Centrifuge 5810 R) to remove intact cells and the supernatant was centrifuged again at 25,000 g for 1 hour (Beckman Coulter JA-20 rotor). The pellet was resuspended in lysis buffer and sodium cholate was added to a final concentration of 1% and stirred at 4°C for 1 hour. The membrane extract was clarified by spinning at 10,000 g for 30 minutes (Beckman Coulter JA-20 rotor). The supernatant was diluted 3 times with NiNTA A buffer (20 mM HEPES pH 7.7, 100 mM NaCl, 10 mM Imidazole, 0.1% C12E10, 10mM βME) and loaded onto a 5 mL HisTrap™ FF crude column (GE Healthcare) equilibrated in the same buffer. The column was washed with NiNTA A, 6% NiNTA B buffer (20 mM HEPES pH 7.7, 25 mM NaCl, 250 mM imidazole pH 8.0, 0.1% C12E10, 10 mM βME) and the protein was eluted with 100% NiNTA B. The eluent was loaded onto HiTrap™ Q HP anion exchange column equilibrated in Hep A buffer (20 mM Tris pH 8.0, 8 mM CHAPS, 2 mM Dithiothreitol (DTT)). A gradient was started with Hep B buffer (20 mM Tris pH 8.0, 500 mM NaCl, 8 mM CHAPS, 2 mM DTT) and the protein was eluted in ~50% Hep B buffer. The eluent was concentrated in a 30,000 MWCO Amicon Concentrator (Millipore) to < 1 mL and injected onto a Superdex™ 75 10/300 GL size exclusion column (GE Healthcare) equilibrated in Gel Filtration buffer (20 mM HEPES pH 7.7, 100 mM NaCl, 10 mM CHAPS, 2 mM TCEP). Fractions containing protein were pooled, concentrated, aliquoted, frozen and stored at -80°C.

Expression and Purification of Lipidated HRas G12V:

Full-length HRas G12V was expressed by infecting 500 mL of Sf9 cells with 5 mL of baculovirus. Cells were harvested after 55 hours of infection and frozen as described above. The frozen cell pellet was resuspended in lysis buffer (50 mM HEPES pH 7.5, 100 mM NaCl, 10 mM βME and protease inhibitor (Protease Inhibitor Cocktail Set III, Sigma)) and sonicated on ice for 1 minute 30 seconds (15s ON, 15s OFF, power level 4.0) on the Misonix sonicator 3000. Triton-X 114 was added to the lysate to a final concentration of 1%, mixed for 10 minutes at 4°C and centrifuged at 25,000 rpm for 45 minutes (Beckman Ti-45 rotor). The supernatant was warmed to 37°C for few minutes until it turned cloudy following which it was centrifuged at 11,000 rpm at room temperature for 10 minutes (Beckman JA-20 rotor) to separate the soluble and detergent-enriched phases. The soluble phase was removed, and Triton-X 114 was added to the detergent-enriched phase to a final concentration of 1%. Phase separation was performed 3 times. Imidazole pH 8.0 was added to the detergent phase to a final concentration of 15 mM and the mixture was incubated with Ni-NTA agarose beads (Qiagen) for 1 hour at 4°C. The beads were washed with 5 column volumes of Ras-NiNTA buffer A (20mM Tris pH 8.0, 100mM NaCl, 15mM imidazole pH 8.0, 10mM βME and 0.5% Sodium Cholate) and the protein was eluted with 2 column volumes of Ras-NiNTA buffer B (20mM Tris pH 8.0, 100mM NaCl, 250mM imidazole pH 8.0, 10mM βME and 0.5% Sodium Cholate). The protein was buffer exchanged to Ras-NiNTA buffer A using a 10,000 kDa MWCO Amicon concentrator, where protein was concentrated to ~1mL and topped up to 15 mL with Ras-NiNTA buffer A and this was repeated a total of 3 times. GTPγS was added in 2-fold molar excess relative to HRas along with 25 mM EDTA. After incubating for an hour at room temperature, the protein was buffer exchanged with phosphatase buffer (32 mM Tris pH 8.0, 200 mM Ammonium Sulphate, 0.1 mM $ZnCl_2$, 10 mM βME and 0.5% Sodium Cholate). 1 unit of immobilized calf alkaline phosphatase (Sigma) was added per milligram of HRas along with 2-fold excess nucleotide and the mixture was incubated for 1 hour on ice. $MgCl_2$ was added to a final concentration of 30 mM to lock the bound nucleotide. The immobilized phosphatase was removed using a 0.22-micron spin filter (EMD Millipore). The protein was concentrated to less than 1 mL and was injected onto a Superdex^{TM} 75 10/300 GL size exclusion column (GE Healthcare) equilibrated in gel filtration buffer (20 mM HEPES pH 7.7, 100 mM NaCl, 10 mM CHAPS, 1 mM $MgCl_2$ and 2 mM TCEP). The protein was concentrated to 1 mg/mL using a 10,000 kDa MWCO Amicon concentrator, aliquoted, snap-frozen in liquid nitrogen and stored at -80°C.

Lipid Vesicle Preparation:

For kinase assays comparing WT and mutant activities, lipid vesicles containing 5% brain phosphatidylinositol 4,5- bisphosphate (PIP_2), 20% brain phosphatidylserine (PS), 50% egg-yolk phosphatidylethanolamine (PE), 10% egg-yolk phosphatidylcholine (PC), 10% cholesterol and 5% egg-yolk sphingomyelin (SM) were prepared by mixing the lipids dissolved in organic solvent. The solvent was evaporated in a stream of argon following which the lipid film was desiccated in a vacuum for 45 minutes. The lipids were resuspended in lipid buffer (20 mM HEPES pH 7.0, 100 mM NaCl and 10 % glycerol) and the solution was sonicated for 15 minutes. The vesicles were subjected to five freeze thaw cycles and extruded 11 times through a 100-nm filter (T&T Scientific: TT-002-0010). The extruded vesicles were sonicated again for 5 minutes, aliquoted and stored at -80°C. For inhibitor response assays, lipid vesicles containing 95% PS and 5% C8-PIP_2 were used. PS was dried and desiccated as described above. The lipid film was mixed and resuspended with C8-PIP_2 solution (2.5 mg/mL in lipid buffer). Following this, vesicles were essentially prepared the same way as described above. All vesicles were stored at 5 mg/mL.

Lipid Kinase assays:

All lipid kinase activity assays employed the Transcreener ADP2 Fluorescence Intensity (FI) Assay (Bellbrook labs) which measures ADP production. For assays comparing the activities of mutants, final concentrations of PM-mimic vesicles were 1 mg/mL, ATP was 100 μM ATP and lipidated Gβγ/HRas were at 1.5 μM. 2 μL of a PI3K solution at 2× final concentration (50-3000 nM final) was mixed with 2 μL substrate solution containing ATP, vesicles and Gβγ/HRas or Gβγ/HRas gel filtration buffer and the reaction was allowed to proceed for 60 minutes at 20°C. The reaction was stopped with 4 μL of 2× stop and detect solution containing Stop and Detect buffer, 8 nM ADP Alexa Fluor 594 Tracer and 93.7 μg/mL ADP2 Antibody IRDye QC-1 and incubated for 50 minutes. The fluorescence intensity was measured using a SpectraMax M5 plate reader at excitation 590 nm and emission 620 nm. This data was normalized against a 0-100% ADP window made using conditions containing either 100 μM ATP/ADP with vesicles and kinase buffer. % ATP turnover was interpolated from an ATP standard curve obtained from performing the assay on 100 μM (total) ATP/ADP mixtures with increasing concentrations of ADP using Prism 7. All specific activities of lipid kinase activity were corrected for the basal ATPase activity by subtracting the specific activity of the WT/mutant protein in the absence of vesicles/activators.

For assays measuring inhibitor response, substrate solutions containing vesicles, ATP and Gβγ at 4× final concentration (as described above) were mixed with 4× solutions of inhibitor dissolved in lipid buffer (<1% DMSO) in serial to obtain 2× substrate solutions with inhibitors at the various 2× concentrations. 2 μL of this solution was mixed with 2 μL of 2× protein solution (4 nM final for the mutant and 8 nM final for WT) to start the reaction and allowed to proceed for 60 minutes at 37 ºC. Following this, the reaction was stopped and the intensity was measured. The raw data was normalized against a 0-100% ADP window as described above. The % inhibition was calculated by comparison to the activity with no inhibitor to obtain fraction activity remaining.

Hydrogen Deuterium Exchange Mass Spectrometry (HDX-MS):

HDX experiments were performed similarly as described before (102). For HDX with mutants, 3 μL containing 13 picomoles of protein was incubated with 8.25 μL of D_2O buffer (20mM HEPES pH 7.5, 100 mM NaCl, 98% (v/v) D_2O) for four different time periods (3, 30, 300, 3000 s at 20 ºC). After the appropriate time, the reaction was stopped with 57.5 μL of ice-cold quench buffer (2M guanidine, 3% formic acid), immediately snap frozen in liquid nitrogen and stored at -80 ºC. For HDX with inhibitors, 5 μL of p110γ or p110γ/p101 at 2 μM was mixed with 5 μL of inhibitor at 4 μM in 10% DMSO or 5 μL of blank solution containing 10% DMSO and incubated for 20 minutes on ice. 40 μL of D2O buffer was added to this solution to start the exchange reaction which was allowed to proceed for four different time periods (3, 30, 300, 3000 s at 20 ºC). After the appropriate time, the reaction was terminated with 20 μL of ice-cold quench buffer and the samples were frozen.

Protein samples were rapidly thawed and injected onto an ultra-high pressure liquid chromatography (UPLC) system at 2 °C. Protein was run over two immobilized pepsin columns (Trajan, ProDx protease column, PDX.PP01-F32 and Applied Biosystems, Porosyme, 2-3131-00) at 10 °C and 2 °C at 200 μl/min for 3 min, and peptides were collected onto a VanGuard precolumn trap (Waters). The trap was subsequently eluted in line with an Acquity 1.7-μm particle, 100 × 1 mm2 C18 UPLC column (Waters), using a gradient of 5–36% B (buffer A, 0.1% formic acid; buffer B, 100% acetonitrile) over 16 min. Mass spectrometry experiments were performed on an Impact II TOF (Bruker) acquiring over a mass range from 150 to 2200 *m/z* using an electrospray ionization source operated at a temperature of 200 °C and a spray voltage of 4.5 kV. Peptides were identified using data-dependent acquisition methods following tandem MS/MS experiments (0.5-s precursor scan from 150–2000 *m/z*; 12 0.25-s fragment scans

from 150–2000 *m/z*). MS/MS datasets were analyzed using PEAKS7 (PEAKS), and a false discovery rate was set at 1% using a database of purified proteins and known contaminants.

HD-Examiner software (Sierra Analytics) was used to automatically calculate the level of deuterium incorporation into each peptide. All peptides were manually inspected for correct charge state and presence of overlapping peptides. Deuteration levels were calculated using the centroid of the experimental isotope clusters. The results for these proteins are presented as the raw percent deuterium incorporation, as shown in Appendix C, with the only correction being applied correcting for the deuterium oxide percentage of the buffer utilized in the exchange (62% for experiments with mutants and 75.5% for experiments with inhibitors). No corrections for back exchange that occurs during the quench and digest/separation were applied. Attempts to generate a fully deuterated class I PI3K sample were unsuccessful, which is common for large macromolecular complexes. Therefore, all deuterium exchange values are relative.

Changes in any peptide at any time point greater than both 5% and 0.4 Da between conditions with a paired t test value of $p < 0.01$ were considered significant. Peptides that crossed these criteria were mapped onto the structures in Figures 2.3A+B and 2.4B-D. The raw HDX data are shown in two different formats. The raw peptide deuterium incorporation graphs for a selection of peptides with significant differences are shown, with the raw data for all analyzed peptides in the appendix. To allow for visualization of differences across all peptides, we utilized number of deuteron difference (#D) plots. These plots show the total difference in deuterium incorporation over the entire H/D exchange time course, with each point indicating a single peptide. These graphs are calculated by summing the differences at every time point for each peptide and propagating the error (example Figure 2.3C-F). This visualization was utilized over the similar strategy of graphing differences at each timepoint separately as it allowed for the display of multiple comparisons on the same graph (example Figure 2.4A). The mass spectrometry proteomics data have been deposited to the ProteomeXchange Consortium via the PRIDE partner repository (118) with the dataset identifier PXD021132.

X-ray crystallography:

p110γ (aas 144-1102) was crystallized from a grid of 2 µl sitting drops at 1:1, 2:1 and 3:1 protein to reservoir ratios at 18°C. Protein at 4 mg/mL (in 20 mM Tris pH 7.2, 0.5 mM $(NH_4)_2SO_4$, 1% ethylene glycol, 0.02% CHAPS and 5 mM DTT) was mixed with reservoir solution containing 100 mM Tris pH 7.5, 250 mM $(NH_4)_2SO_4$ and 20-22% PEG 4000. Large multinucleate crystals were generated in these drops. Inhibitor stocks were prepared at

concentrations of 0.01 mM, 0.1 mM and 1 mM in cryo-protectant solution containing 100 mM Tris pH 7.5, 250 mM $(NH_4)_2SO_4$, 23% PEG 4000 and 14% glycerol. Inhibitors at increasing concentrations were added to the drops stepwise every 1 hour. After overnight incubation with the inhibitor, single crystals were manually broken from the multi-nucleates and soaked in a fresh drop containing 1 mM inhibitor in cryo-protectant before being immediately frozen in liquid nitrogen. The final crystals were rod/needle shaped and had dimensions of roughly 10 x 20 x 80 μm, and were mounted on either 0.1 - 0.2 or 0.05-0.1 mm cryo loops (Hampton Research). Each unique structure of PI3K bound to inhibitors was solved from a single crystal.

Diffraction data for PI3Kγ crystals were collected on beamline 08ID-1 of the Canadian Light Source. Data was collected at 0.97949 Å using a beam width of 50 μm. Diffraction data for each unique crystal was collected using a strategy of 0.2-0.4 sec exposure / 0.2° rotation for each image, over a total rotational range of 180°. Data were processed using XDS (119). Phases were initially obtained by molecular replacement using Phaser (120) using PDB: 2CHW for the IPI-549 complex (121), and 5JHA for Gedatolisib and NVS-PI3-4 (122). Iterative model building and refinement were performed in COOT (123) and phenix.refine (124). Refinement was carried out with rigid body refinement, followed by translation/libration/screw B-factor and xyz refinement, with the final round of refinement optimising X-ray/stereochemistry and X-ray/ADP weighting. The final model was verified in Molprobity (125) to examine all Ramachandran and Rotamer outliers. Data collection and refinement statistics are shown in Appendix E. The crystallography data has been deposited in the protein data bank with accession numbers (PDB: 7JWE, 7JX0, 7JWZ).

2.4 Results

R1021P and R1021C mutations alter the activity of p110γ

The recent discovery of an inactivating disease-linked mutation in *PIK3CG* located near the C-terminus of the p110γ kinase domain (R1021P) in immunocompromised patients led us to investigate the molecular mechanism of this mutation. Intriguingly, this same residue is found to be mutated in the COSMIC database (R1021C) (106). The R1021 residue in p110γ is conserved across all class I PI3K isoforms (Figure 2.1 C), and mutations in the equivalent residue in *PIK3CA* (p110α) are putatively oncogenic (R992L/N). To define the effect of these mutations on protein conformation and biochemical activity, we generated them recombinantly in complex with the p101 regulatory subunit. Both the p110γ R1021C and R1021P complexes with p101 eluted from gel filtration similar to wild-type

p110γ-p101, suggesting they were properly folded (Figure 2.2A+B). However, the yield of the R1021P complex with p101 was dramatically decreased relative to both wild-type and R1021C p110γ, indicating that this mutation may decrease protein stability, consistent with decreased p110γ and p101 expression in patient tissues (74). We also generated the free R1021C p110γ subunit, however we could not express free p110γ R1021P, further highlighting that this mutation likely leads to decreased protein stability.

The R1021 residue forms hydrogen bonds with the carbonyl oxygens of L1055, T1056, and K1059 located in or adjacent to the regulatory arch helices kα10 and kα11 of PI3Kγ (Figure 2.1D). Both R1021C and R1021P would be expected to disrupt these interactions, with the R1021P also expected to distort the secondary structure of the kα8 helix. The R1021P has been previously found to lead to greatly decreased lipid kinase activity *in vitro* (74). To characterize these mutations, we carried out biochemical assays of wild-type, R1021C, and R1021P p110γ/p101 complexes against plasma membrane-mimic lipid vesicles containing 5% PIP_2. Assays were carried out in the presence and absence of lipidated Gβγ and Ras. Lipidated Gβγ leads to a >100-fold activation of lipid kinase activity for wild-type complexes, with Ras causing a ~10-fold activation. These assays revealed that p110γ/p101 R1021C was ~8-fold more active than wild-type both basally and in the presence of Gβγ, and ~2-3 fold more active upon Ras activation (Figure 2.2C). The R1021C mutant also showed a ~8-fold increase in lipid kinase activity compared to wild-type when assaying the free p110γ subunit (Figure 2.2E). This is consistent with the R1021C mutation destabilizing the regulatory motif, potentially disrupting the Tryptophan lock and leading to increased membrane recruitment.

The R1021P complex showed weak but detectable basal lipid kinase activity, however, there was almost no activation by lipidated Gβγ compared to wild-type, suggesting this complex would be almost completely inactive in a physiological context (Figure 2.2C). To examine if the catalytic machinery of the R1021P mutant was intact, we carried out experiments looking at ATPase activity (non-productive turnover of ATP in the absence of lipid substrate). Intriguingly, R1021P p110γ-p101 showed higher basal ATPase activity compared to wild-type p110γ/p101 and R1021C p110γ-p101, revealing that it still has catalytic activity, but almost no activity on membrane substrate (Figure 2.2D). This suggests that the minimal structural features required for ATP hydrolysis are maintained in the R1021P mutant, but that either membrane binding or PIP_2 recognition is severely impaired.

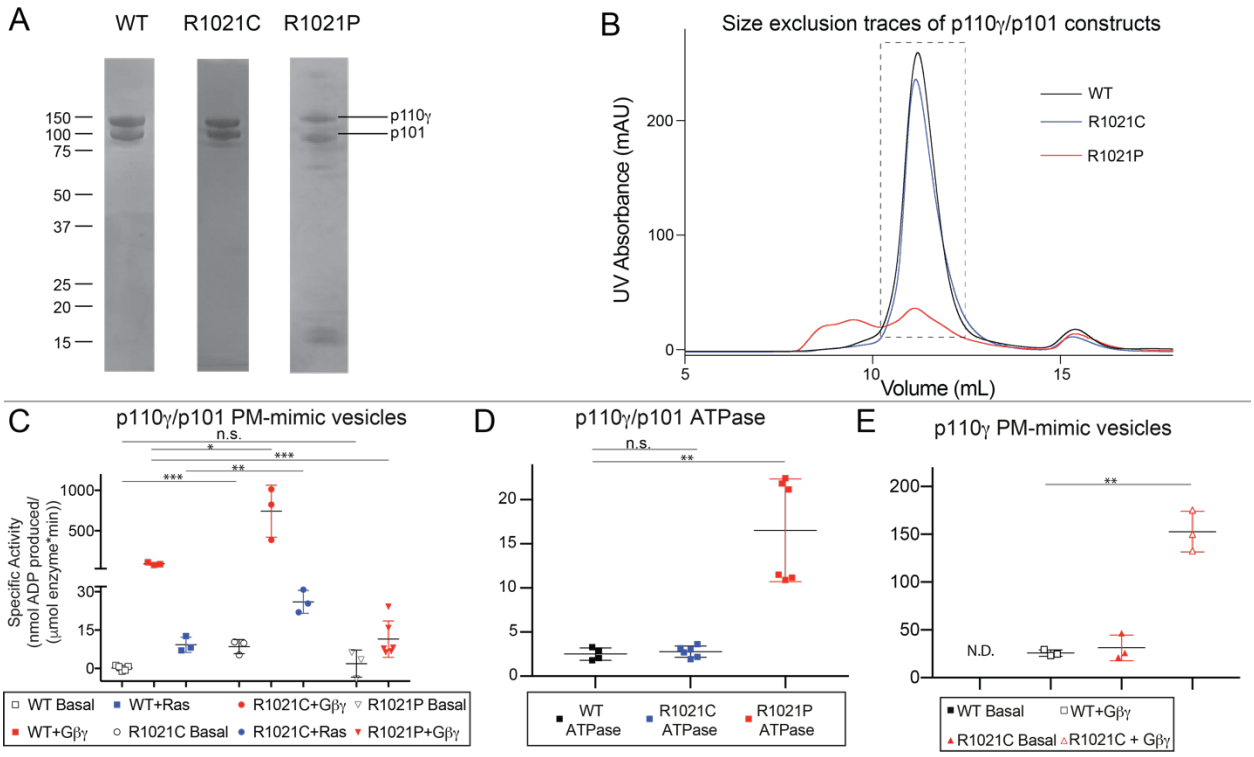

Figure 2.2. Mutations in the regulatory C-terminal motif alter PI3Kγ activity. **(A)** SDS-page analysis of the final complexes after size exclusion chromatography. The location of size markers are shown on the left. **(B)** Gel filtration elution of the wild type and mutant p110γ/p101 complexes on a Superdex™ 200 10/300 GL Increase column **(C).** Lipid kinase activity assays testing the activity of WT, R1021C, and R1021P p110γ/p101 WT basally and in the presence of lipidated Gβγ and HRas. Experiments were carried out with 50-3000 nM kinase, 1500 nM Ras, 1500 nM Gβγ, all in the presence of 100 μM ATP and 1 mg/mL PM-mimic vesicles [5% phosphatidylinositol 4,5 bisphosphate (PI_2), 20% phosphatidylserine (PS), 10% phosphatidyl choline (PC), 50% phosphatidylethanolamine (PE), 10% Cholesterol, 5% sphingomyelin (SM)]. **(D)** Activity assays testing the intrinsic ATPase activity (ATP conversion in the absence of membrane substrate) for wild type and mutant p110γ/p101 complexes. **(E)** Lipid kinase activity assays testing the activity of WT and R1021C for the free p110γ catalytic subunit with and without lipidated Gβγ. Lipid kinase activity was generated by subtracting away non-specific ATPase activity, for unstimulated WT p110γ there was no detectable lipid kinase activity above basal ATPase activity (N.D.). For panels E-G every replicate is plotted, with error shown as standard deviation (n=3-6). Two tailed p-values represented by the symbols as follows: ***<0.001; **<0.01; *<0.05; n.s.>0.05.

R1021P and R1021C cause allosteric conformational changes throughout the regulatory C-terminal motif

We carried out hydrogen deuterium exchange mass spectrometry (HDX-MS) experiments to define the molecular basis for why two different mutations at R1021 have opposing effects on lipid kinase activity. HDX-MS is a technique that measures the exchange rate of amide hydrogens, and as the rate is dependent on the presence and stability of secondary structure, it is an excellent probe of protein conformational dynamics (126). HDX-MS experiments were performed on complexes of wild-type p110γ/p101, R1021C p110γ/p101, and R1021P p110γ/p101.

The coverage map of the p110γ and p101 proteins was composed of 153 peptides spanning ~93% percent of the exchangeable amides (Appendix A).

The R1021C and R1021P mutations led to significant changes in the conformational dynamics of the p110γ catalytic and p101 regulatory subunits (Figure 2.3A-G). The R1021P mutation resulted in large increases in exchange throughout almost the entire C2, helical, and kinase domains (Figure 2.3B+D). Comparing the rates of hydrogen exchange between wild-type, R1021C, and R1021P showed many regions where both R1021C and R1021P mutations caused increased H/D exchange. However, for the majority of these regions, the R1021P mutation led to increased exchange at early (3 s) and late timepoints (3000 s) of exchange, indicating that this mutation was leading to significant disruption of protein secondary structure (Figure 2.3G). This large-scale destabilization throughout the protein may explain the low yield and decreased kinase activity.

The R1021C mutation resulted in increased H/D exchange in the C2, helical and kinase domains of p110γ. Intriguingly, many of the changes in dynamics of the helical and kinase domains are similar to those observed upon membrane binding (86). The largest differences occurred in the helices in the C-terminal regulatory motif (kα7-12) (Figure 2.3A+C). A peptide spanning the C-terminal end of the activation loop and kα7 (976-992) showed increased exchange, with these changes primarily occurring at later timepoints of exchange (3000 s) (Figure 2.3G). This is indicative of these regions maintaining secondary structure, although with increased flexibility. Differences in HDX-MS with R1021C is consistent with a disruption of the inhibitory conformation of the regulatory motif. In addition, the increased dynamics of the activation loop seen in the mutant may pre-organize the catalytic machinery for activation. This is consistent with previous HDX-MS analysis of the regulatory mechanisms of class IA PI3Ks which revealed that increased dynamics of the activation loop occurred concurrently with increased lipid kinase activity (102,127–129).

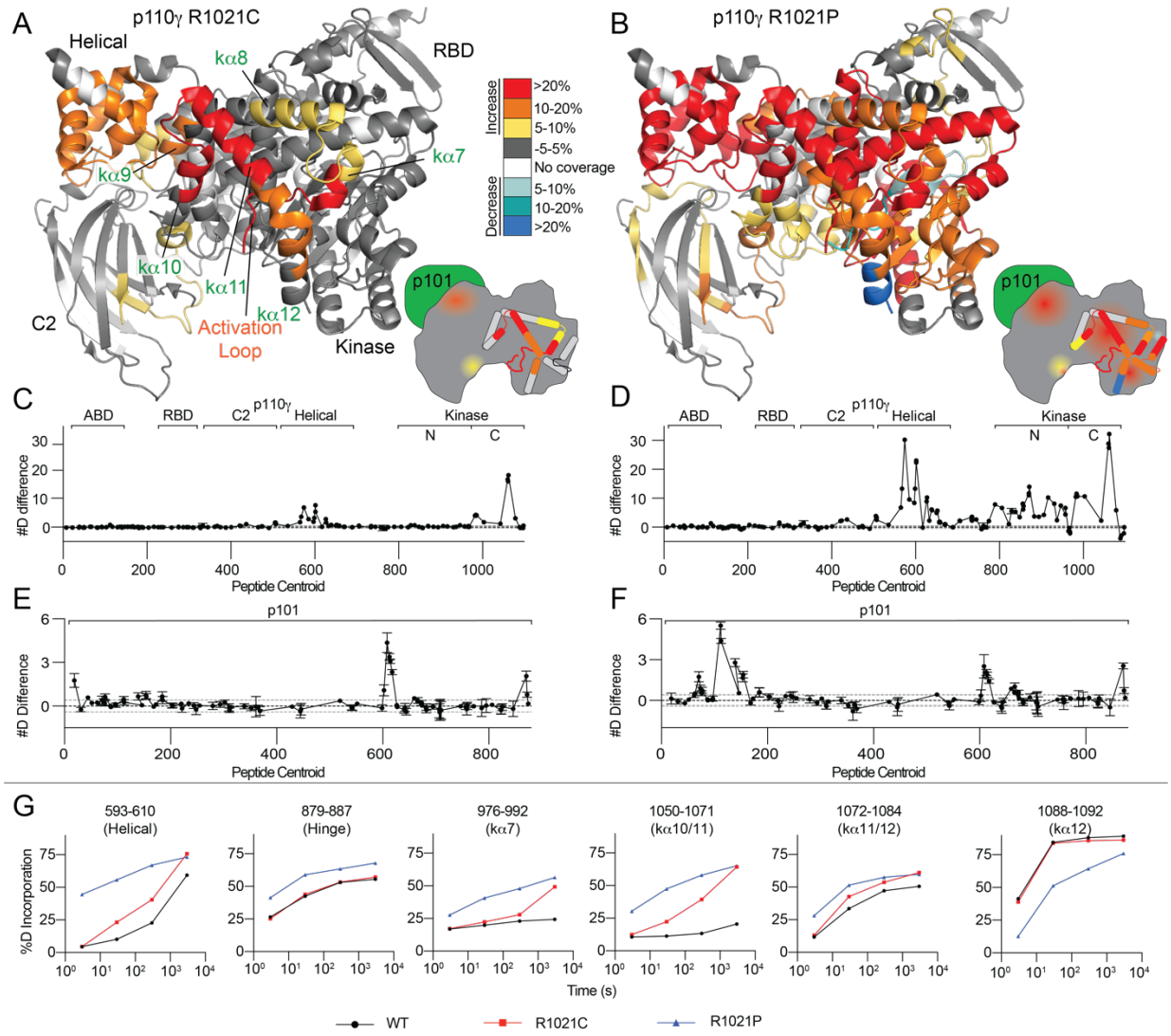

Figure 2.3. R1021P leads to global destabilization while R1021C leads to localised disruption of the C-terminal regulatory W1080 Tryptophan 'lock'. (A+B). Peptides showing significant deuterium exchange differences (>5 %, >0.4 kDa and $p<0.01$ in an unpaired two-tailed t-test) between wild-type and R1021C (A) and wild-type and R1021P (B) p110γ/p101 complexes are coloured on a model of p110γ (PDB: 6AUD) (108). Differences in exchange are coloured according to the legend. **(C+D).** The number of deuteron difference for the R1021C and R1021P mutants for all peptides analyzed over the entire deuterium exchange time course for p110γ. Every point represents the central residue of an individual peptide. The domain location is noted above the primary sequence. A cartoon model of the p110γ structural model is shown according to the legend in panels A+B. Error is shown as standard deviation (n=3). **(E+F).** The number of deuteron difference for the R1021C and R1021P mutants for all peptides analyzed over the entire deuterium exchange time course for p101. Every point represents the central residue of an individual peptide. Error is shown as standard deviation (n=3). **(G)** Deuterium incorporation behaviour over time for selected p110γ peptides that showed decreases and increases in exchange are shown.

The two mutations in R1021C and R1021P both caused increased exchange in the p101 subunit. Peptides spanning 602-623, and 865-877 of p101 showed similar increases in exchange for both R1021C and R1021P, with R1021P also leading to increased exchange in a peptide nearer the N-terminus (102-122) (Figure 2.3E+F). As there is

no structural model for the p101 subunit, it is hard to unambiguously interpret this data, however, these may represent increased H/D exchange due to partial destabilization of the complex.

Multiple PI3Kγ inhibitors lead to allosteric conformational changes

The increased H/D exchange in the regulatory motif for the R1021C mutant is similar to previously observed differences caused by cyclopropyl ethyl containing isoindolinone inhibitors (94). This result suggested it would be worth interrogating the dynamics of p110γ induced by multiple classes of p110γ inhibitors. Specifically, we wanted to understand if inhibitors that promote allosteric conformational changes might be useful in the development of isoform/mutant selective compounds.

We performed HDX-MS experiments with seven potent PI3K inhibitors on free p110γ to define the role of allostery in PI3Kγ inhibition. We analyzed inhibitors that were selective for PI3Kγ (AS-604850 (66), AZ2 (94), NVS-PI3-4 (130), and IPI-549 (72)) as well as pan-PI3K inhibitors (PIK90 (121), Omipalisib (131), and Gedatolisib (132)). Of these compounds, only AS-604850, PIK90, and Omipalisib have been structurally characterized bound to p110γ. A table summarizing these compounds and their selectivity for different PI3K isoforms is shown in Appendix B. Deuterium exchange experiments were carried out with monomeric p110γ over 4 timepoints of deuterium exchange (3,30,300, and 3000 s). We obtained 180 peptides covering ~89% percent of the exchangeable amides (Appendix C).

Based on the H/D exchange differences observed with inhibitors present, we were able to classify the inhibitors into three broad groups. The first group contains the isoquinolinone compound IPI-549, the imidazo[1,2-*c*]quinazoline molecule PIK-90 and the thiazolidinedione compound AS-604850 (Figure 2.4A+B). These compounds caused decreased exchange near the active site, with the primary protected region being the hinge region between the N- and C- lobes of the kinase domain (Figure 2.4B+E). No (IPI-549, AS-604850) or very small (PIK-90) increases in deuterium incorporation were observed (Figure 2.4A, Appendix D), suggesting that there are localized allosteric conformational changes for these compounds.

The H/D exchange experiments revealed a second class of inhibitors that showed decreased exchange at the active site, but also significant increases in exchange in the kinase and helical domains (Figure 2.4A+C, Appendix D). The second group includes the bis-morpholinotriazine molecule Gedatolisib, difluoro-benzene sulfonamide compound Omipalisib, and the PI3Kγ-specific thiazole derivative NVS-PI3-4. Binding of these inhibitors caused increased exchange in multiple regions of the kinase regulatory motif, including kα7, kα10, kα11 and kα12. The peptide

covering kα7 also spans the C-terminal end of the activation loop (Figure 2.4C+E). In addition to these changes, there were also increases in exchange within the helical domain. Intriguingly, for Gedatolisib, the regions of the protein that showed differences in H/D exchange matched very closely to those observed in the R1021C mutant. This suggests that the conformational changes induced by these compounds may partially mimic the activated state that occurs in the R1021C mutant.

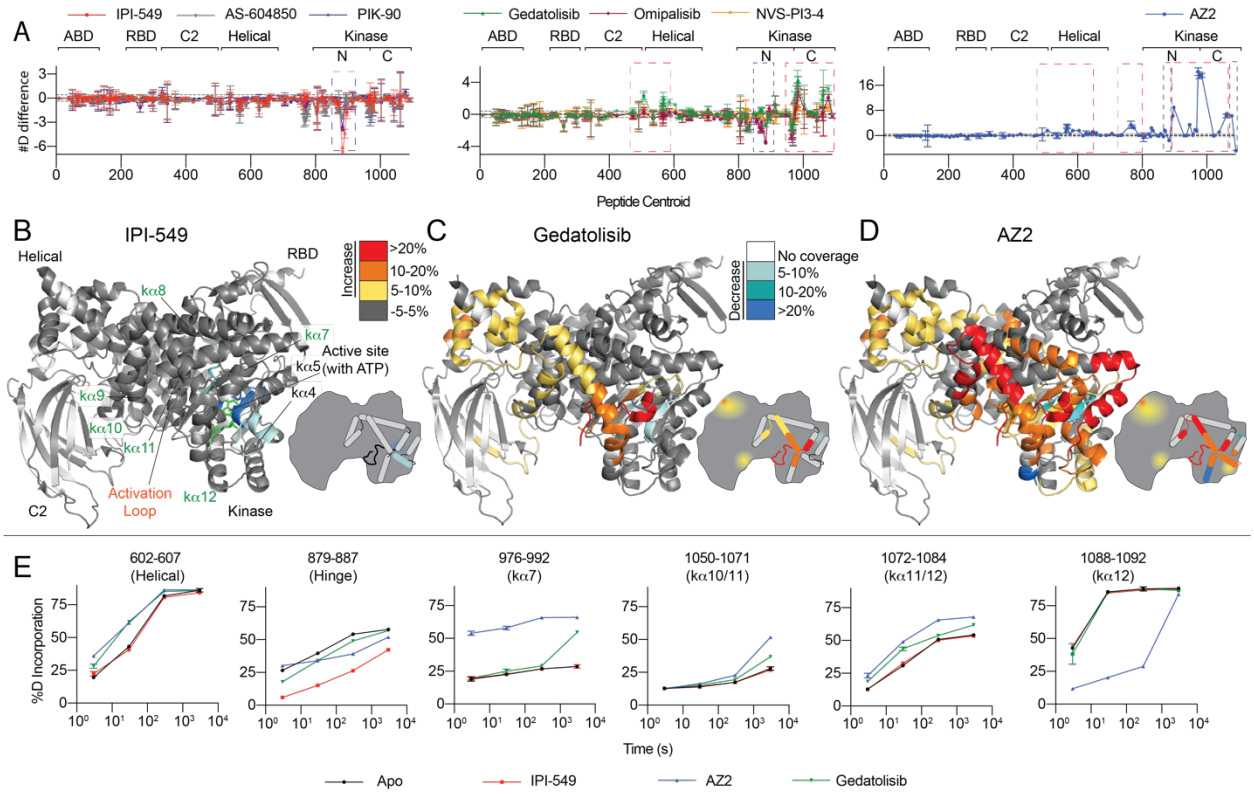

Figure 2.4. HDX-MS reveals that different classes of PI3K inhibitors lead to unique allosteric conformational changes. (A) The number of deuteron difference for the 7 different inhibitors analyzed over the entire deuterium exchange time course for p110γ. Every point represents the central residue of an individual peptide. The domain location is noted above the primary sequence. Error is shown as standard deviation (n=3). **(B-D).** Peptides showing significant deuterium exchange differences (>5%, >0.4 kDa and $p<0.01$ in an unpaired two-tailed t-test) between wild-type and IPI-549 (B), Gedatolisib (C), and AZ2 (D) are coloured on a model of p110γ (PDB: 6AUD). Differences in exchange are mapped according to the legend. A cartoon model in the same format as Figure 2.1 is shown as a reference. **(E).** Selected p110γ peptides that showed decreases and increases in exchange are shown.

Finally, AZ2 caused large scale increased exposure throughout large regions of the helical and kinase domains (Figure 2.4A+D), consistent with previous reports (94). The same regulatory motif regions that showed increased exchange with Gedatolisib showed much larger changes with AZ2. Importantly, increased exchange was observed at earlier timepoints for AZ2 compared to Gedatolisib (example peptide 976-992 covering the activation

loop and kα7), suggesting that AZ2 leads to a complete disruption of secondary structure, with Gedatolisib likely causing increased secondary structure dynamics (Figure 2.4E).

This shows that multiple PI3K inhibitors can cause large scale allosteric conformational changes upon inhibitor binding, however, deciphering the molecular mechanism of these changes were hindered by lack of high-resolution structural information for many of these compounds.

Structures of PI3Kγ bound to IPI-549, Gedatolisib, and NVS-PI3-4

To further define the molecular basis for how different inhibitors lead to allosteric conformational changes we solved the crystal structure of p110γ bound to IPI-549, Gedatolisib, and NVS-PI3-4 at resolutions of 2.55Å, 2.65Å, and 3.15Å, respectively (Figure 2.5A-C). The inhibitor binding mode for all were unambiguous (Figure 2.5H).

These structures revealed insights into how IPI-549 and NVS-PI3-4 can achieve selectivity for PI3Kγ (Figure 2.5I+J, L+M). All inhibitors formed the critical hydrogen bond with the amide hydrogen of V882 in the hinge region, which is a conserved feature of ATP competitive PI3K kinase inhibitors. NVS-PI3-4 leads to opening of a p110γ unique pocket mediated by a conformational change in K883 (Figure 2.5L). The opening of K883 is accommodated by it rotating into contact with D884 and T955. This opening would not be possible in p110α and p110δ as the corresponding K883 residue (L829 in p110δ and R852 in p110α) would clash with the corresponding T955 residue (R902 in p110δ and K924 in p110α) (Figure 2.5M). IPI-549 binds with a characteristic propeller shape, as seen for multiple p110γ and p110δ selective inhibitors (133). IPI-549 leads to a conformational change in the orientation of M804, which opens the specificity pocket, primarily composed of W812 and M804 (Figure 2.5C). Comparison of IPI-549 bound to p110γ to the selective inhibitor Idelalisib bound to p110δ revealed a potential molecular mechanism for p110γ selectivity. Structure activity analysis of IPI-549 and its derivatives showed a critical role for substitutions at the alkyne position in achieving p110γ specificity (72). The *N*-methylpyrazole group in IPI-549 projects out of the specificity pocket towards the kα1-kα2 loop. This loop is significantly shorter in p110δ, with a potential clash with bulkier alkyne derivatives (Figure 2.5I+J). However, this cannot be the main driver of specificity, as a phenyl substituent of the alkyne had decreased selectivity for p110γ over p110δ, with hydrophilic heterocycles in this position being critical in p110γ selectivity (72). A major difference in this pocket between p110γ and p110δ is K802 in p110γ (T750 in p110δ), with this residue making a pi-stacking interaction with W812. The *N*-methylpyrazole group packs

against K802, with a bulkier group in this position likely to disrupt the pi stacking interaction, explaining the decreased potency for these compounds.

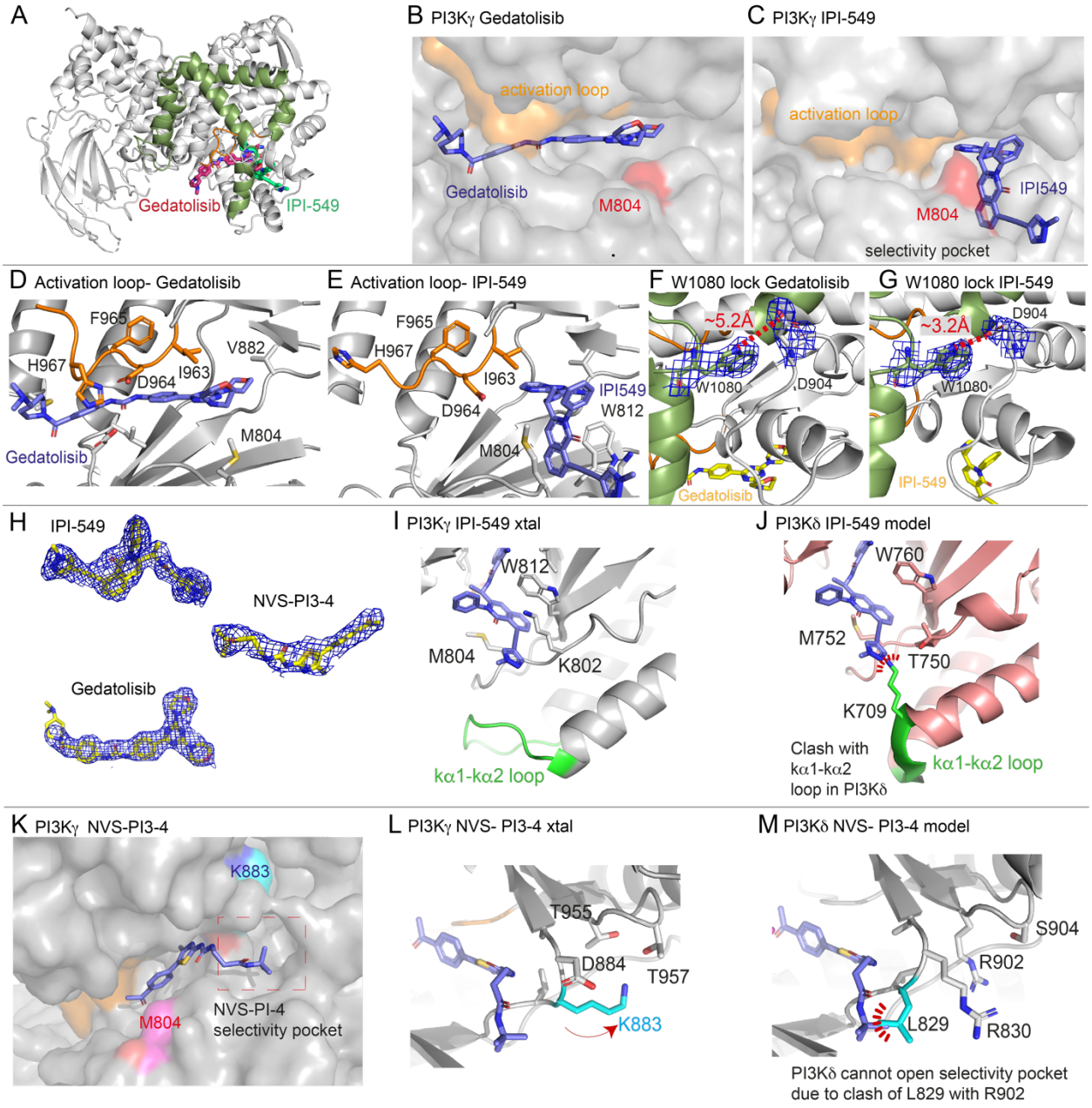

Figure 2.5. Structures of Gedatolisib, IPI-549 and NVS-PI3-4 bound to p110γ (A). Overall structure of Gedatolisib (red) and IPI-549 (green) bound to p110γ. **(B+C).** Comparison of Gedatolisib and IPI-549 bound to p110γ with the activation loop and selectivity pocket highlighted. M804 that changes conformation upon selectivity pocket opening is coloured red. **(D+E).** Comparison of the conformation of the activation loop (orange) of p110γ when Gedatolisib or IPI-549 are bound, with residues in the activation loop labelled, specifically D964 and F965 of the DFG motif labelled. **(F+G).** The Trp lock composed of W0180 is partially disrupted in the Gedatolisib structure compared to the IPI-549 structure. The interaction between W1080 and D904 is shown, with the distance between the two shown on each structure. The electron density from a feature enhanced map (124) around W1080 and D904 in each structure is contoured at 1.5 sigma. **(H).** The electron density from a feature enhanced map around IPI-549, NVS-PI3-4, and

Gedatolisib contoured at 1 sigma. **(I+J).** Molecular basis for IPI-549 specificity for p110γ over p110δ. The structure of p110γ bound to IPI-549 (I) compared to a model of IPI-549 bound to p110δ (**J**), based on the structure of p110δ bound to the specificity pocket inhibitor Idelalisib (PDB: 4XE0) (134). K802 and W812 in p110γ are labelled, along with the corresponding residues in p110δ. The kα1-kα2 loop is green, with potential clashes in p110δ with the methylpyrazole of IPI-549 highlighted. **(K).** NVS-PI3-4 bound to p110γ with the activation loop and selectivity pockets highlighted. M804 and K883 that change conformation are colored in magenta and cyan, respectively. **(L+M).** Molecular basis for NVS-PI3-4 for p110γ over p110α/δ. The structure of p110γ bound to NVS-PI3-4 (L), revealed a conformational change in K883 leading to opening of pocket accommodating the *t*-butyl motif. Comparing this to a model of p110δ (PDB: 5DXU) (135) (M) with NVS-PI3-4 revealed that this pocket is unlikely to open with L829 in p110δ (corresponds to K883 in p110γ) unable to adopt this conformational change due to steric clashes / electrostatic repulsion with R902 in p110δ (corresponds to T955 in p110γ).

One of the most striking differences between the structure of Gedatolisib and IPI-549 bound to p110γ is the conformation of the N-terminus of the activation loop, including the residues that make up the DFG motif (Figure 2.5B). The majority of the activation loop is disordered in PI3Kγ crystal structures, with the last residue being between 967 and 969. Gedatolisib makes extensive contacts with the activation loop, with H967 immediately following the DFG motif in a completely altered conformation. The interaction of the cyclopropyl motif in AZ2 with the activation loop has previously been proposed to be critical in mediating allosteric conformational changes. In addition to the change in the activation loop, there was a minor perturbation of the W1080 lock, with the Gedatolisib structure revealing a disruption of the hydrogen bond between W1080 and D904, with this bond maintained in the IPI-549 structure (Figure 2.5F+G). The C-terminus of the activation loop and kα7 immediately following showed some of the largest changes upon inhibitor binding in HDX experiments. The kα7 helix is directly in contact with W1080, and we postulated that the conformational changes induced in the N-terminus of the activation loop may mediate these changes.

Conformational selective inhibitors show altered specificity towards activating PI3Kγ mutant

We observed that HDX differences occurring in the R1021C mutant were very similar to conformational changes observed for p110γ bound to Gedatolisib. This suggested that both the mutant and Gedatolisib bound forms might be adopting an activated conformation of the regulatory motif. HDX differences were very similar for the region spanning 976-992 in the activation loop (Figure 2.3G, Figure 2.4E). As this region is directly adjacent to the inhibitor binding site, we postulated that there may be altered inhibitor binding for the R1021C mutant. We carried out IC_{50} measurement for wild-type and R1021C p110γ/p101 with both IPI-549 and Gedatolisib (Figure 2.6A). Gedatolisib was roughly three-fold more potent for the R1021C mutant over the wild-type, with no significant difference in IC_{50}

values for IPI-549 compared to wild-type. This provides initial insights into how understanding the dynamics of activating mutations and inhibitors may be useful as a novel strategy towards designing mutant specific inhibitors.

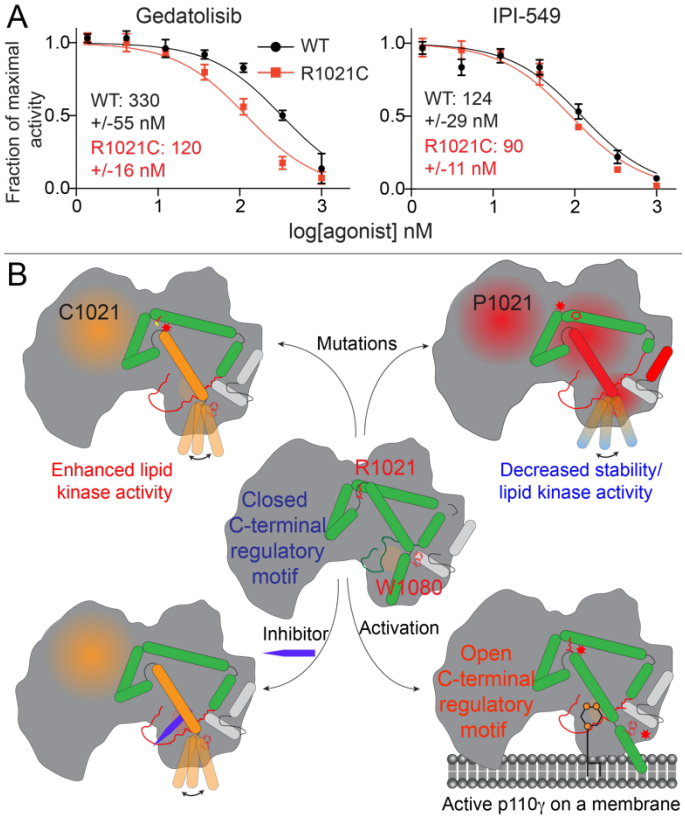

Figure 2.6. Activating mutations show slight differences in inhibition by allosteric inhibitors and model of PI3Kγ regulation. (A). IC_{50} curves for wild-type and R1021C p110γ/p101 complexes. Assays were carried out with 5% C8 PIP_2 / 95% PS vesicles at a final concentration of 1 mg/ml in the presence of 100 μM ATP and 1.5 μM lipidated Gβγ. PI3Kγ concentration was 4 nM for R1021C and 8 nM for WT. Error is shown as standard deviation (n=3). **(B).** Model of conformational changes that occur upon mutation of the C-terminal motif and binding of activation loop interacting conformation selective inhibitors.

2.5 Discussion

Understanding the molecular determinants of how mutations in PI3Ks lead to altered signaling in disease is vital in the design of targeted therapeutic strategies. The PI3Kγ isoform is critical to maintain immune system function, and plays important roles in the regulation of the tumor microenvironment (136,137). Bi-allelic loss of function mutations in p110γ are a driver of human immunodeficiencies, and multiple inactivating mutations located in the C-terminal regulatory motif of the kinase domain have been described (74,107). Initial results linking deletion of PI3Kγ to the development of colon cancer (77) have been disputed (138), and recent studies suggest that tumor growth and

metastasis is attenuated in PI3Kγ deficient mice (56,63) and IPI-549 treated animals (90). Inhibiting PI3Kγ has shown promise as an immunomodulatory agent in generating an anti-tumor immune response. There have also been numerous reports of overexpression and single nucleotide variants in *PIK3CG* linked to cancer development in multiple tissues (54,57–60,60,61). Oncogenic mutations in *PIK3CG* are widely distributed, which is distinct from the oncogenic hotspot mutations seen in the helical and kinase domain of *PIK3CA*. There has been limited analysis of the functional consequences of oncogenic *PIK3CG* mutants, with the R1021 residue in the regulatory motif of the kinase domain being unique, as mutations of this residue exist in both immunodeficiencies and tumors.

Here, we have described the biochemical and biophysical characterisation of both activating and inactivating disease-linked R1021 mutations in the regulatory motif of the p110γ kinase domain. This has revealed that mutation of R1021 can lead to either kinase activation or inactivation. The R1021 in the kα8 helix is conserved across all class I PI3Ks, with it making a number of hydrogen bonds with residues in kα10 and kα11. Both R1021P and R1021C would lead to disruption of the hydrogen bonds with kα10 and kα11, however R1021P would also lead to disruption of the kα8 helix due to the altered dynamics introduced by the proline residue. HDX-MS results were consistent with this hypothesis, with R1021P leading to large scale conformational changes across the entire protein, with the main disruptions occurring in the helical and kinase domain. The R1021P mutation greatly destabilized the protein, with purification yields being >20-fold lower than wild-type, consistent with greatly decreased p110γ and p101 levels in patient T cells (74). Consistent with previous reports, we found greatly decreased lipid kinase activity for R1021P, although the enzyme maintained catalytic ability, as it showed greatly increased basal ATPase activity, which is similar to what occurs upon mutation of the W1080 lock or removal of the kα12 helix (74,94). Overall, this data is consistent with this mutation leading to destabilization of the p110γ protein, leading to both greatly decreased protein levels, and decreased lipid kinase activity.

The R1021C mutation, in contrast, had enhanced lipid kinase activity, both basally, and upon Gβγ activation. HDX-MS suggests that this activation is mediated by a conformational disruption of the inhibitory c-terminal regulatory motif of the kinase domain. Many of these changes in the C-terminal regulatory motif have been previously observed upon membrane binding (86), as well as upon binding to conformational selective inhibitors (94). One of the largest changes in exchange occurred at the C-terminus of the activation loop and the beginning of kα7 which is in contact with the W1080 lock. We propose a model of how mutation of R1021 can lead to either activated or

inactivated lipid kinase activity (Figure 2.6B). The conformation of the C-terminal regulatory motif is critical in regulating lipid kinase activity, where minor perturbations (R1021C) can lead to disruption of multiple inhibitory contacts allowing for reorientation of the kα12 membrane binding helix and increased lipid kinase activity. This suggests that the mutation can pre-organise the enzyme for productive catalysis, either through increased membrane binding, or increased PIP_2 kinase activity. Reinforcing the importance of the R1021 mutant for class I PI3K regulation is the fact that mutation of the equivalent R992 in *PIK3CA* to either Leu or Asn has been found in tumor samples (106).

This work corroborates the important role of the C-terminal regulatory motif in controlling PI3K lipid kinase activity. The orientation of this motif is critical in the regulation of all class I PI3Ks, although this is regulated by different molecular mechanisms in p110α, p110β, p110δ, and p110γ. The class IA PI3Ks require p85 regulatory subunits to stabilize the C-terminal regulatory motif, with the nSH2 of p85 interacting with and stabilizing kα10 for all class IA PI3Ks (129,139), and the cSH2 of p85 stabilizing kα7, kα8, kα11 and kα12 for p110β and p110δ (110,127). The p110γ isoform is unique in that its C-terminal motif adopts an inhibited conformation in the absence of regulatory proteins. The C-terminal regulatory motif of p110γ can be post-translationally modified by phosphorylation of kα9 (T1024) by protein kinase A decreasing lipid kinase activity (140), while protein kinase C phosphorylates an adjacent area in the helical domain (S582) (141) increasing lipid kinase activity.

Extensive work has been carried out toward the development of allosteric inhibitors of PI3Ks. While no allosteric inhibitors that bind out of the ATP binding pocket have been developed, fragment screens have revealed potential druggable pockets that may be targeted in class IA PI3Ks (142). It has previously been noted that PI3Kγ can be selectively targeted through a conformationally selective inhibitor, AZ2 (94). This was mediated through a cyclopropyl moiety on AZ2, which putatively alters the orientation of the activation loop, leading to disruption of the inhibitory conformation of the C-terminal regulatory motif. Many of the changes observed for this inhibitor were similar to those seen in the R1021C mutant. To interrogate if allosteric conformational changes were unique to cyclopropyl containing compounds, we screened a panel of pan-PI3K and PI3Kγ selective inhibitors using HDX-MS. The compounds PIK90, IPI549, and AS-604850 only caused decreased exchange at the active site. Comparison of the crystal structures of these compounds (66,121) revealed similar conformations of the activation loop, with limited interaction between the inhibitors and the activation loop. After this study was submitted for publication, the structure of IPI-549 was released by Arcus Biosciences (143) with a conserved binding mode to the model proposed here.

The AZ2 compound containing the cyclopropyl moiety, led to large scale conformational changes consistent with previous results (94). Intriguingly, the non-specific inhibitors, Gedatolisib and Omipalisib, caused increased exchange in many of the same regions that showed enhanced exchange with the R1021C mutant. Comparison of the crystal structures of these inhibitors revealed more extensive interactions with the activation loop and significant conformational rearrangement of the activation loop. Distinct from the AZ2 compound, neither Gedatolisib and Omipalisib show specificity for PI3Kγ over class IA PI3Ks (131,132). Similar HDX-MS differences were observed for both the R1021C mutant and wild type bound to Gedatolisib. Gedatolisib showed increased potency versus R1021C over wild type PI3Kγ, with a ~3-fold decrease in IC_{50} values. Altogether, this suggests that R1021C induces a conformation similar to the wild type enzyme bound to Gedatolisib. This provides an intriguing approach for designing oncogenic PI3K specific inhibitors through further optimisation of the ATP competitive inhibitor moieties in the activation loop binding region.

Overall, this work provides novel insights into how the C-terminal regulatory motif of PI3Kγ regulates lipid kinase activity, how oncogenic and immunodeficiency mutations can disrupt this regulation, and how one can exploit these conformational changes to develop isoform and mutant selective small molecule inhibitors. Further exploration of the dynamic regulation of the C-terminal regulatory motif of PI3Ks by mutations and inhibitors may reveal unique approaches to develop therapeutics for PI3K related human diseases.

Chapter 3: Nanobodies as tools for biochemical and structural studies on PI3Kγ complexes

Adapted from:

Rathinaswamy, M.K.*, Fleming, K.D.*, Dalwadi, U., Pardon, E., Harris, N.J., Yip, C.K., Steyaert, J., and Burke, J.E. (2021). HDX-MS optimized approach to characterize nanobodies as tools for biochemical and structural studies of class IB phosphoinositide 3-kinases. (2021) Structure (In Press).

* indicates equal contribution

Contributions:

The data presented in this chapter was a collaborative effort between the Burke lab, Yip lab (University of British Columbia) and the Steyaert lab (Vlaams Instituut voor Biotechnologie). **Myself**: Cloning, expression and purification of all proteins, nanobody characterization, HDX-MS and kinase assay development. **Dr. Els Pardon (Steyaert Lab)**: Immunization and generation of nanobody plasmids. **Kaelin Fleming**: Kinase assays and assistance with HDX-MS. **Noah Harris**: Assistance with nanobody characterization. **Udit Dalwadi (Yip Lab)**: EM experiments with proteins generated by me.

3.1 Abstract

There is considerable interest in developing antibodies as modulators of signaling pathways. One of the most important signaling pathways in higher eukaryotes is the phosphoinositide 3-kinase (PI3K) pathway, which plays fundamental roles in growth, metabolism and immunity. The class IB PI3K, PI3Kγ, is a heterodimeric complex composed of a catalytic p110γ subunit bound to a p101 or p84 regulatory subunit. PI3Kγ is a critical component in multiple immune signaling processes and is dependent on activation by Ras and GPCRs to mediate its cellular roles. Here we describe the rapid and efficient characterization of multiple PI3Kγ single chain camelid nanobodies using hydrogen deuterium exchange mass spectrometry (HDX-MS) for structural and biochemical studies. This allowed us to identify nanobodies that stimulated lipid kinase activity, blocked Ras activation and specifically inhibited p101-mediated GPCR activation. Overall, this reveals novel insight into PI3Kγ regulation and identifies sites that may be exploited for therapeutic development.

3.2 Introduction

Class I Phosphoinositide-3-Kinases (PI3Ks) are important lipid signaling proteins which are frequently mis-regulated in human disease (136). These enzymes produce phosphatidylinositol-3,4,5-trisphosphate at the plasma membrane, which recruits numerous downstream effectors that control growth, survival, metabolism and immunity (144). All class I PI3Ks are hetero-dimeric complexes composed of a p110 catalytic subunit bound to a regulatory subunit. The regulatory subunits are crucial in the activation of class I PI3Ks downstream of membrane localized signaling molecules including receptor tyrosine kinases (RTKs), G-protein coupled receptors (GPCRs) and the Ras family of small GTPases (145). The class IB PI3Ks are composed of a single catalytic subunit (p110γ) bound to one of two regulatory subunits, p101 or p84 (also called p87). Both PI3Kγ complexes have important roles in immune cell migration, cytokine production and cardiac function (146) and are therapeutic targets in cancer immunotherapy (63,90) and inflammation (66). The regulatory subunits mediate activation of p110γ, with either p101 or p84 needed for activation by Gβγ, derived from GPCRs (85,147). The p101 subunit is unique as it has a direct binding site for Gβγ (148), while p84 merely potentiates Gβγ binding to p110γ. Both complexes of p110γ are activated by Ras (84), which is mediated by the Ras binding domain (RBD) of p110γ (93).

These differences in regulation translate into distinct cellular functions with p110γ/p101 controlling immune cell migration while p110γ/p84 controls mast cell degranulation and production of reactive oxides from neutrophils (83,92). A full understanding of how PI3Kγ is regulated has been hampered by lack of molecular details on complex assembly, and activation by GPCRs. In addition, due to the severe side effects of pan-PI3K ATP-competitive inhibitors, targeting specific PI3Kγ complexes could be useful for therapeutic approaches in cancer and inflammatory diseases. The development of potent and specific biomolecules that modulate PI3Kγ activity will be useful for structural, biochemical and cellular studies of PI3K regulation.

One of the most powerful biomolecules for optimizing structural studies and modulating signaling pathways are single chain antibodies from camelids, known as nanobodies (149). Nanobodies are the variable domains of the heavy-chain only camelid antibodies (V_{HH}), and lack hydrophobic residues that would normally pack against the light chain (V_L) in conventional antibodies. As a result, nanobodies can be expressed in high yield in multiple expression systems (150). Nanobodies have an enlarged antigen binding surface with a longer CDR3 loop, which normally packs

against the V_L in conventional dual chain antibodies (151). This coupled with their small size (~15 kDa versus 150 kDa for conventional antibodies) provide nanobodies the potential to bind specifically to epitopes that are inaccessible for conventional antibodies, with high affinity. These advantages have resulted in their widespread use in research, testing and therapy (152).

Nanobodies have proven to be exceptional tools for optimizing structural biology approaches of protein assemblies. In X-ray crystallography, they can stabilize flexible protein regions, prevent aggregation/oligomerization, and offer novel crystal contact sites (153–156). Nanobodies are powerful tools to lock protein complexes into specific, functionally-relevant conformational states. For example, nanobodies have provided insight into active/inactive states of receptors or different stages in the transport cycle of membrane channels and pumps (157–160). They have played an important role in understanding PI3K biology, as a specific nanobody was crucial in the crystallization of the 385 kDa class III PI3K complex (161). In addition to crystallography, they have been useful in electron microscopy to assist structural characterization and in the labelling of protein subunits in large complexes (162–164).

In addition to their utilization in structural biology, nanobodies can be used to dissect and target signaling events in cells and organisms (165,166). They are a potent tool to interfere with protein-protein interactions *in vivo,* which has potential applications in multiple human diseases. This is highlighted by their utilization as neutralizing agents in betacoronavirus infection, including SARS CoV-1/2 and MERS CoV, through blocking the interaction of the viral spike protein with ACE2 (167,168). Nanobodies have been particularly powerful in modulating the signaling inputs and outputs of GPCRs (169,170). Conformationally selective nanobodies that bind to GPCRs can modulate agonist binding, receptor phosphorylation, and the recruitment of downstream partners including both G-proteins and β-arrestin (171–173). GPCR activation of G-protein signaling stimulates the dissociation of the heterotrimeric G protein into Gα-GTP and a Gβγ dimer, and nanobodies targeting the effector binding surface of Gβγ inhibit Gβγ signaling (174). Development of nanobodies that disrupt specific inputs from GPCRs and other membrane receptors into distinct signaling pathways will be powerful in dissecting the molecular mechanisms of signaling and in developing novel therapeutics. Critical to determining the usefulness of nanobodies as structural chaperones and signaling modulators is the ability to rapidly determine their binding sites and how they might alter protein conformational dynamics.

Here we report the characterization of multiple PI3Kγ binding nanobodies, and describe their application for both structural biology approaches and modulation/inhibition of the activation and kinase activity of PI3Kγ. We

utilized hydrogen deuterium exchange mass spectrometry (HDX-MS) to rapidly identify binding epitopes in p110γ, p101, and p84. This allowed us to identify and characterize p110γ binding nanobodies that activate lipid kinase activity, block activation by Ras, and a p101 binding nanobody that disrupts GPCR activation. Identified nanobodies were also capable of stabilizing flexible regions/domains, allowing for high resolution cryo electron microscopy (cryo-EM) studies (details described in chapter 4). Overall, this work provides an HDX-MS enabled flow-path for the rapid characterization of nanobodies for structural and biochemical studies (Figure 3.1).

3.3 Materials and Methods

Virus Generation and Amplification:

PI3Kγ complexes were expressed from a MutliBac plasmid with a 10X histidine tag, a 2×-strep tag and a Tobacco Etch Virus protease cleavage site on the N-terminus of the regulatory subunits. The plasmids encoding genes for insect cell expression were transformed into DH10MultiBac cells (MultiBac, Geneva Biotech) containing the baculovirus viral genome (bacmid) and a helper plasmid expressing transposase to transpose the expression cassette harbouring the gene of interest into the baculovirus genome. Bacmids with successful incorporation of the expression cassette into the bacmid were identified by blue-white screening and were purified from a single white colony using a standard isopropanol-ethanol extraction method. Briefly, colonies were grown overnight (16 hours) in 3-5 mL 2×YT (BioBasic #SD7019). Cells were pelleted by centrifugation and the pellet was resuspended in 300 µL P1 Buffer (50 mM Tris-HCl, pH 8.0, 10 mM EDTA, 100 mg/mL RNase A), chemically lysed by the addition of 300 µL Buffer P2 (1% sodium dodecyl sulfate (SDS) (w/v), 200 mM NaOH), and the lysis reaction was neutralized by addition of 400 µL Buffer N3 (3.0 M potassium acetate, pH 5.5). Following centrifugation at 21130 RCF and 4 ºC (Rotor #5424 R), the supernatant was separated and mixed with 800 mL isopropanol to precipitate the DNA out of solution. Further centrifugation at the same temperature and speed pelleted the Bacmid DNA, which was then washed with 500 µL 70% Ethanol three times. The bacmid DNA pellet was then dried for 1 minute and re-suspended in 50 mL Buffer EB (10 mM Tris-Cl, pH 8.5; All buffers from QIAprep Spin Miniprep Kit, Qiagen #27104). Purified bacmid was then transfected into Sf9 cells. 2 mL of Sf9 cells between 0.3-0.5X10^6 cells/mL were aliquoted into the wells of a 6-well plate and allowed to attach, creating a monolayer of cells at ~70-80% confluency. Transfection reactions were prepared by the addition of 2-10 ug of bacmid DNA to 100 µL 1xPBS and 12 mL polyethyleneimine (PEI) at 1 mg/mL (Polyethyleneimine ‘‘Max’’ MW 40.000, Polysciences #24765, USA) to 100 µL 1xPBS. The bacmid-PBS and the

PEI-PBS solutions were mixed together, and the reaction occurred for 20-30 minutes before addition drop-by-drop to an Sf9 monolayer containing well. Transfections were allowed to proceed for 5-7 days before harvesting virus containing supernatant as a P1 viral stock.

Purification of PI3Kγ complexes

PI3Kγ catalytic and regulatory subunits were co-expressed in Spodoptera frugiperda (Sf9) cells using the baculovirus expression system. After 55 hours, the cells were harvested and the pellets were resuspended in lysis buffer (20 mM Tris pH 8.0, 100 mM NaCl, 10 mM imidazole pH 8.0, 2 mM beta-mercaptoethanol (βME), 5% (v/v) glycerol, Protease Inhibitor Cocktail (Millipore Protease Inhibitor Cocktail Set III, Animal-Free)) on ice. The resuspended pellets were sonicated for 2.5 minutes at level 4.0 with cycles consisting of 15 seconds ON/OFF using the Misonix Sonicator 3000. Triton X-100 was added to the cell lysate at a final concentration of 0.1% (v/v), and the lysates were centrifuged at 14,000 rpm at 4℃ for 45 minutes in a JA-20 rotor. The supernatant was loaded onto a HisTrap™ FF column (GE Healthcare Life Sciences) equilibrated with NiNTA A buffer (20 mM Tris pH 8.0, 100 mM NaCl, 10 mM imidazole pH 8.0, 5% (v/v) glycerol) and a high salt wash was performed using NiNTA A High Salt Buffer (20 mM Tris pH 8.0, 1 M NaCl, 10 mM imidazole pH 8.0, 5% (v/v) glycerol, 2mM βME). The protein was washed on an AKTA Start FPLC (GE) system with 4 column volumes (CV) of NiNTA A, 4 CV of 94% NiNTA A/6% NiNTA B (20 mM Tris pH 8.0, 100 mM NaCl, 200 mM imidazole pH 8.0, 2 mM βME, 5% (v/v) glycerol), and eluted in 2 CV of NiNTA B buffer. The eluted protein was loaded onto a StrepTrap™ column (GE) equilibrated with gel filtration buffer (GFB) (20 mM Tris pH 8.5, 100 mM NaCl, 50 mM (NH4)2SO4, 0.5 mM Tris (2-carboxyethyl) phosphine (TCEP)). For pulldowns, the column was washed with 2 CV GFB and the tagged protein was eluted in 2 CV GFB containing 2.5 mM Desthiobiotin. For studies using untagged protein, the washed column was incubated on ice overnight with 100 uL Tobacco Etch Virus Protease (1 mg/mL) diluted in GFB and eluted the following day. The protein was concentrated in an Amicon 50K Concentrator (Millipore Sigma). Gel filtration chromatography was performed on an AKTA Pure (GE) using a Superdex™ 200 10/300 Increase column (GE) equilibrated in GFB. The fractions containing the protein were pooled and concentrated, flash frozen in liquid nitrogen, and stored at -80℃. All purification steps were analyzed using SDS-PAGE.

Nanobody generation and small scale nanobody purification.

Nanobody discovery was carried out as previously described by the Steyaert lab at the VIB-VUB Center for Structural Biology (170). Briefly, one llama was immunized 6 times with in total 900µg of p110γ/p101, another llama was immunized 6 times with in total 830µg of p110γ/p84 complex. Four days after the final boosts, peripheral blood lymphocytes were collected from both animals and RNA was extracted and used for creating cDNA encoding the ORFs of nanobodies. After PCR amplification, each library of Nanobody ORFs was cloned in the pMESy4 phage display vector (GenBank KF415192) creating 2 phage display libraries. Nanobodies were obtained after phage display selection on either p110γ/p101 or p110γ/p84 complex. In total, 88 nanobodies were identified and classified into 49 families according to CDR3 sequence similarity. Nanobodies were expressed from pMYESy4 vectors in the periplasms of Escherichia coli WK6 cells. For pulldowns and HDX-MS, 5 mL cultures were grown to OD600 of 0.7 in Terrific Broth containing 0.1% glucose and 2mM $MgCl_2$ in the presence of 100 µg/mL ampicillin and was induced with 0.5 mM isopropyl-β-D-thiogalactoside (IPTG). For assays and EM studies, nanobodies were expressed in 1L cultures. Cells were harvested the following day by centrifuging at 2500 RCF (Eppendorf Centrifuge 5810 R) and the pellet was snap-frozen in liquid nitrogen. Nanobodies were isolated from these pellets by osmotic shock. Cell pellets were resuspended TES buffer (3 mL for pellets from 5mL cultures or 15 mL for pellets from 1L cultures) (0.2 M Tris pH 8.0, 0.5 mM ethylenediaminetetraacetic acid (EDTA), 0.5 M sucrose) with Protease Inhibitor Cocktail Set III and rotated for 45 minutes at 4℃. Twice the volume of TES/4 buffer was added to the cells and rotated for 30 minutes at 4℃, followed by centrifugation at 14,000 rpm for 30 minutes at 4℃ in a JA-20 rotor. The periplasmic extract was loaded onto a HisTrap™ HP column (GE) equilibrated with NiNTA buffer (1X PBS pH 7.4, 1 M NaCl), followed by a wash with 5 CV NiNTA A wash buffer (1X PBS pH 7.4, 15 mM imidazole, 1 M NaCl). The protein was eluted with 2 CV of NiNTA B buffer (1X PBS pH 7.4, 200 mM imidazole, 1 M NaCl). The protein elution was exchanged into PI3K GFB with a 5 mL HiTrap™ Desalting column (GE). The success of purification was determined by SDS-PAGE.

Purification of lipidated Gβγ:

Full length, lipidated human Gβγ ($G\beta_1\gamma_2$) was expressed in Sf9 insect cells and purified as described previously (117) . After 65 hours of expression, cells were harvested and the pellets were frozen as described above. Pellets were resuspended in lysis buffer (20 mM HEPES pH 7.7, 100 mM NaCl, 10 mM βME, protease inhibitor

(Protease Inhibitor Cocktail Set III, Sigma)) and sonicated for 2 minutes (15s on, 15s off, level 4.0, Misonix sonicator 3000). The lysate was spun at 500 RCF (Eppendorf Centrifuge 5810 R) to remove intact cells and the supernatant was centrifuged again at 25,000 g for 1 hour (Beckman Coulter JA-20 rotor). The pellet was resuspended in lysis buffer and sodium cholate was added to a final concentration of 1% and stirred at 4ºC for 1 hour. The membrane extract was clarified by spinning at 10,000 g for 30 minutes (Beckman Coulter JA-20 rotor). The supernatant was diluted 3 times with NiNTA A buffer (20 mM HEPES pH 7.7, 100 mM NaCl, 10 mM Imidazole, 0.1% $C_{12}E_{10}$, 10mM βME) and loaded onto a 5 mL HisTrap™ FF crude column (GE Healthcare) equilibrated in the same buffer. The column was washed with NiNTA A, 6% NiNTA B buffer (20 mM HEPES pH 7.7, 25 mM NaCl, 250 mM imidazole pH 8.0, 0.1% C12E10, 10 mM βME) and the protein was eluted with 100% NiNTA B. The eluent was loaded onto HiTrap™ Q HP anion exchange column equilibrated in Hep A buffer (20 mM Tris pH 8.0, 8 mM CHAPS, 2 mM Dithiothreitol (DTT)). A gradient was started with Hep B buffer (20 mM Tris pH 8.0, 500 mM NaCl, 8 mM CHAPS, 2 mM DTT) and the protein was eluted in ~50% Hep B buffer. The eluent was concentrated in a 30,000 MWCO Amicon Concentrator (Millipore) to < 1 mL and injected onto a Superdex™ 75 10/300 GL size exclusion column (GE Healthcare) equilibrated in Gel Filtration buffer (20 mM HEPES pH 7.7, 100 mM NaCl, 10 mM CHAPS, 2 mM TCEP). Fractions containing protein were pooled, concentrated, aliquoted, frozen and stored at -80ºC.

Expression Purification of Lipidated HRas G12V

Full-length HRas G12V was expressed by infecting 500 mL of Sf9 cells with 5 mL of baculovirus. Cells were harvested after 55 hours of infection and frozen as described above. The frozen cell pellet was resuspended in lysis buffer (50 mM HEPES pH 7.5, 100 mM NaCl, 10 mM βME and protease inhibitor (Protease Inhibitor Cocktail Set III, Sigma)) and sonicated on ice for 1 minute 30 seconds (15s ON, 15s OFF, power level 4.0) on the Misonix sonicator 3000. Triton-X 114 was added to the lysate to a final concentration of 1%, mixed for 10 minutes at 4°C and centrifuged at 25,000 rpm for 45 minutes (Beckman Ti-45 rotor). The supernatant was warmed to 37°C for few minutes until it turned cloudy following which it was centrifuged at 11,000 rpm at room temperature for 10 minutes (Beckman JA-20 rotor) to separate the soluble and detergent-enriched phases. The soluble phase was removed, and Triton-X 114 was added to the detergent-enriched phase to a final concentration of 1%. This phase separation was performed for a total of 3 times. Imidazole pH 8.0 was added to the detergent phase to a final concentration of 15 mM and the mixture was incubated with Ni-NTA agarose beads (Qiagen) for 1 hour at 4°C. The beads were washed with

5 column volumes of Ras-NiNTA buffer A (20mM Tris pH 8.0, 100mM NaCl, 15mM imidazole pH 8.0, 10mM βME and 0.5% Sodium Cholate) and the protein was eluted with 2 column volumes of Ras-NiNTA buffer B (20mM Tris pH 8.0, 100mM NaCl, 250mM imidazole pH 8.0, 10mM βME and 0.5% Sodium Cholate). The protein was buffer exchanged to Ras-NiNTA buffer A using a 10,000 kDa MWCO Amicon concentrator, where protein was concentrated to ~1mL and topped up to 15 mL with Ras-NiNTA buffer A and this was repeated a total of 3 times. GTPγS was added in 2-fold molar excess relative to HRas along with 25 mM EDTA. After incubating for an hour at room temperature, the protein was buffer exchanged with phosphatase buffer (32 mM Tris pH 8.0, 200 mM Ammonium Sulphate, 0.1 mM $ZnCl_2$, 10 mM βME and 0.5% Sodium Cholate). 1 unit of immobilized calf alkaline phosphatase (Sigma) was added per milligram of HRas along with 2-fold excess nucleotide and the mixture was incubated for 1 hour on ice. $MgCl_2$ was added to a final concentration of 30 mM to lock the bound nucleotide. The immobilized phosphatase was removed using a 0.22-micron spin filter (EMD Millipore). The protein was concentrated to less than 1 mL and was injected onto a Superdex^{TM} 75 10/300 GL size exclusion column (GE Healthcare) equilibrated in gel filtration buffer (20 mM HEPES pH 7.7, 100 mM NaCl, 10 mM CHAPS, 1 mM $MgCl_2$ and 2 mM TCEP). The protein was concentrated to 1 mg/mL using a 10,000 kDa MWCO Amicon concentrator, aliquoted, snap-frozen in liquid nitrogen and stored at -80°C.

Streptavidin Pulldown assays

To confirm binding, purified nanobodies at 3μM final concentration were mixed with tagged p110γ-p84 at 2μM final concentration in PI3K GFB and incubated for 15 minutes on ice. To this mixture, streptavidin beads (GE Healthcare) equilibrated in GFB was added and incubated again for 15 minutes. The beads were spun down at 500 g (Eppendorf centrifuge 5424 R) and the supernatant was removed. The beads were then washed for a total of three times in GFB. Following the final wash, the beads were spun down, the supernatant was removed and the proteins were eluted in GFB containing 2.5 mM desthiobiotin. The beads were spun down again following which the supernatant was mixed with loading dye and run on a 4-12% Nu-PAGE gel (Invitrogen: NP0321BOX). Binders to both p110γ and p84 were identified by the presence of bands corresponding to the nanobodies (~15 kDa). Pull down assays were performed again on all nanobodies with tagged p110γ-p101 to identify binders to p101.

Differential Scanning Fluorimetry

Differential scanning fluorimetry was performed using the Applied Biosystems StepOnePlus™ RT-PCR instrument (ThermoFisher Scientific, cat. 4376600) with the excitation and emission wavelengths set to 587 and 607 nm, respectively. Briefly, p110γ-p101/ p110γ-p84 at a concentration of ~1 μM was dispensed into a 96-well plate and mixed with ~2 μM nanobody in PI3K GFB. SYPRO orange (Invitrogen) was diluted to 2.5x concentration, from a 5,000x stock. For thermal stability measurements, the temperature scan rate was fixed at 0.5 °C/min and the temperature range spanned 20 °C to 95 °C. Data analysis was performed using Protein Thermal Shift Software v1.4 (ThermoFisher Scientific, cat. 4466038), which determined melting temperatures (T_ms) of individual replicates by fitting fluorescence data to a two-state Boltzman model.

Hydrogen-Deuterium Exchange Mass Spectrometry (HDX-MS)

Preliminary HDX with p110γ-p101, and p110γ-p84 with nanobodies.

HDX was performed by pre-incubating either p110γ-p101 or p110γ-p84 and 2-fold excess of nanobody for 2 minutes. After equilibration H/D exchange was carried out by dilution into a D2O buffer for either 3 or 300 seconds at 18℃ in a 50 ul reaction volume. The final total amount of PI3Kγ (with either p101 or p84) and nanobody were 20 pmol and 30 pmol, respectively. D2O buffer (20 mM HEPES pH 7.5, 100 mM NaCl, 96% D2O) was added to the protein samples to initiate hydrogen-deuterium exchange (final 84.5% D2O) and the reaction was quenched with an acidic quench solution (0.6 M guanidine-HCl, 0.9% formic acid final). The samples were immediately frozen in liquid nitrogen at -80˚C.

Protein digestion and MS/MS data collection

Protein samples were rapidly thawed and injected onto an integrated fluidics system containing a HDx-3 PAL liquid handling robot and climate-controlled chromatography system (LEAP Technologies), a Dionex Ultimate 3000 UHPLC system, as well as an Impact HD QTOF Mass spectrometer (Bruker). The protein was run over either one (at 10°C) or two (at 10°C and 2°C) immobilized pepsin columns (Applied Biosystems; Poroszyme Immobilized Pepsin Cartridge, 2.1 mm x 30 mm; Thermo-Fisher 2-3131-00; Trajan; ProDx protease column, 2.1 mm x 30 mm PDX.PP01-F32) at 200 mL/min for 3 minutes. The resulting peptides were collected and desalted on a C18 trap column (Acquity

UPLC BEH C18 1.7mm column (2.1 x 5 mm); Waters 186003975). The trap was subsequently eluted in line with a C18 reverse-phase separation column (Acquity 1.7 mm particle, 100 x 1 mm^2 C18 UPLC column, Waters 186002352), using a gradient of 3-35% B (Buffer A 0.1% formic acid; Buffer B 100% acetonitrile) over 11 minutes immediately followed by a gradient of 35-80% over 5 minutes. Mass spectrometry experiments acquired over a mass range from 150 to 2200 *m/z* using an electrospray ionization source operated at a temperature of 200C and a spray voltage of 4.5 kV.

Peptide identification

Peptides were identified from the non-deuterated samples of p110γ alone or p110γ complexed with p101 or p84 using data-dependent acquisition following tandem MS/MS experiments (0.5 s precursor scan from 150-2000 *m/z*; twelve 0.25 s fragment scans from 150-2000 *m/z*). MS/MS datasets were analyzed using PEAKS7 (PEAKS), and peptide identification was carried out by using a false discovery based approach, with a threshold set to 1% using a database of of known contaminants found in Sf9 cells (175). The search parameters were set with a precursor tolerance of 20 ppm, fragment mass error 0.02 Da, charge states from 1-8, leading to a selection criterion of peptides that had a -10logP score of 21.7.

Mass Analysis of Peptide Centroids and Measurement of Deuterium Incorporation

HD-Examiner Software (Sierra Analytics) was used to automatically calculate the level of deuterium incorporation into each peptide. All peptides were manually inspected for correct charge state, correct retention time, appropriate selection of isotopic distribution, etc. Deuteration levels were calculated using the centroid of the experimental isotope clusters. Results are presented as relative levels of deuterium incorporation, with the only correction being applied correcting for the deuterium oxide percentage of the buffer utilized in the exchange (84.5% and 86.8%). Differences in exchange in a peptide were considered significant if they met all two of the following criteria: ≥5% change in exchange and ≥0.4 Da difference in exchange. The raw HDX data are shown in two different formats. To allow for visualization of differences across all peptides, we utilized number of deuteron difference (#D) plots (Figure 3.2B). These plots show the total difference in deuterium incorporation over the entire H/D exchange time course, with each point indicating a single peptide. Samples were only compared within a single experiment and were never compared to experiments completed at a different time with a different final D_2O level. The mass

spectrometry proteomics data have been deposited to the ProteomeXchange Consortium via the PRIDE partner repository (118) with the dataset identifier PXD025207.

Lipid vesicle preparation

For kinase assays, lipid vesicles containing 5% brain phosphatidylinositol 4,5- bisphosphate (PIP_2), 20% brain phosphatidylserine (PS), 35% egg-yolk phosphatidylethanolamine (PE), 10% egg-yolk phosphatidylcholine (PC), 25% cholesterol and 5% egg-yolk sphingomyelin (SM) were prepared by mixing the lipids dissolved in organic solvent. The solvent was evaporated in a stream of argon following which the lipid film was desiccated in a vacuum for 45 minutes. The lipids were resuspended in lipid buffer (20 mM HEPES pH 7.0, 100 mM NaCl and 10 % glycerol) and the solution was sonicated for 15 minutes. The vesicles were subjected to five freeze thaw cycles and extruded 11 times through a 100-nm filter (T&T Scientific: TT-002-0010). The extruded vesicles were sonicated again for 5 minutes, aliquoted and stored at -80°C.

In vitro lipid kinase assays

All lipid kinase activity assays employed the Transcreener ADP2 Fluorescence Intensity (FI) Assay (Bellbrook labs) which measures ADP production. For assays with nanobodies, PM-mimic vesicles (5% PIP_2, 20% PS, 10% PC, 35% PE, 25% cholesterol, 5% SM) were used at a final concentration of 1 mg/mL, with ATP at a final concentration of 100 μM ATP and Gβγ/HRas at 1.5 μM final concentration were used. The protein solution at 2× final concentration was mixed with nanobody at 2× final concentration in a black 385 well microplate (Corning). 2 μL of the protein-nanobody solution was mixed with 2 μL substrate solution containing ATP, vesicles and Gβγ/HRas or Gβγ/HRas gel filtration buffer and the reaction was allowed to proceed for 60 minutes at 20°C. Final concentration of kinase was 1200-3500nM for all basal conditions with or without nanobody. For conditions with Gβγ (with or without nanobody), p110γ-p84: 400-1500 nM and p110γ-p101: 25-750 nM. For conditions with Ras (with or without nanobody), p110γ-p84: 1000-3000 nM and p110γ-p101: 750-3000 nM. For conditions with Gβγ and Ras (with or without nanobody), p110γ-p84: 120-3000 nM and p110γ-p101: 5-3000 nM. The final nanobody concentration was 6 μM. The reaction was stopped with 4 μL of 2× stop and detect solution containing Stop and Detect buffer, 8 nM ADP Alexa Fluor 594 Tracer and 93.7 μg/mL ADP2 Antibody IRDye QC-1 and incubated for 50 minutes. The fluorescence intensity was measured using a SpectraMax M5 plate reader at excitation 590 nm and emission 620 nm. This data was

normalized was normalized against the measurements obtained for 100 μM ATP and 100 μM ADP. The % ATP turnover was interpolated from a standard curve (0.1-100 μM ADP). This was then used to calculate the specific activity of the enzyme.

3.4 Results

Characterization and identification of a panel of PI3Kγ nanobodies

Llamas were immunized with either the p110γ/p101 or p110γ/p84 complex and putative binders were identified using phage display from the B-cells as previously described (170)(Figure 3.1A). We identified 88 potential binders, which were classified according to the sequence of the third complementarity determining region (CDR3), into 49 families. Representative nanobodies from all families were recombinantly expressed in WK6 *E.coli* cells and purified using Nickel affinity chromatography. Members of four families could not be expressed, leading to 45 purified nanobodies. Streptavidin pulldown assays were performed using strep-tagged p110γ/p101 and p110γ/p84 complexes with the purified nanobodies to determine binding. To identify nanobodies that bound to p110γ, p101, or p84 we carried out pull downs on both p110γ/p101 and p110γ/p84. Nanobodies that bound both complexes were assumed to bind p110γ, while ones that bound specifically to either p110γ/p101 or p110γ/p84 were assumed to be p101 or p84 binders. Twenty-six nanobodies were identified as positive hits, of which twenty-two bound to p110γ, three bound to p101, and one to p84 (Figure 3.1B, Appendix F). We used differential scanning fluorimetry (DSF) with nanobodies bound to PI3Kγ to identify possible stabilizing effects. DSF measures the unfolding of proteins as a function of temperature, which allows for the identification of stabilizing binding partners by observing increases in the melting temperature (T_m) (Figure 3.1C). Fifteen nanobodies showed higher T_m values, including eight nanobodies which induced differences of 0.5°C or greater, indicating significant stabilizing effects (Appendix F).

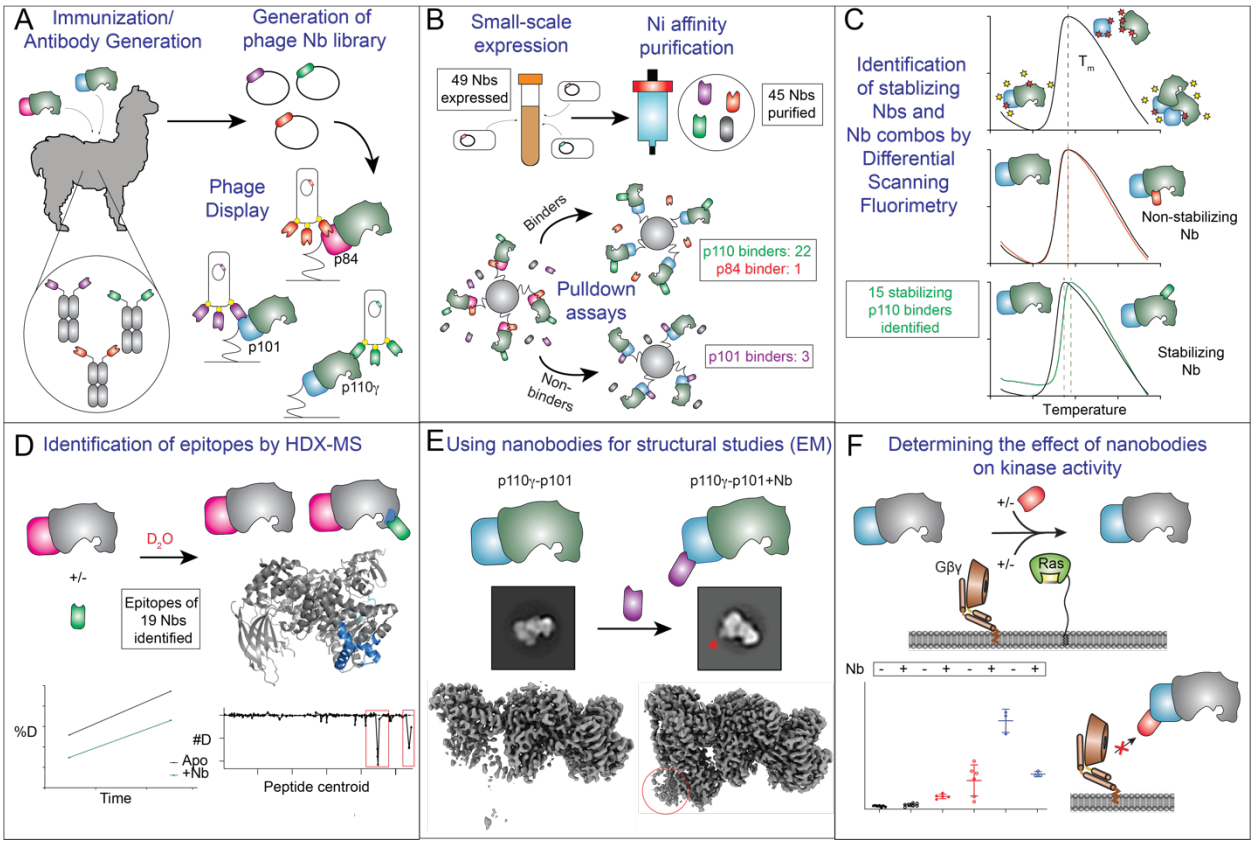

Figure 3.1. Schematic describing the flow-path for characterizing nanobodies that bind PI3Kγ as tools for structural and biochemical analysis. (A) Isolation of nanobodies through immunization with PI3Kγ complexes, p110γ-p101 and p110γ-p84 and nanobody selection by phage display. **(B)** Small scale expression and purification of nanobodies for pulldown assays to select for binders to p110γ, p101 and p84. **(C)** Differential scanning fluorimetry (DSF) to obtain nanobodies with stabilizing effects. **(D)** Identification of nanobody epitopes on p110γ, p101 and p84 by hydrogen-deuterium exchange mass spectrometry (HDX-MS). **(E)** Utilizing nanobodies in electron microscopy to label PI3Kγ subunits and to facilitate high resolution structural studies. **(F)** Utilizing nanobodies as tools to modulate PI3Kγ regulation in kinase activity assays.

HDX-MS enabled identification of nanobody binding epitopes

The p110γ/p101 and p110γ/p84 complexes were subjected to hydrogen deuterium exchange mass spectrometry (HDX-MS) in the presence of 19 different nanobodies confirmed by pulldowns, in order to determine the binding epitope, and possible differences in conformational dynamics. HDX-MS measures the exchange rate of hydrogens on the protein amide backbone with the deuterium from a deuterated buffer. These exchange rates are primarily dependent on protein secondary structure, and thus it is a powerful tool to examine protein conformational dynamics (176). The changes in HDX as a result, allow for the identification of potential binding interfaces or conformational changes induced upon complex formation with nanobodies. The full details of HDX data collection and analysis are shown in Appendix G-I.

HDX-MS was used to identify the epitopes of nineteen nanobodies, including the fifteen p110γ binding and four p101/p84 nanobodies (Figure 3.1D). HDX experiments were carried out at two timepoints of H/D exchange (3 or 300 seconds at 18°C). The p110γ-binding nanobodies caused decreased exchange at regions spanning almost the entire p110γ sequence (Figure 3.2 and Appendix J+K). Multiple nanobodies caused decreased exchange in the helical domain of p110γ, which has been observed for previous p110γ antibody and small molecule binding partners (94,177,178) due to the propagation of allosteric changes to the helical domain.

Of the nanobodies studied by HDX, we were able to identity putative epitopes for the majority (Figure 3.2, Appendix F, Appendix J+K). Of this group, we will focus the discussion on nanobodies that were further characterized. The nanobody NB5-PIK3CG caused decreased HDX in a region spanning the end of the uncharacterized adaptor binding domain (ABD) and the first helix in the ABD-RBD linker (122-157) (Figure 3.2B). Nanobody NB7-PIK3CG caused decreased HDX throughout the helical domain, with the largest decrease being localized in the Ras binding domain (RBD) which is essential for Ras binding (196-211) (Figure 3.2C). The p101-binding nanobody, NB1-PIK3R5, induced large scale decreases in exchange within multiple regions in the final 200 amino acids, which has been identified as a critical region for Gβγ activation (148). The p101 region previously identified as the putative Gβγ binding site (816-828) had a >25% protection in deuterium incorporation.

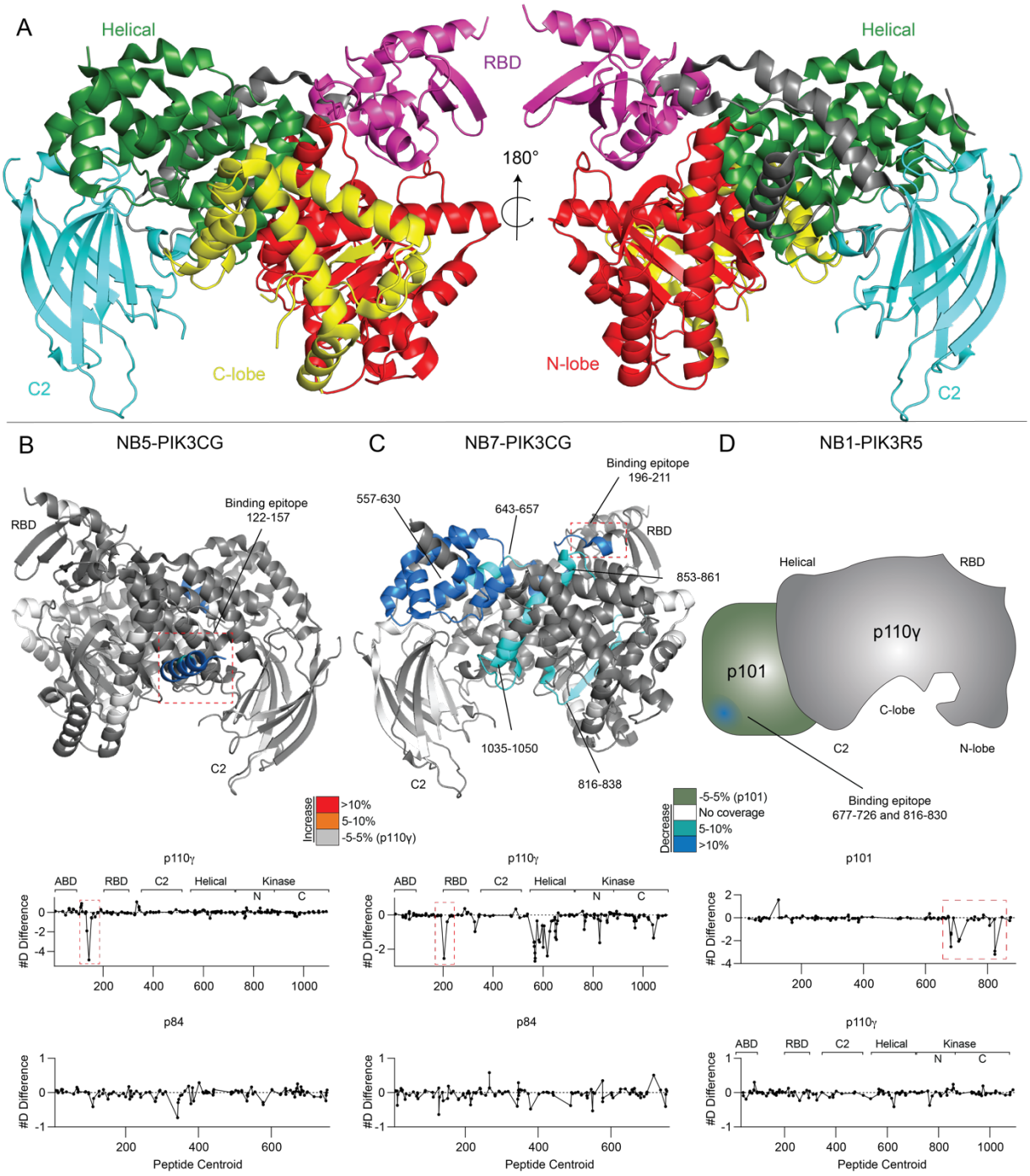

Figure 3.2. Using HDX-MS to identify nanobody epitopes on PI3Kγ. (A) Domain organization of p110γ subunit with domains colored on the crystal structure of the 144-1102 crystal construct. (PDB ID: 6aud) **(B)** HDX-MS differences in p110γ-p84 with the addition of NB5-PIK3CG mapped on a structural model of p110γ. The number of deuteron difference for all peptides analyzed over the entire deuterium exchange time course is shown for p110γ and p84. In panels (B-D), peptides showing significant difference in deuterium exchange (>5%,>0.4 kDa) between conditions with and without nanobody are colored on the cartoon. **(C)** HDX-MS differences in p110γ-p84 with the addition of NB7-PIK3CG mapped on a model of p110γ. The number of deuteron difference for all peptides analyzed over the entire deuterium exchange time course is shown for p110γ and p84. **(D)** HDX-MS differences in p110γ-p101 with the addition of NB1-PIK3R5 mapped on a cartoon representation of p110γ/p101, as changes only occur in

the p101 subunit, which has not been structurally characterized. The number of deuteron difference for all peptides analyzed over the entire deuterium exchange time course is shown for p110γ and p101.

Nanobodies stabilize protein conformations enabling high resolution Cryo-EM analysis

Many nanobodies bound to regions of either p110γ or the p101 and p84 subunits that have not been characterized structurally up to this point. We first used utilized negative stain electron microscopy to analyze three nanobodies that bind novel regions of the p110γ-p101 complex: NB1-PIK3R5 (p101 C-terminus), NB2-PIK3R5 (p101) and NB5-PIK3CG (p110γ ABD) (Figure 3.3A). 2D analysis revealed that additional densities along the periphery of the complex corresponding to unique binding sites of these nanobodies. We were able to model the approximate location of these binding sites by integrating data from HDX-MS and negative stain EM (Figure 3.3D). We also conducted cryo-EM analysis of the p110γ-p101 complex, generating a map at an overall resolution of 3.4 Å. However, this 3D reconstruction revealed that a large portion of p101 was poorly resolved in the EM density map, with this region matching the area where NB1-PIK3R5 bound based on the negative stain analysis and HDX-MS. Hence, we reconstituted a ternary complex of p110γ-p101 with NB1-PIK3R5 and vitrified this sample for cryo-EM analysis. We were able to obtain a 3D reconstruction at an overall resolution of 2.9 Å, with greatly improved local resolution compared to the apo complex at the NB1-PIK3R5 binding site (Figure 3.3B+C). The improved quality of the EM density map resulting from the nanobody serves as a proof of principle for the HDX-MS guided approach to rapidly optimize nanobodies as structural chaperones. This enabled us to efficiently narrow down to the best possible nanobody to overcome the challenges facing structural investigations of p110γ-p101 (Figure 3.3D).

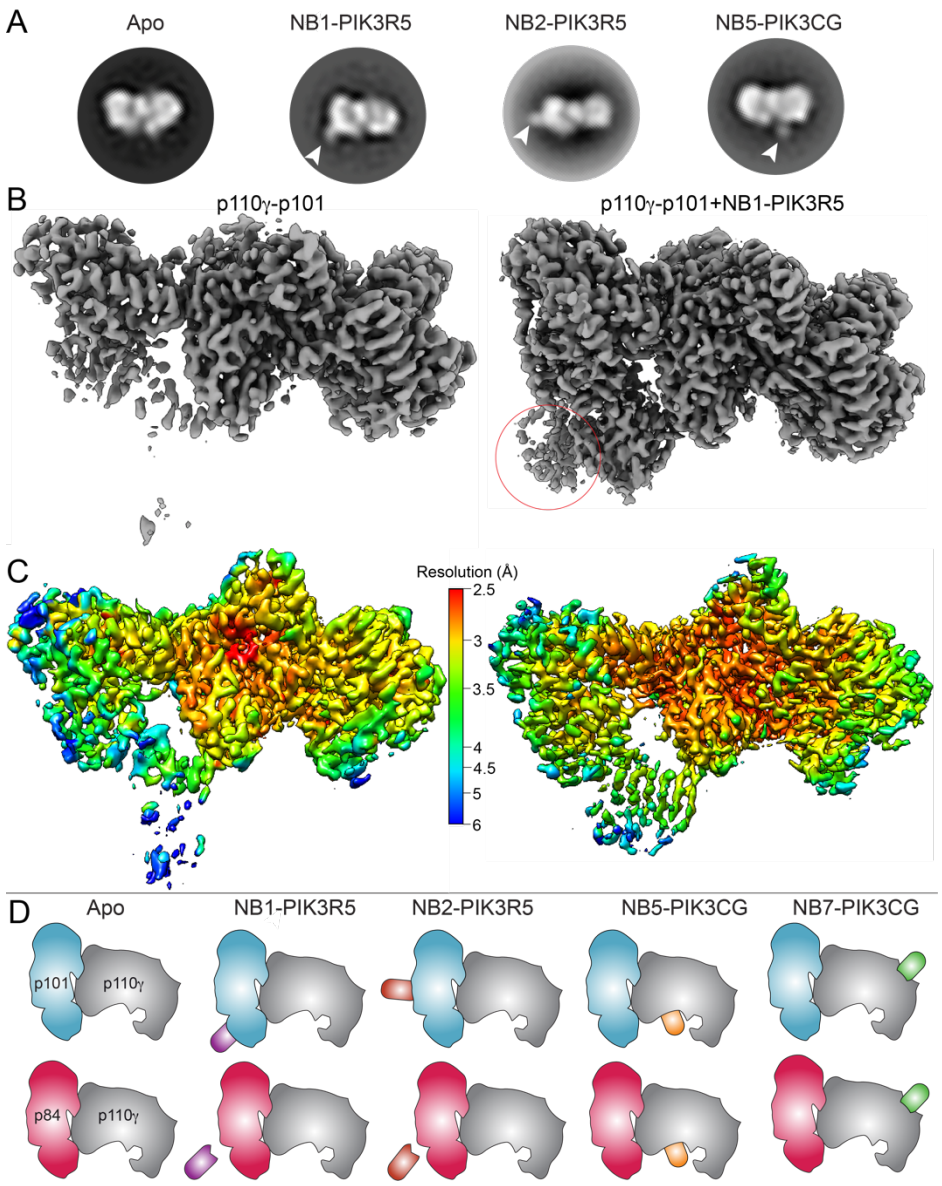

Figure 3.3. Nanobodies facilitate structural studies by EM. (A) Representative 2D class averages of p110γ-p101 indicating positions of the nanobodies NB1-PIK3R5, NB2-PIK3R5 and NB5-PIK3CG as seen on negative stain EM. **(B)** Cryo-EM 3D reconstructions of p110γ-p101 and NB1-PIK3R5 bound p110γ-p101 showing the stabilizing effect of this nanobody. Density for the nanobody is circled. **(C)** p110γ-p101 reconstructions with and without NB1-PIK3R5 colored according to local resolution as estimated using cryoSPARC v3.1 **(D)** Cartoons showing approximate binding sites of NB1-PIK3R5, NB2-PIK3R5, NB5-PIK3CG and NB7-PIK3CG as determined by HDX-MS and negative stain EM.

Nanobodies can both inhibit and activate PI3Kγ *lipid kinase activity*

The identification of nanobodies that bound at the protein interfaces for the upstream activators Ras (which binds the RBD of p110γ) and Gβγ (binds the c-terminus of p101) led us to characterize their effects on lipid kinase activity and activation by lipidated Ras and Gβγ. We hypothesized that nanobodies sharing the same binding epitopes

as known PI3Kγ activators could potentially disrupt PI3Kγ activation and signaling. Additionally, the important role of the ABD domain in regulating class I PI3Ks, led to investigate the potential role of nanobodies binding this region. We selected three nanobodies for full biochemical characterization (the RBD binding nanobody NB5-PIK3CG, the p101 binding nanobody NB1-PIK3R5, and the ABD binding nanobody NB7-PIK3CG) using in vitro lipid kinase assays of its basal activity and activation by lipidated Gβγ and Ras (Figure 3.1F, Figure 4). Assays were carried out with both the p110γ-p101 and p110γ-p84 complexes, to determine any complex specific modulatory effects. The development of biomolecules that can specifically target unique p110γ complexes would be an important tool to decipher PI3Kγ signaling, as ATP competitive inhibitors will equally inhibit both complexes.

The RBD-binding nanobody NB7-PIK3CG had no effect on basal lipid kinase activity of either p110γ-p101 or p110γ-p84 (Figure 3.4A+D). For both complexes it completely blocked activation by lipidated Ras (Figure 3.4A+D). This nanobody appeared to have a limited effect on Gβγ activation of the p110γ-p101 complex, as it was still robustly activated, however, for the p110γ-p84 complex it caused complete disruption of both Ras and Gβγ activation (Figure 3.4A+D). This potentially could be utilized as a biased inhibitor that would preferentially inhibit p110γ-p84 over p110γ-p101. The contact site of the p101 binding nanobody NB1-PIK3R5 partially overlapped with the one identified for lipidated Gβγ on membranes (148). In light of this, we hypothesized that this nanobody would be able to specifically inhibit Gβγ-mediated activation of p110γ/p101. Gβγ activation of p110γ/p101 was almost completely inhibited in the presence of NB1-PIK3R5 (Figure 3.4B), with no effect on Ras activation. This nanobody caused no significant differences in lipid kinase activity under any conditions for the p110γ/p84 complex (Figure 3.4E). Due to its ability to potently inhibit only GPCR activation of the p110γ-p101 complex, NB1-PIK3R5 will be a powerful tool to selectively inhibit only p110γ-p101 over p110γ-p84 to decipher their specific roles in PI3Kγ signaling.

We tested the effect of the p110γ ABD binding nanobody (NB5-PIK3CG) on lipid kinase activity. The ABD of p110γ is structurally uncharacterized, but the ABD domain of class IA PI3Ks is known to be a critical regulator of lipid kinase activity (95). The NB5-PIK3CG nanobody activated lipid kinase activity under all conditions tested for both p110γ-p101 and p110γ-p84 (Figure 3.4C+F). This reveals an unexpected and previously undescribed role of the ABD as a regulator of p110γ signaling, with molecules targeting this region able to modulate lipid kinase activity.

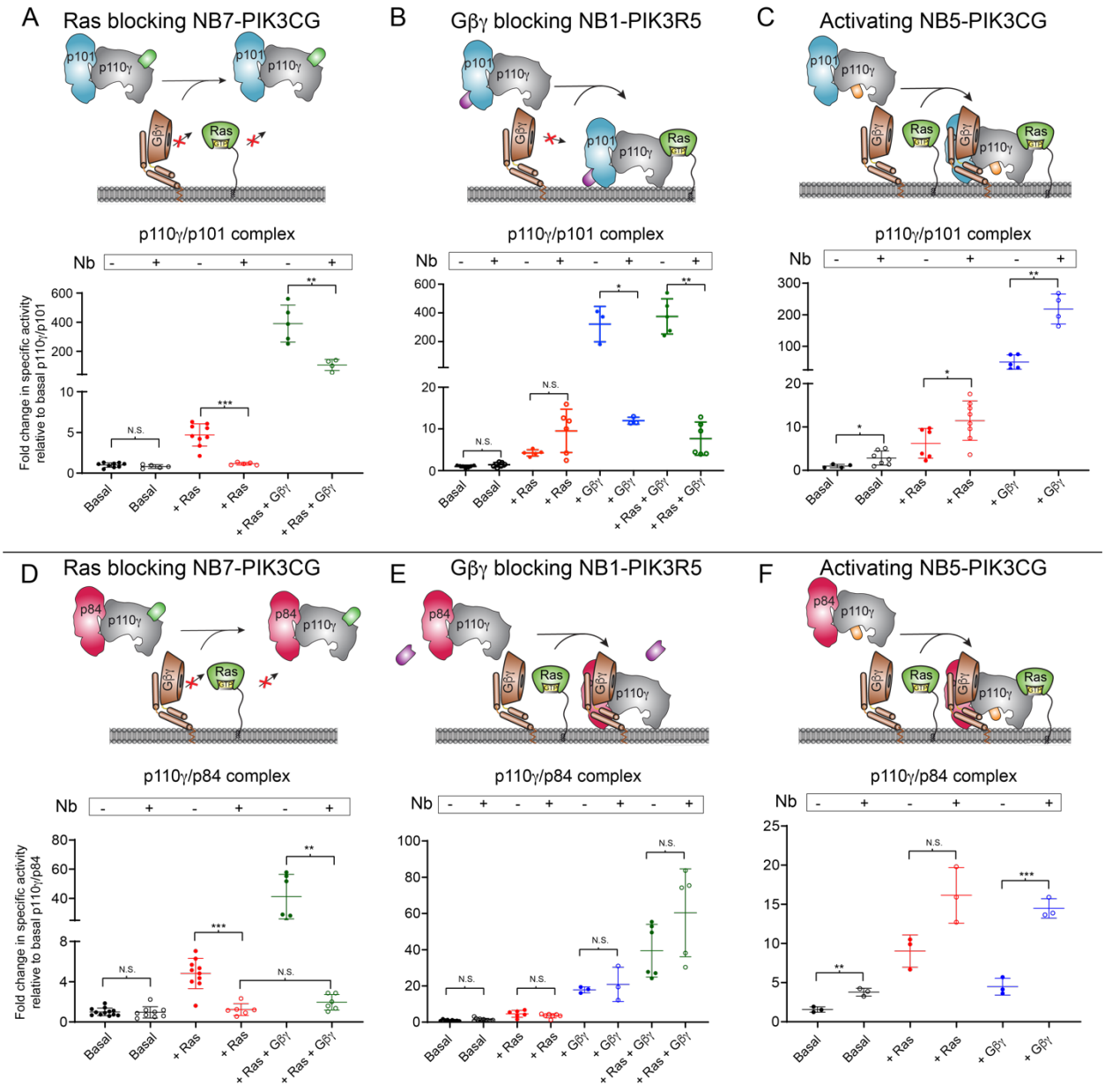

Figure 3.4. Nanobodies modulate PI3Kγ regulation. (A) Lipid kinase activity assay showing the effect of NB7-PIK3CG binding on the specific activity of p110γ-p101 under the indicated conditions. For assays in (A-F), plasma membrane mimic vesicles (20% phosphatidylserine (PS), 50% phosphatidylethanolamine (PE), 10% Cholesterol, 10% phosphatidylcholine (PC), 5% sphingomyelin (SM) and 5% phosphatidylinositol-3,4,5-trisphosphate (PIP2)) at 0.5 mg/mL final concentration were used. Final concentration of ATP was 100 μM. Final concentration of nanobody was 6 μM. Lipidated Gβγ and HRas G12V were present at 1.5 μM concentration. Two tailed p-values represented by the symbols as follows: ***<0.001; **<0.01; *<0.05; N.S.>0.05. **(B)** Lipid kinase activity assay showing the effect of NB5-PIK3CG binding on the specific activity of p110γ-p101 under the indicated conditions. **(C)** Lipid kinase activity assay showing the effect of NB1-PIK3R5 binding on the specific activity of p110γ-p101 under the indicated conditions. Biochemical assays in panels A-C were carried out with p110γ-p101 at 50-3,000 nM final concentration. **(D)** Lipid kinase activity assay showing the effect of NB7-PIK3CG binding on the specific activity of p110γ-p84 under the indicated conditions. **(E)** Lipid kinase activity assay showing the effect of NB5-PIK3CG binding on the specific activity of p110γ-p84 under the indicated conditions. **(F)** Lipid kinase activity assay showing the effect of

NB1-PIK3R5 binding on the specific activity of p110γ-p84 under the indicated conditions. Biochemical assays in panels D-F were carried out with p110γ-p84 at 1,500-3,000 nM final concentration.

3.5 Discussion

The class I PI3Ks are master regulators of growth, metabolism, and immunity (136). Mutations leading to activation of the PI3K pathway are the most frequent alterations in human cancer (179). Small molecule inhibitors of class I PI3Ks are in clinical and pre-clinical development for cancer, immune disorders, developmental disorders, and inflammatory disorders. Partially limiting this approach is the severe side effects associated with pan-PI3K ATP-competitive inhibitors (180). Further development of biomolecules that can selectively modulate distinct PI3K isoforms and complexes will be critical in fully understanding PI3K signaling, and may prove useful as therapeutics for multiple human diseases. Here we describe an HDX-MS optimized flow-path for the rapid identification of a panel of class IB binding nanobodies. These identified nanobodies enabled high resolution structural studies, and selectively modulated different p110γ regulatory complexes.

Nanobodies can be powerful tools in preventing protein-protein interactions, and they are rapidly entering the clinic for treatment of multiple diseases (181), with the first nanobody drug Cablivi approved as a treatment for acquired thrombotic thrombocytopenic purpura (182). In addition to this therapeutic role, one of the first applications of nanobodies was as chaperones facilitating structural biology approaches. This has enabled high resolution structures of multiple signaling proteins, highlighted by the foundational impact nanobodies have had on GPCR structural biology (158). A complication of generating optimized nanobodies, is the extensive screening required for biomolecules that enable either EM or X-ray approaches. Here we have described how HDX-MS can be utilized to rapidly identify epitopes for nanobodies and stabilizing conformational changes induced upon binding. HDX-MS is a well-established technique for efficiently defining antibody binding sites for biopharmaceuticals (183), and has been used to define nanobody binding sites (161,184). The identification of the NB1-PIK3R5 nanobody, which stabilized the dynamic C-terminus of the p101 subunit, allowed us to obtain a high-resolution map of the p110γ-p101 complex by cryo-EM, which is described in depth in chapter 4. Overall, our HDX-MS based approach allows for a repeatable method to rapidly identify the most suitable nanobodies to optimize X-ray crystallography and cryo-EM approaches.

Our combined HDX-MS and EM structural studies revealed multiple nanobodies that bound at critical regulatory interfaces involved in the binding of Ras and Gβγ in both p110γ and p101. We identified two nanobodies

(NB6-PIK3CG, NB7-PIK3CG) that bound to the RBD in p110γ, which contains the Ras binding interface (93). Membrane reconstitution assays of Ras activation showed that NB7-PIK3CG potently inhibited Ras activation for both the p110γ-p101 and p110γ-p84 complexes. Intriguingly, for p110γ-p84, this nanobody also disrupted activation by Gβγ. The p110γ-p84 complex is proposed to strictly require Ras for activation *in vivo* (84), however, this data suggests a key role of the RBD in the activation by both Ras and Gβγ in this complex. NB7-PIK3CG induced large-scale allosteric changes within the helical domain of p110γ (Figure 3.2C). It has been shown that the Gβγ binding interface in p110γ lies within the helical domain (148), and thus a potential molecular mechanism for this inhibition is the disruption of the helical domain-Gβγ interaction through nanobody-induced allosteric changes. The p110γ-p101 complex has a second Gβγ binding site in p101 (85,185) which potentially allows it to overcome this inhibitory effect and still be activated by Gβγ. This difference between the two PI3Kγ complexes will likely enable this nanobody to be used as a biased p110γ-p84 inhibitor. A similar effect was seen with a C2 binding antibody that was able to selectively inhibit GPCR activation of p110γ-p84 over p110γ-p101 (178). Together these biomolecules will be useful as tools to study the specific roles of p110γ-p84 in cell signaling.

The p110γ-p101 complex contains Gβγ binding sites in both p110γ and p101 (85,148,185,186), with the unique p101 Gβγ binding site being an attractive target for the development of molecules to selectively inhibit GPCR activation of the p110γ-p101 complex. Nanobodies have been developed that can inhibit/modulate GPCR signaling at multiple levels (187), including ones that target the extracellular (188) and intracellular (158,189) faces of GPCRs, as well as the released Gβγ heterodimer (174) . The development of molecules that can specifically block activation of a single Gβγ effector will have major advantages both as tools, and as potential therapeutics. The NB1-PIK3R5 nanobody bound to p101 at a site previously proposed as the Gβγ binding site (148), and selectively inhibited Gβγ activation of only the p110γ-p101 complex. Selectively inhibiting the p110γ-p101 complex has potential applications and advantages in targeting p110γ in disease. In heart failure, the p110γ-p101 complex is upregulated, while the p110γ-p84 complex plays an important role in maintaining cardiac contractility (71,140) , highlighting the potential advantage of specifically targeting p110γ-p101. Initiation of toll-like receptor (TLR) signaling activates p110γ through engagement with Rab8 (82), with this being proposed to selectively activate p110γ-p101 through an unknown mechanism. This might indicate an advantage of targeting p110γ-p101 in TLR driven inflammation. Further structural

and biochemical optimization of biomolecules binding at this site in p101 may play an important role in understanding p110γ signaling and designing potential therapeutics.

Overall, this study using HDX-MS to probe a family of PI3Kγ binding nanobodies identified a wide variety of biomolecules that were useful in both high-resolution structural analysis and as selective modulators of PI3K activity. This approach can be employed for other large multi-component protein complexes, and is uniquely well-suited to develop and identify biomolecules that can allosterically modulate enzyme activity outside of the active site.

Chapter 4: Molecular basis for the regulation of p110γ-p101 by GPCRs

Adapted from:

Rathinaswamy, M.K.*, Dalwadi, U.*, Fleming, K.D., Adams, C., Stariha, J.T.B., Pardon, E., Minkyung, B., Vadas, O., DiMaio, F., Steyaert, J., Hansen, S.D., Yip, C.K. and Burke, J.E. (2021). Structure of the phosphoinositide 3-kinase p110γ-p101 complex reveals molecular mechanism of GPCR activation. (2021) Science Advances (In Press)

* indicates equal contribution

Contributions:

The data presented in this chapter was a collaborative effort between the Burke lab, Yip lab (University of British Columbia), DiMaio lab (University of Washington) and Hansen lab (University of Oregon). **Myself**: Cloning, expression and purification of all proteins, kinase assays, HDX-MS and biolayer interferometry. **Udit Dalwadi (Yip Lab)**: EM experiments using protein produced by me and 3D map generation. **Kaelin Fleming/Jordan Stariha**: Assistance with HDX-MS. **Carson Adams (DiMaio Lab)**: Assistance with model building. **Dr. Scott Hansen (Hansen Lab)**: Single molecule microscopy experiments using proteins purified by me.

4.1 Abstract

The class IB phosphoinositide 3-kinase (PI3K), PI3Kγ, is a master regulator of immune cell function, and a promising drug target for both cancer and inflammatory diseases. Critical to PI3Kγ function is the association of the p110γ catalytic subunit to either a p101 or p84 regulatory subunit, which mediates activation by G-protein coupled receptors (GPCRs). Here, we report the cryo-EM structure of a heterodimeric PI3Kγ complex, p110γ-p101. This structure reveals a unique assembly of catalytic and regulatory subunits that is distinct from other class I PI3K complexes. p101 mediates activation through its Gβγ binding domain, recruiting the heterodimer to the membrane and allowing for engagement of a secondary Gβγ binding site in p110γ. Multiple oncogenic mutations mapped to

these novel interfaces and enhanced Gβγ activation. A nanobody that specifically binds to the p101-Gβγ interface blocks activation providing a novel tool to study and target p110γ-p101-specific signaling events *in vivo*.

4.2 Introduction

The class IB p110 isoform p110γ, encoded by *PIK3CG* is a master regulator of immune cell function (137), chemotaxis (76,77), cytokine release (78), and reactive oxygen species generation (75), which are important processes for both the innate and adaptive immune systems. It is a key factor in multiple inflammatory diseases, including rheumatoid arthritis (66), atherosclerosis (190), Lupus (68), allergy (69,78,83), cardiovascular diseases (71), obesity related changes in metabolism (67), and pulmonary fibrosis (87). The immunomodulatory effects of PI3Kγ are drivers of pancreatic ductal adenocarcinoma (89) and targeting PI3Kγ in combination with checkpoint inhibitors has shown promise as an anti-cancer therapeutic (63,90). Its ability to mediate multiple immune cell functions is controlled by its activation downstream of diverse cell surface receptors, including G-protein coupled receptors (GPCRs) (79), the IgE/Antigen receptor (78), receptor tyrosine kinases (80), and Toll-like receptors (TLRs) (81,82).

Structural and biophysical analysis have provided initial insight into the regulation of p110γ and its activation by upstream stimuli. The structure of a p110γ fragment revealed a conserved molecular architecture shared by all p110 subunits composed of a Ras Binding Domain (RBD) which mediates activation by the small GTPase Ras (93), a C2 domain, an armadillo repeat helical domain, and an archetypal bi-lobal kinase domain, similar to protein kinases (91) (Figure 4.1A). Sequence analysis suggested the presence of a ubiquitin-like domain at the N-terminus, possibly playing a similar function as the Adaptor Binding Domain (ABD) of class IA PI3Ks. Both p101 and p84 differ from the class IA PI3K regulatory subunits, as they are not essential for p110 stability and do not inhibit lipid kinase activity (85,191) , but instead mediate activation by upstream stimuli. The molecular basis for why regulatory subunits differentially regulate class IA and IB PI3Ks has remained elusive.

The class I PI3Ks are frequently mis-regulated in multiple human diseases (192). This is most evident by the high frequency of hotspot somatic activating mutations found in *PIK3CA* (encodes for p110α) in multiple human cancers (98,179). The other class I PI3K isoforms are also potentially involved in cancer, with overexpression of these p110 catalytic subunits leading to oncogenic transformation in cells (97). Both overexpression of *PIK3CG* and rare point mutations spanning the catalytic subunit have been identified in tumor biopsies (55,56,58,193). The mechanisms

by which these mutations affect lipid kinase activity cannot be clearly explained by the existing structure of the catalytic subunit alone, highlighting the importance of understanding the molecular details of PI3Kγ regulatory complexes.

PI3Kγ is mainly activated downstream of GPCRs, where the presence of different adaptor subunits greatly modulates activation. The p84 and p101 subunits show distinct expression profiles, and alter PI3Kγ signaling responses to distinct upstream inputs (186). *In vivo,* the p110γ catalytic subunit alone is unable to be activated downstream of GPCRs and requires either the p101 or p84 regulatory subunits to respond to GPCRs (185). p101 and p84 play unique roles, with neutrophils lacking p84 having reduced reactive oxide species generation and neutrophils lacking p101 showing impaired migration (92). The distinct signaling responses were attributed to differential sensitivity of each of the PI3Kγ heterodimers to Gβγ subunits, with the p110γ-p101 complex being preferentially activated by Gβγ (85,148) and p110γ-p84 requiring Ras binding for activation (84). To better understand how preferences for activating inputs translate into differences in function, there is a need for molecules that selectively inhibit one of the two p110γ complexes without affecting the other.

To decipher the molecular mechanism of how the p101 subunit regulates p110γ activation, we determined the structure of the p110γ-p101 complex using cryo-electron microscopy (cryo-EM). This structure reveals a novel binding interface between p101 and p110γ, which is completely distinct with the interface of class IA PI3K adaptors. Our structure also validates the presence of an ABD in p110γ similar to other class I PI3Ks, although with a unique orientation. Unlike class IA ABDs, the p110γ ABD does not directly bind p101, but instead orients the RBD-C2 linker for productive binding to this regulatory subunit. Intriguingly, oncogenic mutations found in p110γ localize at the interfaces of the ABD and p101. Hydrogen deuterium exchange mass spectrometry analysis revealed the altered dynamics of the p110γ-p101 interfaces upon mutation, leading to increased activation by Gβγ. The structure also showed that the Gβγ binding domain (GBD) in p101 contains a putative membrane binding surface that positions p110γ for catalysis. Single molecule fluorescence microscopy experiments indicated that the full activation of the p110γ-p101 complex requires the engagement of two Gβγ molecules to p101 and p110γ, respectively. Finally, a nanobody used in the cryo-EM analysis was found to be a potent inhibitor of GPCR activation of only p110γ-p101, with no effect on p110γ-p84. This nanobody could be used to decipher the complex specific roles of PI3Kγ in immune cell signaling, while also providing a novel potential therapeutic strategy for targeting unique PI3Kγ complexes.

4.3 Materials and Methods

Expression and purification of nanobody:

Nanobody NB1-PIK3R5 with a C-terminal 6X His tag was expressed from a pMESy4 vector in the periplasm of WK6 E.coli. A 1L culture was grown to OD600 of 0.7 in Terrific Broth containing 0.1% glucose and 2mM $MgCl_2$ in the presence of 100 μg/mL ampicillin and was induced with 0.5 mM isopropyl-β-D-thiogalactoside (IPTG). Cells were harvested the following day by centrifuging at 2500 RCF (Eppendorf Centrifuge 5810 R) and the pellet was snap-frozen in liquid nitrogen. The frozen pellet was resuspended in 15 mL of buffer containing 200 mM Tris pH 8.0, 0.5mM ethylenediaminetetraacetic acid (EDTA) and 500 mM Sucrose and was mixed for 1 hour at 4°C. To this mixture, 30 mL of resuspension buffer diluted four times in water was added and mixed for 45 minutes at 4°C to induce osmotic shock. The lysate was clarified by centrifuging at 14,000 rpm for 30 minutes (Beckman Coulter JA-20 rotor). Imidazole was added to the supernatant to final concentration of 10mM loaded onto a 5 mL HisTrap™ FF crude column (GE Healthcare) equilibrated in NiNTA A buffer (20 mM Tris pH 8.0, 100 mM NaCl, 20 mM imidazole pH 8.0, 5% (v/v) glycerol, 2 mM β-mercaptoethanol (βME)). The column was washed with high salt NiNTA A buffer (20 mM Tris pH 8.0, 1 M NaCl, 20 mM imidazole pH 8.0, 5% (v/v) glycerol, 2 mM βME), NiNTA A buffer, 6% NiNTA B buffer (20 mM Tris pH 8.0, 100 mM NaCl, 250 mM imidazole pH 8.0, 5% (v/v) glycerol, 2 mM βME) and the protein was eluted with 100% NiNTA B. The eluent was concentrated in a 10,000 MWCO Amicon Concentrator (Millipore) to <1 mL and injected onto a Superdex™ 75 10/300 GL Increase size-exclusion column (GE Healthcare) equilibrated in gel filtration buffer (20mM Tris pH 8.5, 100 mM NaCl, 50 mM Ammonium Sulfate and 0.5 mM tris(2-carboxyethyl) phosphine (TCEP)). Following size exclusion, the protein was concentrated, frozen and stored at -80ºC.

Plasmid Generation for PI3Kγ constructs:

PI3Kγ constructs without the regulatory subunit (p110γ full length and p110γ 144-1102) were encoded in a pACEBac vector while the complexes were expressed from MutliBac (WT) or biGBac (mutants) vectors. For purification, a 10X histidine tag, a 2×-strep tag and a Tobacco Etch Virus protease cleavage site were cloned to the N-terminus of the regulatory subunits for the complex and to p110γ for constructs without regulatory subunits. All mutations were made in pLib vectors encoding p110γ using site-directed mutagenesis according to published

commercial protocols (QuickChange Site-Directed Mutagenesis, Novagen). Oligonucleotides spanning the region of interest containing altered nucleotides were used in PCR reactions (Q5 High-Fidelity 2× MasterMix, New England Biosciences #M0492L) and the resulting reaction mixture was transformed into XL10 E.coli. Single colonies were grown overnight and purified using QIAprep Spin Miniprep Kit (Qiagen #27104). Plasmid identity was confirmed by sequencing.

Virus Generation and Amplification:

The plasmids encoding genes for insect cell expression were transformed into DH10MultiBac cells (MultiBac, Geneva Biotech) containing the baculovirus viral genome (bacmid) and a helper plasmid expressing transposase to transpose the expression cassette harbouring the gene of interest into the baculovirus genome. Bacmids with successful incorporation of the expression cassette into the bacmid were identified by blue-white screening and were purified from a single white colony using a standard isopropanol-ethanol extraction method. Briefly, colonies were grown overnight (16 hours) in 3-5 mL 2×YT (BioBasic #SD7019). Cells were pelleted by centrifugation and the pellet was resuspended in 300 µL P1 Buffer (50 mM Tris-HCl, pH 8.0, 10 mM EDTA, 100 mg/mL RNase A), chemically lysed by the addition of 300 µL Buffer P2 (1% sodium dodecyl sulfate (SDS) (W/V), 200 mM NaOH), and the lysis reaction was neutralized by addition of 400 µL Buffer N3 (3.0 M potassium acetate, pH 5.5). Following centrifugation at 21130 RCF and 4 ^{o}C (Rotor #5424 R), the supernatant was separated and mixed with 800 µL isopropanol to precipitate the DNA out of solution. Further centrifugation at the same temperature and speed pelleted the Bacmid DNA, which was then washed with 500 µL 70% Ethanol three times. The Bacmid DNA pellet was then dried for 1 minute and re-suspended in 50 µL Buffer EB (10 mM Tris-Cl, pH 8.5; All buffers from QIAprep Spin Miniprep Kit, Qiagen #27104). Purified bacmid was then transfected into Sf9 cells. 2 mL of Sf9 cells between 0.3-0.5X10^{6} cells/mL were aliquoted into the wells of a 6-well plate and allowed to attach, creating a monolayer of cells at ~70-80% confluency. Transfection reactions were prepared by the addition of 2-10 µg of bacmid DNA to 100 µL 1xPBS and 12 µL polyethyleneimine (PEI) at 1 mg/mL (Polyethyleneimine ‘‘Max’’ MW 40.000, Polysciences #24765, USA) to 100 µL 1xPBS. The bacmid-PBS and the PEI-PBS solutions were mixed together, and the reaction occurred for 20-30 minutes before addition drop-by-drop to an Sf9 monolayer containing well. Transfections were allowed to proceed for 5-7 days before harvesting virus containing supernatant as a P1 viral stock.

Viral stocks were amplified by adding P1 viral stock to suspension Sf9 cells between 1-2×10^6 cells/mL at a 2/100 volume ratio. This amplification produces a P2 stage viral stock that can be used in final protein expression. The amplification proceeded for 4-5 days before harvesting, with cell shaking at 120 RPM in a 27ºC shaker (New Brunswick). Harvesting of P2 viral stocks was carried out by centrifuging cell suspensions in 50 mL Falcon tubes at 2281 RCF (Beckman GS-15), collecting the supernatant in a fresh sterile tube, and adding 5-10% inactivated foetal bovine serum (FBS; VWR Canada #97068-085).

Expression and purification of PI3Kγ constructs:

The PI3Kγ complexes (Human p110γ-porcine p101 WT/mutants and Human p110γ-mouse p84 WT) were expressed in Sf9 insect cells using the baculovirus expression system. Following 55 hours of expression, cells were harvested by centrifuging at 1680 RCF (Eppendorf Centrifuge 5810 R) and the pellets were snap-frozen in liquid nitrogen. Constructs without the regulatory subunit (Human p110γ full length and Human p110γ 144-1102) were expressed in insect cells for 55 hours from a pACEBac vector. Both the monomer and the complex were purified identically through a combination of nickel affinity, streptavidin affinity and size exclusion chromatographic techniques.

Frozen insect cell pellets were resuspended in lysis buffer (20 mM Tris pH 8.0, 100 mM NaCl, 10 mM imidazole pH 8.0, 5% glycerol (v/v), 2 mM βME), protease inhibitor (Protease Inhibitor Cocktail Set III, Sigma)) and sonicated for 2 minutes (15s on, 15s off, level 4.0, Misonix sonicator 3000). Triton-X was added to the lysate to a final concentration of 0.1% and clarified by spinning at 15,000 RCF for 45 minutes (Beckman Coulter JA-20 rotor). The supernatant was loaded onto a 5 mL HisTrap™ FF crude column (GE Healthcare) equilibrated in NiNTA A buffer (20 mM Tris pH 8.0, 100 mM NaCl, 20 mM imidazole pH 8.0, 5% (v/v) glycerol, 2 mM βME). The column was washed with high salt NiNTA A buffer (20 mM Tris pH 8.0, 1 M NaCl, 20 mM imidazole pH 8.0, 5% (v/v) glycerol, 2 mM βME), NiNTA A buffer, 6% NiNTA B buffer (20 mM Tris pH 8.0, 100 mM NaCl, 250 mM imidazole pH 8.0, 5% (v/v) glycerol, 2 mM βME) and the protein was eluted with 100% NiNTA B. The eluent was loaded onto a 5 mL StrepTrap™ HP column (GE Healthcare) equilibrated in gel filtration buffer (20mM Tris pH 8.5, 100 mM NaCl, 50 mM Ammonium Sulfate and 0.5 mM TCEP). The column was washed with the same buffer and loaded with tobacco etch virus protease. After cleavage on the column overnight, the protein was eluted in gel filtration buffer. For the complex with nanobody, the eluted protein was incubated with two-fold molar excess of purified nanobody on ice for

15 minutes. The protein was concentrated in a 50,000 MWCO Amicon Concentrator (Millipore) to <1 mL and injected onto a Superdex™ 200 10/300 GL Increase size-exclusion column (GE Healthcare) equilibrated in gel filtration buffer. After size exclusion, the protein was concentrated, aliquoted, frozen and stored at -80ºC.

Expression and Purification of lipidated Gβγ for kinase activity assays:

Full length, lipidated human Gβγ ($G\beta_1\gamma_2$) was expressed in Sf9 insect cells and purified as described previously (117). After 65 hours of expression, cells were harvested and the pellets were frozen as described above. Pellets were resuspended in lysis buffer (20 mM HEPES pH 7.7, 100 mM NaCl, 10 mM βME, protease inhibitor (Protease Inhibitor Cocktail Set III, Sigma)) and sonicated for 2 minutes (15s on, 15s off, level 4.0, Misonix sonicator 3000). The lysate was spun at 500 RCF (Eppendorf Centrifuge 5810 R) to remove intact cells and the supernatant was centrifuged again at 25,000 RCF for 1 hour (Beckman Coulter JA-20 rotor). The pellet was resuspended in lysis buffer and sodium cholate was added to a final concentration of 1% and stirred at 4ºC for 1 hour. The membrane extract was clarified by spinning at 10,000 RCF for 30 minutes (Beckman Coulter JA-20 rotor). The supernatant was diluted 3 times with NiNTA A buffer (20 mM HEPES pH 7.7, 100 mM NaCl, 10 mM Imidazole, 0.1% $C_{12}E_{10}$, 10mM βME) and loaded onto a 5 mL HisTrap™ FF crude column (GE Healthcare) equilibrated in the same buffer. The column was washed with NiNTA A, 6% NiNTA B buffer (20 mM HEPES pH 7.7, 25 mM NaCl, 250 mM imidazole pH 8.0, 0.1% C12E10, 10 mM βME) and the protein was eluted with 100% NiNTA B. The eluent was loaded onto HiTrap™ Q HP anion exchange column equilibrated in Hep A buffer (20 mM Tris pH 8.0, 8 mM CHAPS, 2 mM Dithiothreitol (DTT)). A gradient was started with Hep B buffer (20 mM Tris pH 8.0, 500 mM NaCl, 8 mM CHAPS, 2 mM DTT) and the protein was eluted in ~50% Hep B buffer. The eluent was concentrated in a 30,000 MWCO Amicon Concentrator (Millipore) to < 1 mL and injected onto a Superdex™ 75 10/300 GL size exclusion column (GE Healthcare) equilibrated in Gel Filtration buffer (20 mM HEPES pH 7.7, 100 mM NaCl, 10 mM CHAPS, 2 mM TCEP). Fractions containing protein were pooled, concentrated, aliquoted, frozen and stored at -80ºC.

Lipid vesicle preparation for kinase activity assays:

Lipid vesicles containing 5% brain phosphatidylinositol 4,5- bisphosphate (PIP_2), 20% brain phosphatidylserine (PS), 50% egg-yolk phosphatidylethanolamine (PE), 10% egg-yolk phosphatidylcholine (PC), 10% cholesterol and 5% egg-yolk sphingomyelin (SM) were prepared by mixing the lipids solutions in organic

solvent. The solvent was evaporated in a stream of argon following which the lipid film was desiccated in a vacuum for 45 minutes. The lipids were resuspended in lipid buffer (20 mM HEPES pH 7.0, 100 mM NaCl and 10 % glycerol) and the solution was sonicated for 15 minutes. The vesicles were subjected to five freeze thaw cycles and extruded 11 times through a 100-nm filter (T&T Scientific: TT-002-0010). The extruded vesicles were sonicated again for 5 minutes, aliquoted and stored at -80°C. Final vesicle concentration was 5 mg/mL.

Lipid kinase activity assays:

All lipid kinase activity assays employed the Transcreener ADP2 Fluorescence Intensity (FI) Assay (Bellbrook labs) which measures ADP production. For assays comparing the activities of p110γ, p110γ-p101 and p110γ-p84, PM-mimic vesicles at a final concentration of 1 mg/mL, ATP at a final concentration of 100 μM ATP and Gβγ at 1.5 μM final concentration were used. Final concentration of kinase was 3000nM for all basal conditions. For conditions with Gβγ, p110γ: 3000 nM, p110γ-p84: 1000 nM and p110γ-p101: 30 nM. 2 μL kinase solution at 2× final concentration was mixed with 2 μL substrate solution containing ATP, vesicles and Gβγ or Gβγ gel filtration buffer and the reaction was allowed to proceed for 60 minutes at 20°C. For assays comparing mutants, kinase was mixed with vesicles at 1mg/mL, ATP at 100 μM and Gβγ at 75 nM or 1.5 μM final concentrations and the reaction was allowed to proceed for 60 minutes at 37°C. The reactions were stopped with 4 μL of 2× stop and detect solution containing Stop and Detect buffer, 8 nM ADP Alexa Fluor 594 Tracer and 93.7 μg/mL ADP2 Antibody IRDye QC-1 and incubated for 50 minutes. The fluorescence intensity was measured using a SpectraMax M5 plate reader at excitation 590 nm and emission 620 nm. This data was normalized against the measurements obtained for 100 μM ATP and 100 μM ADP. The % ATP turnover was interpolated from a standard curve (0.1-100 μM ADP). This was then used to calculate the specific activity of the enzyme.

For assays measuring nanobody inhibition at saturating Gβγ concentrations, kinase at 4× concentration was mixed with nanobody at 4× concentration to obtain 2× enzyme-nanobody solution (6 μM final nanobody). Final concentration of kinase was 3000nM for all basal conditions. For conditions with Gβγ, p110γ-p84: 1500 nM and p110γ-p101: 50 nM. 2 μL of this solution was mixed with 2 μL of 2× substrate solution containing ATP (100 μM final), vesicles (1 mg/mL final) with or without Gβγ (1.5 μM final) to start the reaction and allowed to proceed for 60 minutes at 20 ºC. Following this, the reaction was stopped, the intensity was measured, the data was normalized and

specific activity calculated as described above. For the nanobody IC_{50} curve, kinase at 4× concentration was mixed with nanobody at 4× concentration to obtain 2× enzyme-nanobody solution (200nM final kinase; 41-10,000 nM final nanobody). 2 µL of this solution was mixed with 2 µL of 2× substrate solution containing ATP (100 µM final), vesicles (2 mg/mL final) and Gβγ (600 nM final) to start the reaction and allowed to proceed for 60 minutes at 20 °C. Following this, the reaction was stopped, the intensity was measured, and the data was normalized as described above. The normalized values for conditions with nanobody were then further normalized against the condition with maximal activity (no nanobody).

Bio-layer interferometry:

Biolayer interferometry was performed using Octet K2 (Fortebio, Inc.). His-tagged nanobody was immobilized on an Anti-Penta-His biosensor for 600 seconds and the sensor was dipped into solutions of p110γ-p101 at 1.5, 6 and 25 nM final concentrations diluted in kinetics buffer (KB) containing 20mM Tris pH 8.5, 100mM NaCl, 50mM ammonium sulphate, 0.1% bovine serum albumin and 0.02% tween-20. The association step was allowed to proceed for 600 seconds followed by a dissociation step in KB without protein for 600 seconds. The baseline was obtained by dipping sensor without nanobody into a solution containing 25 nM p110γ-p101 in a similar fashion. The average K_d was calculated from the three binding curves based on their global fit to a 1:1 binding model.

Hydrogen Deuterium Exchange Mass Spectrometry (HDX-MS) (STAR methods)

HDX-MS sample preparation

For HDX reactions comparing p110γ alone and p110γ in complex with p101 or p84, exchange was carried out in a 50 µl reaction containing 20 picomoles of protein, either p110γ, p110γ-p84 or p110γ-p101. To initiate hydrogen-deuterium exchange, 1.5µL of either protein was incubated with 48.5 µL of D_2O buffer solution (20mM HEPES pH 7.5, 100mM NaCl, 94.3% D_2O) for five time points (3s on ice, 3s, 30s, 300s, 3000s at room temperature) to give a final concentration of 91.5% D_2O.

HDX reactions comparing full length p110γ and ABD truncated p110γ were conducted in 50 µl reaction volumes with a final p110γ amount of 15 pmol. Exchange was carried out for four time points (3s, 30s, 300s and 3000s

at room temperature). To initiate hydrogen-deuterium exchange, 1.2 µL of either protein was incubated with 48.8 µL of D_2O buffer solution (20mM HEPES pH 7.5, 100mM NaCl, 94.3% D_2O) to give a final concentration of 92% D_2O.

HDX reactions comparing p110γ-p101 with and without nanobody were conducted in 50 µl reaction volumes with a final p110γ amount of 16 pmol and a final nanobody amount of 7 pmol. Exchange was carried out for two time points (3s and 300s at room temperature). To initiate hydrogen-deuterium exchange, 1µL of p110γ-p101 and 1µL of nanobody was incubated with 48 µL of D_2O buffer solution (20mM HEPES pH 7.5, 100mM NaCl, 94.3% D_2O) to give a final concentration of 90.5% D_2O.

HDX reactions comparing wild-type p110γ-p101, R472C p110γ-p101, and E347K p110γ-p101 were conducted in 50 µl reaction volumes with a final protein amount of 12.5 pmol. Exchange was carried out for five time points (3s on ice, 3s, 30s, 300s and 3000s at room temperature). To initiate hydrogen-deuterium exchange, 2 µL of protein was incubated with 48 µL of D_2O buffer solution (20mM HEPES pH 7.5, 100mM NaCl, 94.3% D_2O) to give a final concentration of 90.5% D_2O. All exchange reactions were terminated by the addition of ice-cold quench buffer to give a final concentration 0.6M guanidine-HCl and 0.9% formic acid and samples were frozen in liquid nitrogen and stored at -80°C. All experiments were carried out in independent triplicate.

Protein digestion and MS/MS data collection

Protein samples were rapidly thawed and injected onto an integrated fluidics system containing a HDx-3 PAL liquid handling robot and climate-controlled chromatography system (LEAP Technologies), a Dionex Ultimate 3000 UHPLC system, as well as an Impact HD QTOF Mass spectrometer (Bruker). The protein was run over either one (at 10°C) or two (at 10°C and 2°C) immobilized pepsin columns (Applied Biosystems; Poroszyme Immobilized Pepsin Cartridge, 2.1 mm x 30 mm; Thermo-Fisher 2-3131-00; Trajan; ProDx protease column, 2.1 mm x 30 mm PDX.PP01-F32) at 200 µL/min for 3 minutes. The resulting peptides were collected and desalted on a C18 trap column (Acquity UPLC BEH C18 1.7mm column (2.1 x 5 mm); Waters 186003975). The trap was subsequently eluted in line with a C18 reverse-phase separation column (Acquity 1.7 mm particle, 100 x 1 mm^2 C18 UPLC column, Waters 186002352), using a gradient of 5-36% B (Buffer A 0.1% formic acid; Buffer B 100% acetonitrile) over 16 minutes. Mass spectrometry experiments acquired over a mass range from 150 to 2200 *m/z* using an electrospray ionization source operated at a temperature of 200°C and a spray voltage of 4.5 kV.

Peptide identification

Peptides were identified from the non-deuterated samples of p110γ alone, p110γ-p84, or p110γ-p101 using data-dependent acquisition following tandem MS/MS experiments (0.5 s precursor scan from 150-2000 *m/z*; twelve 0.25 s fragment scans from 150-2000 *m/z*). MS/MS datasets were analyzed using PEAKS7 (PEAKS), and peptide identification was carried out by using a false discovery-based approach, with a threshold set to 1% using a database of purified proteins and known contaminants. The search parameters were set with a precursor tolerance of 20 ppm, fragment mass error 0.02 Da, charge states from 1-8, leading to a selection criterion of peptides that had a -10logP score of 21.7.

Mass Analysis of Peptide Centroids and Measurement of Deuterium Incorporation

HD-Examiner Software (Sierra Analytics) was used to automatically calculate the level of deuterium incorporation into each peptide. All peptides were manually inspected for correct charge state, correct retention time, appropriate selection of isotopic distribution, etc. Deuteration levels were calculated using the centroid of the experimental isotope clusters. The results for these proteins are presented as the raw percent deuterium incorporation, as shown in the Appendix, with the only correction being applied correcting for the deuterium oxide percentage of the buffer utilized in the exchange (91.7% for comparing p110γ to p110γ-p101 and p110γ-p84, 86.8% for comparing p110γ-p101 with NB1-PIK3R5, 92% for the ABD deletion, and 90.5% for the oncogenic mutants). No corrections for back exchange that occurs during the quench and digest/separation were applied. Attempts to generate a fully deuterated class I PI3K sample were unsuccessful, which is common for large macromolecular complexes. Therefore, all deuterium exchange values are relative.

Differences in exchange in a peptide were considered significant if they met all three of the following criteria: ≥5% change in exchange, ≥0.4 Da difference in exchange, and a p value <0.01 using a two tailed student t-test. The raw HDX data are shown in two different formats.

The raw peptide deuterium incorporation graphs for a selection of peptides with significant differences are shown, with the raw data for all analyzed peptides in the appendix. To allow for visualization of differences across all peptides, we utilized number of deuteron difference (#D) plots. These plots show the total difference in deuterium

incorporation over the entire H/D exchange time course, with each point indicating a single peptide. These graphs are calculated by summing the differences at every time point for each peptide and propagating the error. For a selection of peptides, we are showing the %D incorporation over a time course, which allows for comparison of multiple conditions at the same time for a given region. Samples were only compared within a single experiment and were never compared to experiments completed at a different time with a different final D_2O level. The data analysis statistics for all HDX-MS experiments are in Appendix P according to the guidelines (194). The mass spectrometry proteomics data have been deposited to the ProteomeXchange Consortium via the PRIDE partner repository (118) with the dataset identifier PXD025209.

4.4 Results

Structure of the p110γ-p101 complex

Full length human p110γ alone, as well as the p110γ-p84 and p110γ-p101 complexes were purified (Figure 4.1A+B). Gel filtration elution profiles of the p110γ-p84 and p110γ-p101 complexes confirmed their heterodimeric stoichiometry. Lipid kinase assays testing Gβγ activation revealed a ~100-200-fold activation of p110γ-p101, a less potent ~6-fold activation of p110γ-p84, and limited activation for p110γ alone, results that are consistent with previous work (148) (Figure 4.1C). To delineate the molecular basis for how p101 protein controls the activation of p110γ we examined its architecture using an approach combining hydrogen deuterium exchange mass spectrometry (HDX-MS) and Cryo-EM.

We first conducted cryo-EM analysis of the p110γ-p101 complex. Although negative stain analysis revealed that purified p110γ-p101 was homogeneous (data not shown) and high-quality vitrified specimens from this relatively small-sized and asymmetric complex could be obtained, the region encompassing the p101 regulatory subunit was poorly resolved in our initial 3D reconstruction of p110γ-p101. This could be attributed to the highly dynamic nature of the C-terminal region of p101. To obtain a more "rigid" complex for cryo-EM analysis, we screened nanobodies targeting p110γ-p101 and found one that specifically stabilized the p101 C-terminal domain (NB1-PIK3R5, described in chapter 3). We purified the nanobody-bound p110γ-p101 complex and confirmed its 1:1:1 stoichiometry by gel filtration (Figure 4.1B). Using this sample, we were able to obtain a cryo-EM reconstruction of the ternary complex of nanobody-bound p110γ-p101 at 2.9 Å overall resolution from 320,179 particles (Appendix L). The density map

was of sufficient quality to allow for automated and manual building of the majority of the p110γ and p101 subunits (Figure 4.1D-F). We were able to unambiguously fit available crystal structures of p110γ (aas 144-1102) (195) into our map and build an additional 210 residues that constitute the ABD, the linkers connecting the RBD-C2 and C2-helical domains, and the kinase domain activation loop (Appendix M). The region with the lowest local resolution was the Gβγ binding domain (GBD) of p101, along with the bound nanobody. The GBD forms a beta sandwich structure composed of two sheets, and initial automated and manual model building only allowed for partial building of one of the two sheets. To build the remainder of the GBD, we utilized computational approaches. This allowed us to build a complete model of the structured regions of p101 (Appendix N).

The p101 regulatory subunit structure (Appendix N) features a helical solenoid (aas 11-149, 186-267) and a α/β barrel (aas 150-185, 268-670, 867-877) that together we refer to as the p110γ binding domain (PBD), and a beta sandwich Gβγ binding domain (aas 671-834, GBD). In addition to these motifs, there are four linker regions that were not resolved in the electron density map (aas 311-512, 560-603, 623-650, and 835-866). Comparisons between p101 and p84 revealed that the structured regions of the PBD and GBD are partially conserved (28% identity and 47% similarity for the PBD, and 24% identity and 44% similarity for the GBD) (Appendix N). We analyzed our p101 model using the DALI server (196) and found multiple lipid kinases that shared a similar arrangement of an α/β barrel and β sandwich domain, including Diacylglycerol kinase (197), the phosphatidyl kinase YegS (198) and Sphingosine kinase 1 (199) (Appendix N). The catalytic residues at the active site were not conserved, suggesting that p101 has no kinase activity. However, comparing the previously identified lipid binding region of Sphingosine kinase 1 (200) with p110γ-p101 showed that the corresponding region of p101 is oriented towards the putative membrane interface (Figure 4.1E+F), indicating a membrane binding site in p101.

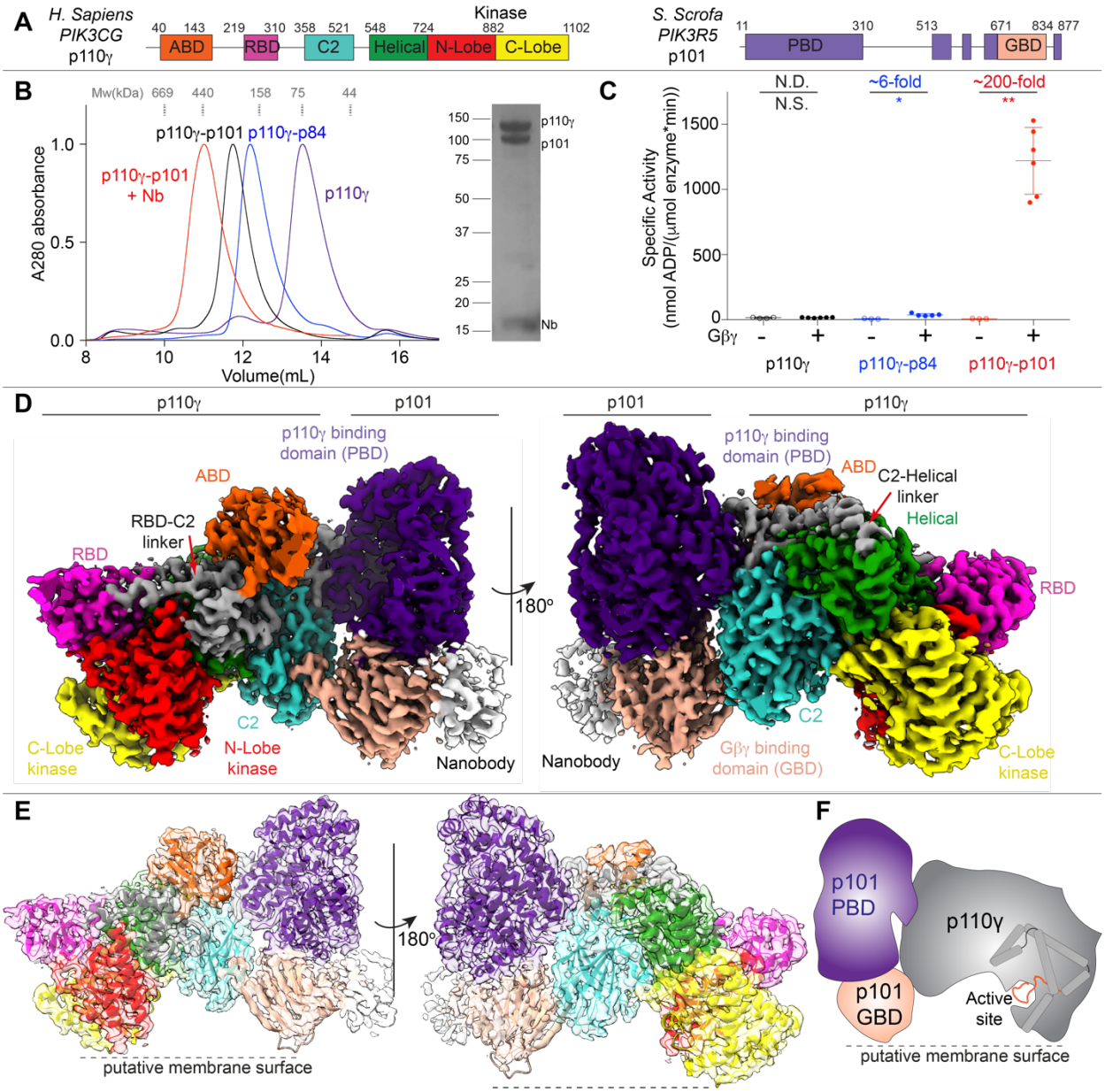

Figure 4.1. Cryo-EM structure of the p110γ p101 complex. (A) Domain schematic of *H. Sapiens* p110γ and *S. Scrofa* p101 used in this study. **(B)** Gel filtration elution profile of different p110γ complexes (i.e. apo or bound to p84, p101, and p101-NB1-PIK3R5). An SDS-PAGE image of the p110γ-p101-NB1-PIK3R5 complex is shown, with MW standards indicated. **(C)** Lipid kinase activity assays of different p110γ complexes (concentration 30-3,000 nM) with and without lipidated Gβγ (1.5 μM concentration) using 5% PIP2 vesicles mimicking the plasma membrane (20% phosphatidylserine (PS), 50% phosphatidylethanolamine (PE), 10% Cholesterol, 10% phosphatidylcholine (PC), 5% sphingomyelin (SM) and 5% phosphatidylinositol-3,4,5-trisphosphate (PIP_2)). The fold change upon Gβγ activation is indicated. Every replicate is plotted, with error shown as standard deviation (n = 3–6). Two tailed p-values represented by the symbols as follows: **<0.001; *<0.02; N.S.>0.02. **(D).** Density map of the p110γ-p101-NB1-PIK3R5 complex colored according to the schematic in panel **A**. **(E)** Cartoon representation of the p110γ-p101 complex colored according to the schematic in panel **A**. **(F)** Cartoon schematic of the p110γ-p101 complex.

Molecular details of the p110γ-p101 interface

Our cryo-EM structure revealed that p101 engages p110γ in an extended interface resulting in buried surface area of ~1202 Å^2 (Figure 4.2A+B, Appendix O). There are three specific regions of p110γ that bound to p101: the C2 domain, and the two linkers between the RBD-C2 and the C2-helical domains (Figure 4.2A). These inter-domain linkers were not resolved in previous structures of p110γ alone and contain critical contact residues with p101. The primary binding interface on p101 is composed of the helices α5+6 and the intervening turn in the PBD which interacts with the C2 domain and linkers. The C2 domain also makes an additional interaction with the C-terminal proline of p101. These interfacial residues are strongly conserved across evolution (Appendix N). Intriguingly, we found that the PBD contact residues in p101 were also conserved with p84 (78% identical, 89% similar), revealing a likely shared mode of binding for both regulatory subunits.

A secondary contact site between p101 and p110γ is formed between two beta strands in the GBD of p101 (aas 729-741) and the C2 domain of p110γ (Appendix O). This interface is formed by multiple electrostatic interactions between positively charged residues from the GBD of p101 and an anionic surface in the C2 domain of p110γ (Figure 4.2B, Appendix O). This anionic surface in the C2 is absent in all other class I PI3Ks. Residues forming this contact site are conserved in the evolutionary history of both p101 and p110γ, but are only partially conserved in p84 (57% identical, 86% similar), suggesting that the dynamics of this contact may be altered between the two complexes. This unique interface could explain how a previously designed C2 binding antibody specifically inhibited GPCR activation of p110γ-p84 over p110γ-p101 (178).

To verify the contacts observed in the cryo-EM structure of p110γ-p101, and to compare to dynamics at the p110γ-p84 interfaces, we carried out HDX-MS experiments on p110γ alone and with the two regulatory subunits. Consistent with our previous work (86,141), we found that with both p84 and p101, there was protection of large sections of the ABD and C2 domains along with the RBD-C2 and C2-helical linkers (Figure 4.2 D-F, Appendix O). The same regions were protected in both complexes, however, the differences were larger in the presence of p101, indicating enhanced stability of the p101-bound complex. These differences in stability can be explained by the only partial conservation of the secondary interface residues between p101 and p84, in line with previous data (186).

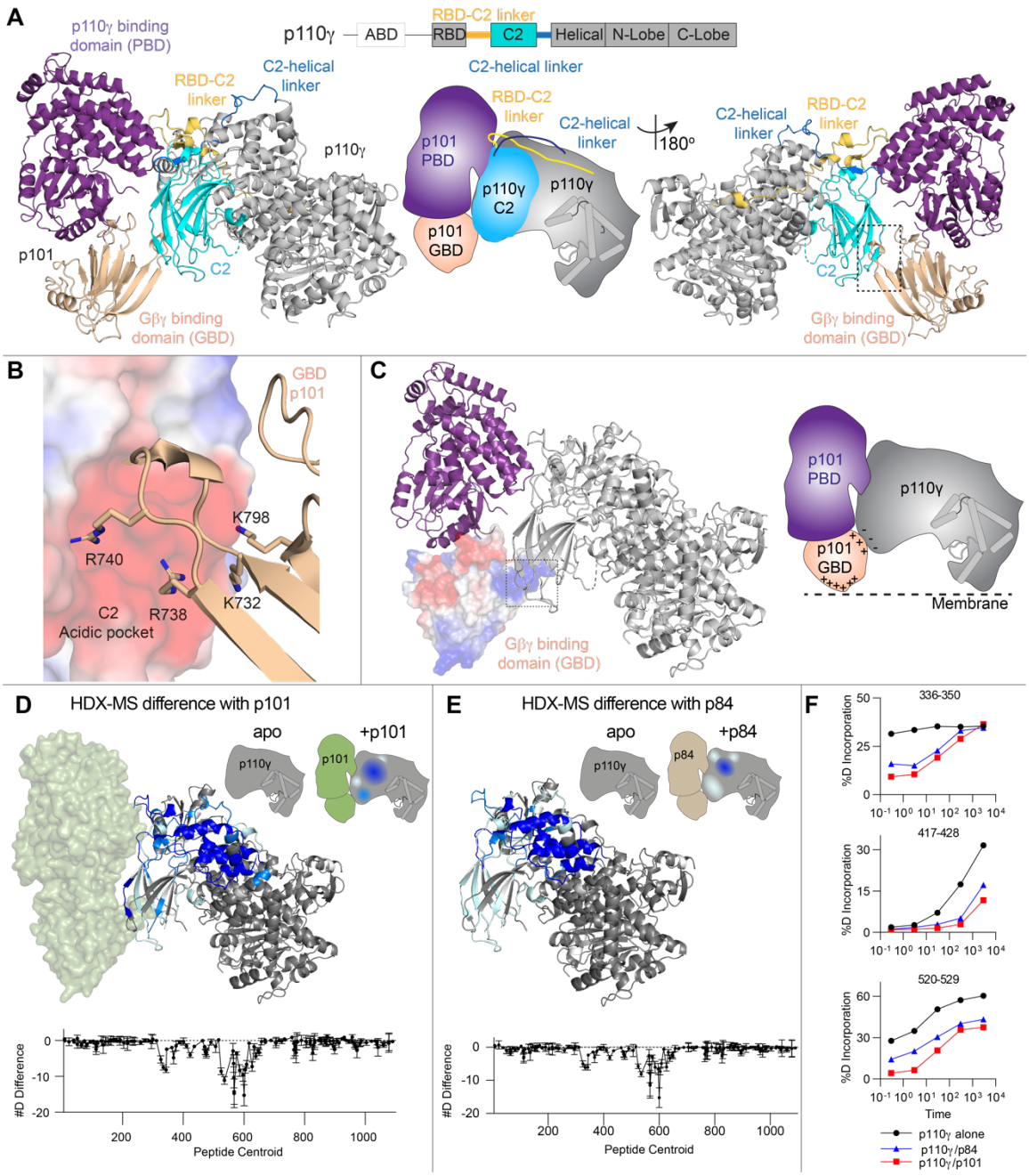

Figure 4.2. Structural basis of the p110γ-p101 binding interface. (A) Cartoon representation of the p110γ-p101 complex, with p101 colored as in Figure 1, and p110γ colored according to the attached schematic, with p101 interacting regions (RBD-C2 linker, C2, and the C2-helical linker) indicated. Important features are shown in a cartoon schematic. **(B)** Interaction between the GBD of p101 and the C2 domain of p110γ. The p110γ C2 domain is shown as an electrostatic surface with p101 shown as sticks. **(C)** The electrostatic surface of the GBD of p101. A cartoon schematic highlighting potential electrostatic interactions between the GBD of p101 and the C2 domain of p110γ and membranes. **(D)** HDX-MS differences in p110γ with the addition of the p101 subunit. **(E)** HDX-MS differences in p110γ with the addition of the p84 subunit mapped on a model of p110γ. The number of deuteron difference for p110γ-p84 for all peptides analyzed over the entire deuterium exchange time course is shown for p110γ. **(D+E)** Peptides showing significant deuterium exchange differences (>5%,>0.4 kDa and p<0.01 in an unpaired two-tailed t-test) between conditions are colored on a cartoon model of p110γ-p101 or p110γ alone. A cartoon schematic is shown

indicating the two conditions compared using HDX-MS. The number of deuteron difference for p110γ-p101 for all peptides analyzed over the entire deuterium exchange time course is shown for p110γ. Every point represents the central residue of an individual peptide. Error is shown as standard deviation (n = 3). **(F)** Selected p110γ peptides that showed decreases and increases in exchange between p110γ alone, p110γ-p101, and p110γ-p84.

Previous work showed that the interaction of the p110γ with its regulatory partners required the presence of the N-terminal ABD (141). Intriguingly, the ABD in p110γ does not directly interact with the regulatory subunit, but instead forms extensive contacts with the RBD-C2 linker (Figure 4.3A) to orient the two linkers for binding the PBD of p101 (Figure 4.3B). To verify these interactions, we performed HDX-MS comparing full length p110γ and the crystal construct of p110γ (aas 144-1102) which lacks the ABD. Consistent with the structural data, presence of the ABD resulted in significant protection in the peptides spanning the RBD-C2 linker (Figure 4.3C).

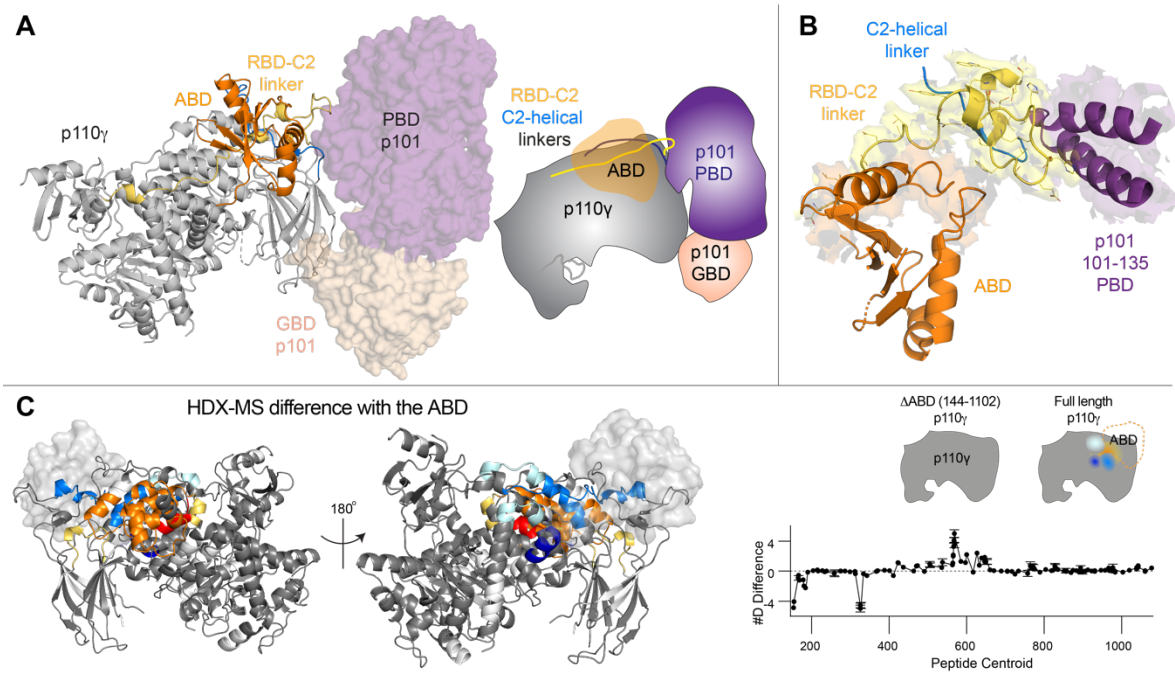

Figure 4.3. Structural basis of the ABD interface with the resit of p110γ. (A) The structure of p110γ-p101 complex, highlighting the orientation of the p110γ ABD, with p101 shown as a transparent surface. The different domains are colored as indicated according to the cartoon schematic. **(B)** The ABD of p110γ coordinates the RBD-C2 linker of p110γ to interact with p101. The RBD-C2 linker, ABD, and the region of p101 that binds the RBD-C2 linker are shown in a cartoon representation. The electron density of the ABD interface, RBD-C2 linker and region of p101 that binds the RBD-C2 linker are visible. **(C)** HDX-MS differences in p110γ with the presence of the ABD mapped on a model of p110γ. The number of deuteron difference for the p110γ ABD deletion for all peptides analyzed over the entire deuterium exchange time course is shown for p110γ.

Comparison of regulatory subunit interactions in class IB to class IA PI3Ks

All class I PI3Ks bind to regulatory subunits, with the class IA PI3Ks binding to five different p85 regulatory subunits. p85 binding has three main effects: (1) it stabilizes the p110 catalytic subunit, (2) inhibits basal lipid kinase activity, and (3) allows activation downstream of pYXXM motifs (95). In contrast, association with class IB regulatory subunits neither stabilizes nor inhibits the p110γ catalytic subunit. To explain these differences in regulation, we compared the orientation of adaptor subunits and the ABD between class IA and class IB PI3Ks (Figure 4.4A-D).

The binding interface with regulatory subunits is completely distinct in class IA PI3Ks compared to class IB. While the C2 domain of class IA PI3Ks does interact with the iSH2 and nSH2 of p85 regulatory subunits, the interface is different from the one that binds the PBD and GBD of p101. Regulatory subunits in class IA PI3Ks make extensive inhibitory interactions with the C-lobe of the kinase domain, while no such contact is observed in the p110γ-p101 complex. Although ABDs of class IA and IB share a similar overall fold (Appendix Q), there are extensive conformational differences in secondary structure elements, consistent with the limited sequence conservation (identity ranging from 13-16% for p110α, p110β, and p110δ). The ABD from class IA PI3Ks is required for forming a high affinity interaction with the iSH2 from p85, mediated by contacts between beta strands β1 and β2, and helix α3. This region is at the surface in the p110γ ABD, making no interactions with the rest of the p110γ subunit (Appendix Q). For all class IA PI3Ks, the ABD forms an inhibitory contact with the N-lobe of the kinase domain, through its N-terminus and the β4-α3 loop. The ABD in p110γ is rotated 180° around the ABD-RBD linker allowing the β4-α3 loop to bind to the RBD-C2 linker. The residues in these regions are highly conserved in the evolution of p110γ, with no conservation with other class I PI3Ks (Appendix Q). Overall, this comparison reveals why p110γ is not inhibited by p101 unlike class IA PI3Ks which are potently inhibited by extensive intra- and inter-subunit contacts with regulatory partners. (Figure 4.4E).

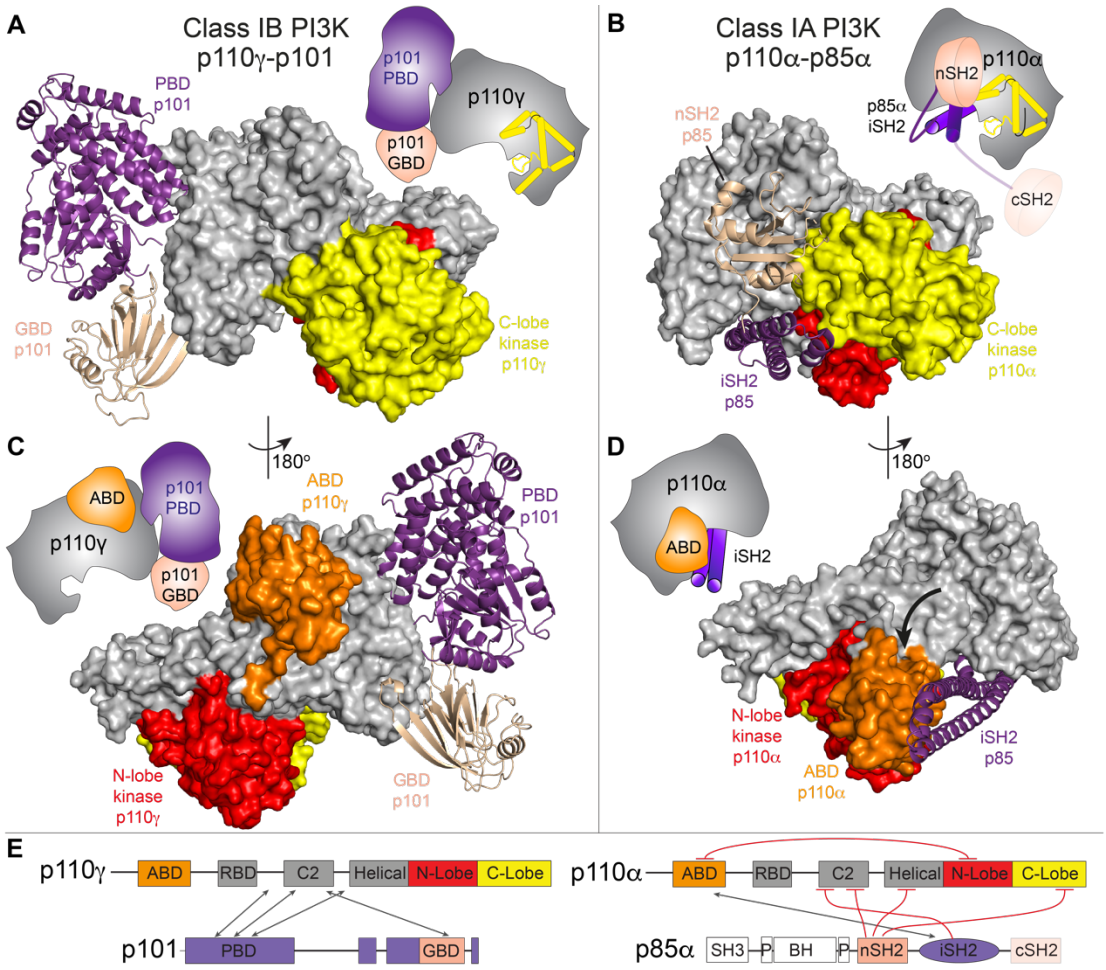

Figure 4.4. Class IA and IB PI3Ks form distinct interfaces with regulatory subunits and the ABD. (A) The structure of p110γ-p101 complex, with p110γ shown as a surface and p101 shown as a ribbon, and the domains colored according to the cartoon schematic as indicated in panel **E**. **(B)** The structure of p110α-p85α complex (PDB:4JPS), with p110α shown as a surface and the nSH2 and iSH2 domains of p85α shown as a ribbon, and the domains colored according to the cartoon schematic as indicated in panel **E**. **(C)** The ABD of p110γ does not interact with either the regulatory subunit or kinase domain. The p110γ-p101 complex is shown as in panel **A**. **(D)** The ABD of p110α interacts with both the regulatory subunit and kinase domain. The p110α-p85α complex is shown as in panel **B**. The altered orientation of the ABD compared to p110γ is indicated by the black arrow. (Cartoon schematics indicating the differences between class IA and class IB are shown for panels **A-D**). **(E)** Domain schematic comparing the interactions between p110 catalytic and the p101 / p85 regulatory subunits. Inhibitory interactions are colored in red, with interacting regions indicated by the arrows.

Rare oncogenic mutations cluster at the p101 and ABD interfaces in p110γ

The PI3K-Akt pathway is the most commonly activated pathway in human cancer, primarily driven by activating oncogenic mutations in the *PIK3CA* gene encoding p110α. The role of the p110γ isoform in cancer development has been ambiguous, with overexpression and rare somatic mutations of *PIK3CG* implicated in multiple cancers, including pancreatic, prostate, renal, and breast. To further explore if activating mutations potentially exist in

PIK3CG we analyzed the Catalog Of Somatic Mutations In Cancer (COSMIC) (106), which showed mutations spanning the primary sequence of p110γ. Intriguingly, many of the most frequent mutations in p110γ mapped to interfaces with either the ABD or p101 (Figure 4.5A).

To identify the consequence of these interfacial mutations we purified mutant complexes of p101 with p110γ E347K (p101 interface) and p110γ R472C (ABD interface). Mutant complexes eluted from gel filtration similar to wild-type (Figure 4.5B), demonstrating that they can still form heterodimers. Lipid kinase assays showed that the mutations resulted in a ~2-3-fold increased activity at both saturating and sub-saturating amounts of Gβγ (Figure 4.5C). To understand the mechanism of how these mutations lead to increased kinase activity, we carried out comparative HDX-MS experiments between the wild-type and mutant p110γ-p101 complexes. The E347K mutant caused increased dynamics at the p101 interface with p110γ, while the R472C mutant led to increased dynamics of the ABD, and the RBD-C2 linker (Figure 4.5D, Appendix R). This suggests that altering the orientation of p101 and ABD relative to the rest of p110γ, may allow for increased access to membrane localized Gβγ subunits.

In addition to the disease-associated mutations at the primary interface between p110γ and p101, we also wanted to determine the role of the GBD-C2 interface in regulating Gβγ activation. This was motivated by analysis of the electron density maps between the free p110γ-p101 complex, and the p110γ-p101 complex with the NB1-PIK3R5 nanobody, which showed that the GBD is highly dynamic in the absence of the nanobody (Figure 4.5E). We mutated a residue in the C2 domain (D369R) that interacts with R738 and R740 in the GBD (Figure 4.5F). The p110γ D369R-p101 mutant eluted from gel filtration as a heterodimer, showing that this contact is not required for p101 binding. Lipid kinase activity assays revealed that this mutation led to a ~2-fold decrease in activation by Gβγ subunits, indicating that the secondary p110γ-p101 interface is crucial in mediating full activation (Figure 4.5G).

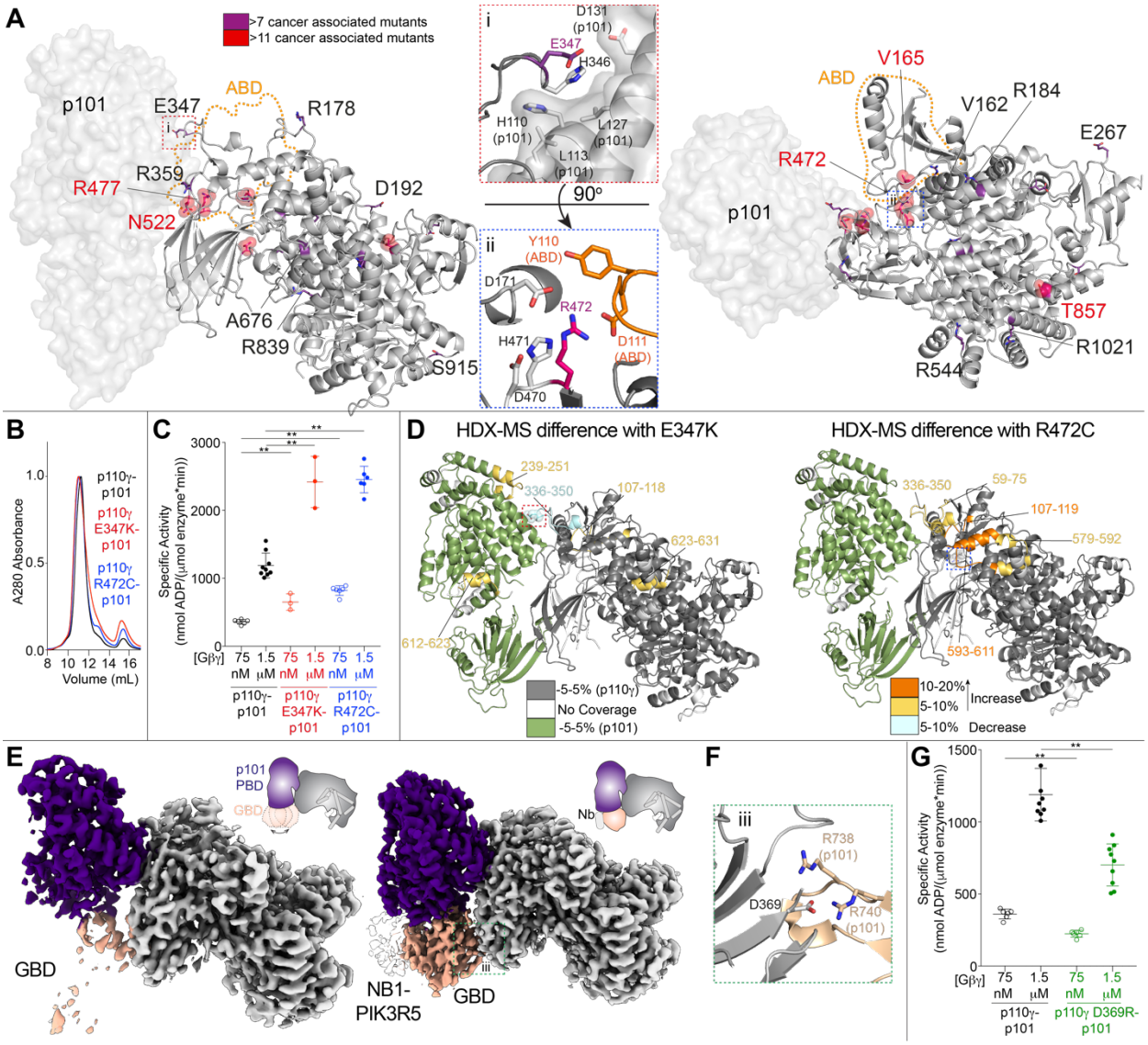

Figure 4.5. Disease-linked and engineered p110γ mutations at the interface with p101 and the ABD modulate Gβγ activation. (A) Somatic mutations found in *PIK3CG* from the Catalogue of Somatic Mutations in Cancer Database (COSMIC) are indicated on the structure, with frequency indicated by the legend. Mutations found in more than 7 tumors are shown as sticks, with mutations found in more than 11 tumors shown as spheres. The orientation of residues around mutations located at the p110γ-p101 interface (i, E347) and ABD interface (ii, R472) are shown. **(B)** Mutations do not disrupt the p110γ-p101 complex. Gel filtration elution profiles of complexes of p110γ (wild-type, E347, and R472) bound to p101. **(C)** Mutations at the p110γ-p101 and ABD interface can lead to enhanced activation by Gβγ. Lipid kinase activity assays of different p110γ complexes (concentration 10-1,000 nM) with and without Gβγ (concentration indicated). **(D)** Hydrogen deuterium exchange mass spectrometry (HDX-MS) revealed enhanced protein dynamics at p101 and ABD interfaces induced by E347K and R472 mutants. Peptides showing significant deuterium exchange differences (>5%,>0.4 kDa and $p<0.01$ in an unpaired two-tailed t-test) between p110γ-p101 complexes of wild-type and E347K (left) and wild-type and R472C (right) are colored on a cartoon model of p110γ-p101 according to the legend. **(E)** The GBD is dynamic in solution, but is stabilized by nanobody (NB1-PIK3R5) binding. Electron density maps of p110γ-p101 alone (left) and p110γ-p101 bound to NB1-PK3R5 (right). **(F)** Charged residues in p110γ-p101 mediate the interaction of the p110γ C2 domain to the p101 GBD. **(G)** Mutation of the p110γ-C2 p101-GBD interface (p110γ D369R) leads to decreased activation by Gβγ. Biochemical assays in panels **(C+G)** were carried out with p110γ-p101 complexes (concentration 10-1,000 nM) and Gβγ (concentration indicated). 5%

PIP_2 membranes were made mimicking the plasma membrane. Every replicate is plotted, with error shown as standard deviation (n = 3–9). Two tailed p-values represented by the symbols as follows: **<0.001; *<0.02.

The Gβγ binding domain is critical for membrane binding and Gβγ activation

To decipher how p101 mediates activation by Gβγ, we have previously examined the dynamic consequences of p110γ-p101 binding to membranes, and membrane localized Gβγ subunits using HDX-MS (86). Our current model of p110γ-p101 allowed us to better understand these data in the context of the full complex. Analysis of the HDX differences upon membrane binding indicated the presence of a membrane binding region in the GBD and protection at the secondary interface between p110γ and p101 (Figure 4.6A, Appendix R). Upon binding to Gβγ subunits, many of these same regions showed greatly decreased exchange indicating enhanced membrane recruitment. Additionally, the Gβγ binding sites (p101 GBD and p110γ helical domain) showed decreases in exchange (Figure 4.6B, Appendix R). Combined with our observations of the GBD flexibility in cryo-EM and activity assays with the p110γ D369R mutant, this HDX-MS data indicated that the GBD forms the secondary interface upon membrane binding, potentially explaining the inability of non-lipidated soluble Gβγ (C68S, Gγ) to interact with p110γ-p101.

A p101 binding nanobody prevents activation by Gβγ subunits

HDX-MS analysis of the NB1-PIK3R5 nanobody used in cryo-EM experiments of p110γ-p101(Figure 4.6D, 5C, Appendix R) showed that it binds with high affinity (~3 nM) to the identified Gβγ binding site in the GBD (Figure 4.6D). This suggested that this nanobody might be useful in specifically disrupting Gβγ activation of the p110γ-p101 complex. We utilized lipid kinase assays with both p110γ-p101 and p110γ-p84 to study the effects of NB1-PIK3R5 on GPCR activation. The NB1-PIK3R5 nanobody at 6 μM led to a ~50-100-fold reduction in Gβγ activation for p110γ-p101, with no effect on p110γ-p84 activation (Figure 4.6E). The nanobody was capable of potently inhibiting the p110γ-p101 complex (IC50 ~1.5 μM) at super-physiological levels of Gβγ (600 nM) (Figure 4.6F), thereby providing a novel tool that may aid in deciphering the exact roles of the p110γ-p101 complex in cells/tissues (Figure 4.6G), and in designing complex-specific therapeutic strategies.

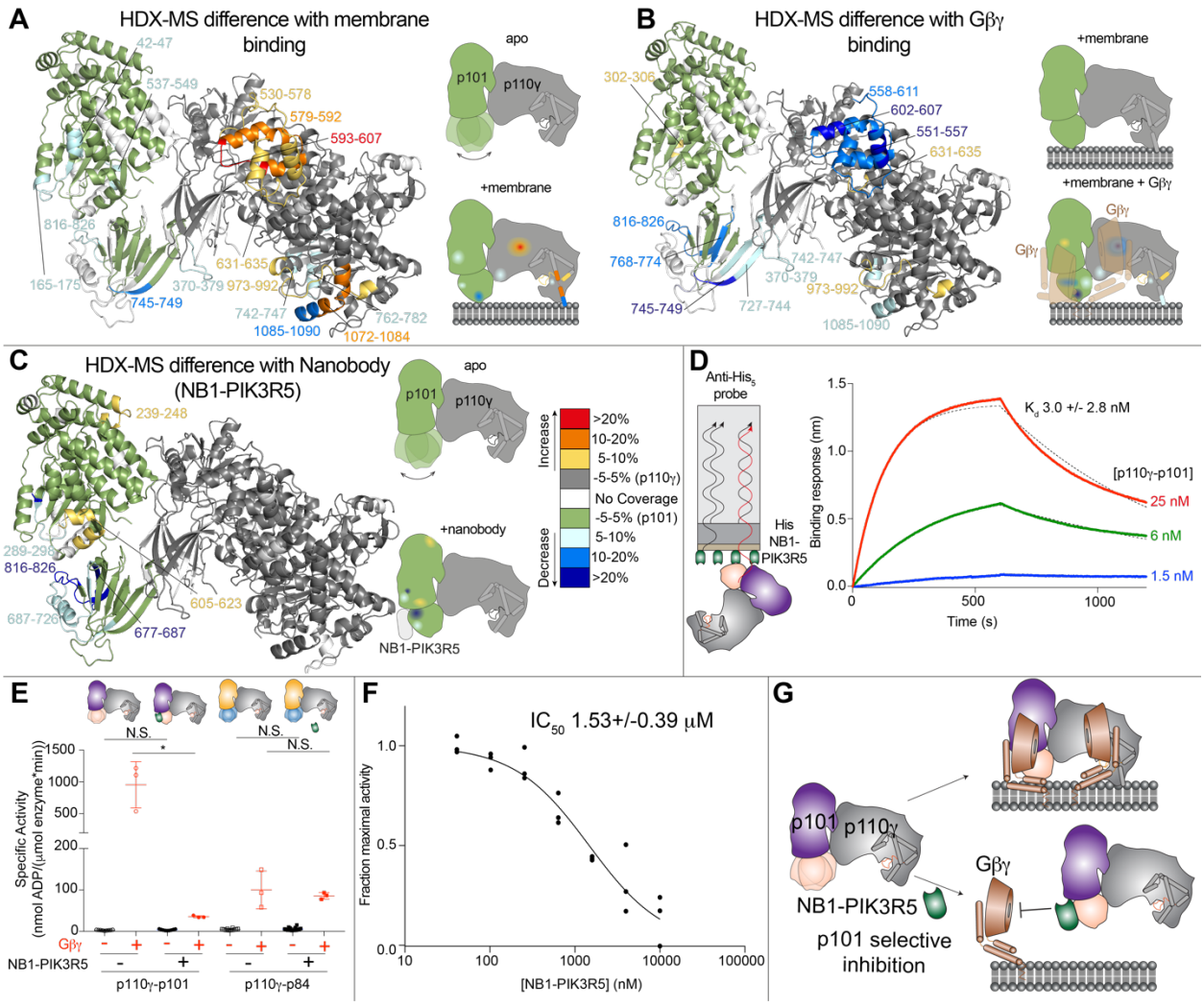

Figure 4.6. Full activation of p110γ by lipidated Gβγ requires the GBD domain of p101 and the GBD-Gβγ interface can be disrupted by a p101 specific nanobody. (A) HDX-MS revealed that interaction of p110γ-p101 with membranes leads to altered protein dynamics in both the p110γ and p101 subunits, with stabilization of the GBD of p101. For panels **(A-C)**, peptides showing significant deuterium exchange differences (>5%,>0.4 kDa and p<0.01 in an unpaired two-tailed t-test) between conditions are colored on a cartoon model of p110γ-p101 according to the legend in panel B. A cartoon schematic is shown indicating the two conditions compared using HDX-MS. **(B)** HDX-MS revealed that interaction of p110γ-p101 with lipidated Gβγ subunits stabilizes the GBD and C2-helical/helical domain of p110γ. HDX-MS data from panels **(A+B)** are reproduced with permission from (148). **(C)** HDX-MS revealed that interaction of p110γ-p101 with NB1-PIK3R5 protects the same surface of GBD that is stabilized upon binding Gβγ on membranes. **(D)** Biolayer interferometry (BLI) analysis of the binding of the immobilized NB1-PIK3R5 nanobody to p110γ-p101. **(E)** The NB1-PIK3R5 nanobody specifically inhibits only the p110γ-p101 complex from GPCR activation, while not affecting the p110γ-p84 complex. Biochemical assays were carried out with p110γ-p101 (50-3,000 nM) and p110γ-p84 (1,500-3,000 nM) using plasma membrane mimic vesicles with and without NB1-PK3R5 (1 μM). Lipidated Gβγ was present at 1.5 μM concentration. **(F)** IC50 measurement of p110γ-p101 inhibition using varying concentrations of the NB1-PIK3R5 nanobody in the presence of 600 nM Gβγ. For panels **(E+F)** every replicate is plotted, with error shown as standard deviation (n = 3–6). Two tailed p-values represented by the symbols as follows: **<0.001; *<0.02. N.S.>0.02. **(G)** Model of the inhibition of GPCR activation of the p110γ-p101 complex by the NB1-PIK3R5 nanobody.

Defining the molecular basis of how Gβγ subunits activate the p110γ-p101 complex

Structural analysis of the Gβγ binding sites in p110γ and p101 from HDX-MS indicated that these regions are separated by ~50 Å, which is greater than the ~40 Å diameter of the Gβγ propeller domain. This suggested that activation of p110γ-p101 is potentially mediated by interactions with two membrane anchored Gβγ molecules. To gain new insight about the mechanism of Gβγ dependent activation of p110γ-p101 we performed single molecule Total Internal Reflection Fluorescence (TIRF) Microscopy experiments on supported lipid bilayers (SLBs) (Figure 4.7A). Experiments were carried out using fluorescently tagged proteins (DY647-p110γ, DY647-p110γ-p101, and Alexa488-SNAP-Gβγ) to track membrane binding. For these experiments, we flowed farnesylated Alexa488-SNAP-Gβγ over a SLB, leading to passive insertion into the membrane ($t_{1/2}$ ~8 min). Single molecule dwell time measurements of fluorescently tagged DY647-p110γ and DY647-p101-p110γ revealed no appreciable membrane binding in the absence of Gβγ (Figure 4.7B). In the presence of membrane anchored Gβγ, we observed an increased binding frequency of DY647-p110γ and transient dwell times that lasted 10-100 ms (Figure 4.7B+C). By contrast, DY647-p101-p110γ bound strongly to membrane anchored Gβγ and exhibited single molecule dwell times that lasted several seconds (Figure 4.7B+D).

Since both subunits in the p110γ-p101 complex contain Gβγ binding interfaces we hypothesized that the single molecule dwell times of DY647-p101-p110γ would strongly depend on the concentration of membrane anchored Gβγ. When we titrated the concentration of Gβγ, we observed a density dependent switch in p110γ-p101 membrane binding behavior (Figure 4.7E). In the presence of low Gβγ concentration (i.e. $\leq$ 100 nM), the dwell time distribution of DY647-p101-p110γ was best described by a single exponential decay curve with dwell times ranging from 100-400 ms. In contrast, we observed longer lived membrane binding interactions when our measurements were performed using more than 100 nM Gβγ. Under these conditions, the dwell time distribution shifted from a single to double exponential decay curve.

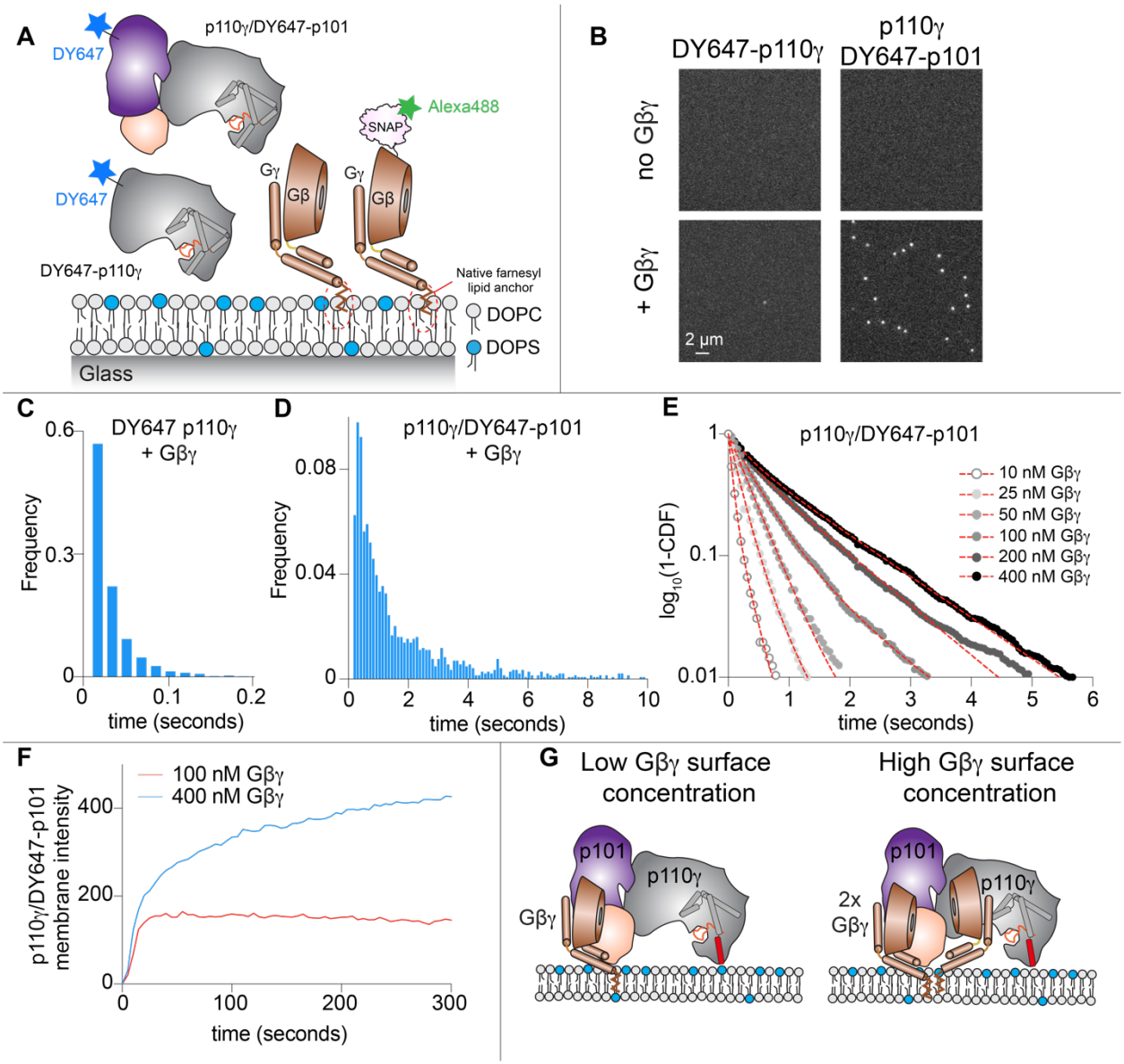

Figure 4.7. Single molecule characterization of p110γ-p101 reveals both subunits can engage membrane anchored Gβγ (A) Schematic showing proteins examined using the single molecule fluorescence approach. Experiments measured the association of fluorescently tagged proteins (Alexa488-SNAP-Gβγ, DY647-p110γ, and DY647-p101-p110γ to a supported lipid bilayer. **(B)** Membrane association of DY647-p110γ or DY647-p101-p110γ requires membrane anchored Gβγ. Single molecule localization measurements were measured in the presence of either 100 pM DY647-p110γ or 10 pM DY647-p101-p110γ. **(C-D)** Single molecule dwell time distributions of DY647-p110γ or DY647-p101-p110γ, measured in the presence of membrane anchored Gβγ. DY647-p110γ transiently associates with membrane anchored Gβγ (**C** τ_1= 22 ms, n=2832 events). DY647-p101-p110γ binds strongly to membrane anchored Gβγ (τ_1= 0.334 sec (31%), τ_2= 1.31 sec (69%), n=3996 events). **(E)** Gβγ membrane density dependent changes in the membrane binding behavior of DY647-p101-p110γ. Concentration of Gβγ represents the solution concentration. **(F)** DY647-p101-p110γ absorption kinetics at different Gβγ membrane densities. **(G)** Model of p110γ-p101 recruitment to Gβγ subunits at both low and high membrane densities.

Consistent with the concentration of Gβγ modulating the dwell time of DY647-p101-p110γ, we also observed changes in the bulk membrane absorption kinetics of p110γ-p101 (Figure 4.7F). In the presence of low Gβγ concentrations (100 nM), DY647-p101-p110γ rapidly associated with the membrane and reached an equilibrium within ~30 seconds (Figure 4.7F). This is the expected kinetic profile for a simple biomolecular interaction between two proteins. In contrast, the membrane absorption kinetics of DY647-p101-p110γ was biphasic in the presence of 400 nM Gβγ (Figure 4.7F). Under these conditions, DY647-p101-p110γ association kinetics are described by rapid binding to the first Gβγ, followed by slow engagement with a second Gβγ (Figure 4.7F). This type of biphasic membrane absorption is similar to how BTK reportedly interacts with two $PI(3,4,5)P_3$ lipids (201). In summary, our TIRF microscopy measurements show that the p110γ-p101 can engage up to two Gβγ molecules depending on the level of GPCR activation (Figure 4.7G).

4.5 Discussion

Understanding how p110γ activity is regulated by p84 or p101 regulatory subunits has been critical in deciphering physiological roles (83,92,185), and will be important in effective PI3K therapeutic design. The class IB p110γ catalytic subunit is a key regulator of immune cell signaling and is a therapeutic target for inflammatory diseases (66,146,202) and immunomodulatory cancer treatment (63,90). Here we report the architecture of the p110γ-p101 complex and a new mechanism of how it can be activated during GPCR signaling.

Our cryo-EM structure of p110γ-p101 reveals important differences in the assembly of catalytic and regulatory subunits between class IA and class IB PI3Ks, and provides novel insight into PI3K regulation. Previous X-ray crystallographic studies of a p110γ fragment revealed its domain organization and the molecular basis for interaction with the upstream activator Ras (91,93,195). Our cryo-EM structure showed an evolutionarily well-conserved binding surface between the regulatory p101 subunit and p110γ. The p110γ ABD does not directly bind p101, but instead coordinates the p101 interaction site on the RBD-C2 linker. This unique architecture is distinct from the ABD in class IA PI3Ks, which mediates direct contacts with the iSH2 of p85 and forms an inhibitory interface with the N-lobe of the kinase domain (203,204).

The architecture of the p110γ-p101 complex reveals how the GBD of p101 orients the kinase domain of p110γ towards the membrane upon Gβγ binding. The p101 protein was identified as a key regulator of the activation

of p110γ by GPCRs (85,147), however, defining the full details of this mechanism was hampered by a paucity of structural information. Complicating structural analysis of p101 is the lack of homologous proteins, with p84 being the only protein with greater than 20% sequence identity in the human proteome. Our p101 structural model validated and defined at high resolution the presence of a Gβγ binding surface on the GBD of p101 (86). The structural similarity of the α/β barrel and the GBD of p101 with the lipid binding surfaces of the lipid kinases diacylglycerol kinase and sphingosine kinase (200) support the idea that the GBD participates in membrane binding upon Gβγ activation. Cellular studies revealed that Gβγ was able to activate membrane localized p110γ, suggesting that Gβγ may orient p110γ in a catalytically competent state (205). Our structure reveals how the GBD participates in membrane and Gβγ binding, which orients the kinase domain for catalysis. Once recruited to the membrane, the p110γ-p101 complex can engage a second Gβγ binding site located on the helical domain of p110γ, leading to full activation. Further structural analysis of the GBD bound to Gβγ will be required to narrow down the exact molecular details of GPCR activation.

The ability of p110γ to generate discrete PIP_3 signals upon activation by a unique set of upstream stimuli is critical to their role in immune cells (144) and is ultimately controlled by the p101 and p84 regulatory subunits. This has been highlighted by responses in neutrophils and mast cells, where p101 complexes mediate cell migration, and p84 complexes mediate reactive oxide production and degranulation (83,92). Various stimuli have been identified that can activate p110γ, including G-protein coupled receptors (85) , Ras (93), Toll like receptors (TLR, mediated by Rab8 activation) (82,206), and the IgE antigen receptor (partially mediated by protein kinase C phosphorylation of p110γ) (141). The p101 and p84 regulatory subunits confer the ability to be preferentially stimulated by a specific subset of these stimuli. The p110γ-p84 complex is uniquely sensitive to Ras activation (84), and is less responsive to signals downstream of GPCRs in comparison to the p101 complex (185). Our TIRF microscopy data reveals how p110γ-p101 is uniquely situated to generate varying PIP_3 responses depending on the different Gβγ membrane surface densities (Figure 4.8). The GBD of p101 uniquely responds to low Gβγ surface densities and allows for distinct p110γ-p101 stimulated PIP_3 responses compared to p110γ-p84. In combination with the membrane localized activators Ras and Rab8 this allows for a multi-faceted set of PIP_3 responses generated by p110γ-p101.

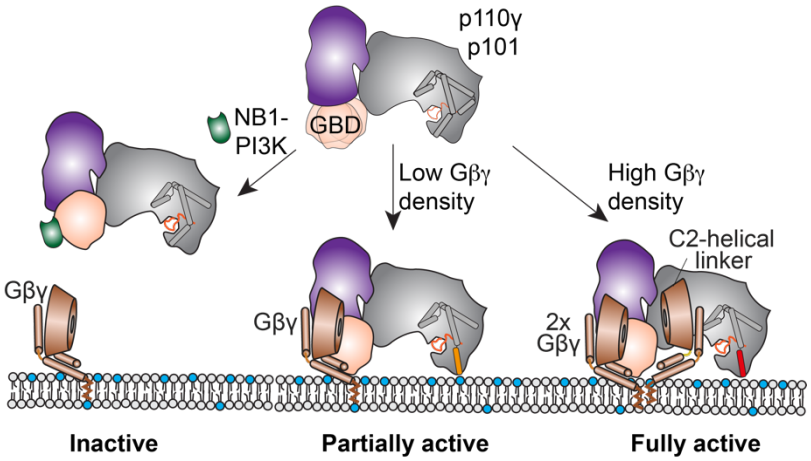

Figure 4.8. Model for regulation of p110γ-p101 activation by Gβγ membrane density. Schematic of how Gβγ subunits can lead to p110γ-p101 activation at different Gβγ surface densities, and how this can be disrupted by the NB1-PIK3R5 nanobody.

Activating mutations in the class I PI3K pathway are the most frequent alterations in human cancer(179), with this primarily driven by oncogenic mutations of p110α (98,128). p110γ is often overexpressed in cancer, specifically in pancreatic ductal adenocarcinoma (54–56,89). Supporting this role of increased expression of p110γ in cancer is the knockdown of a microRNA targeting *PIK3CG* in patients that promotes metastasis in triple negative breast cancer (58). Tumor associated mutations in p110γ are rare compared to p110α (1739 for *PIK3CG* compared to 17,359 for *PIK3CA,* from the COSMIC database as of April 2021 (106)). However, multiple studies have found an association of somatic mutations in *PIK3CG* with cancer development and progression (56,59,60,207). Whether these mutants function within the tumor or the surrounding immune environment remains to be confirmed. Activating oncogenic mutants in the regulatory motif of the kinase domain of p110γ (R1021C) have been identified (177), with bi-allelic inactivating mutations involving the same site (R1021P, R982 frameshift) causing primary immunodeficiencies (74). We found oncogenic mutations clustered at ABD and p101 interfaces in *PIK3CG.* These mutants led to increased kinase activity upon Gβγ stimulation, which is explained by the altered interaction between p110γ and p101 as observed by HDX-MS. This may lead to a reorientation of the GBD allowing for increased binding to membranes or lipidated Gβγ. Further analysis of the effect of these mutations on membrane recruitment, and their effects in cells and model organisms, will be required to understand their complete mechanism of regulation.

The association of p110γ in human disease has driven intense interest in the generation of PI3K selective small molecule inhibitors, however, severe side-effects have limited their efficacy, particularly for pan-PI3K

inhibitors (208). Multiple p110γ isoform selective inhibitors are currently in clinical trials for cancer, and are in development for COPD, and inflammatory disease. Inhibition of p110γ has also been found to improve anti-tumor properties of CAR T-cells (73). Regulatory subunits are differentially involved in the onset and progression of p110γ associated diseases. Upregulation of p110γ-p101 is involved in congestive heart failure (140), while p110γ-p84 plays a protective role by maintaining cardiac contractility (71). The p110γ-p101 complex could also be involved in TLR9-induced inflammation (209,210) due to its sensitivity to Rab8 activation downstream of TLRs (82). In pancreatic cancer models, targeting p110γ is protective in cancer development (56), however, its applicability is limited by hepatotoxicity. Therefore, targeting p110γ in these disease states could benefit from specifically inhibiting p110γ-p101 signaling. We have identified the structural basis for how the NB1-PIK3R5 nanobody can selectively inhibit Gβγ activation of the p110γ-p101 complex, which can be used to determine potential advantages of p110γ-p101 specific inhibition in p110γ-linked diseases, and may allow for design of novel therapeutic strategies.

Collectively, our detailed biochemical and structural analysis of the p110γ-p101 complex provides unique insight into the assembly and regulation of PI3Kγ complexes. This work provides a framework for the design of selective modulators outside of the ATP binding pocket, which will be useful to decipher PI3Kγ signaling roles and for the generation of potential therapeutics in inflammatory diseases and cancer.

Chapter 5: Discussion and Future Directions

5.1 Summary of research objectives

PI3Kγ is a lipid kinase of the class I PI3K family with vital roles in immunity and cardiac function. Its ability to integrate a unique set of upstream activating signals depends on the presence of regulatory features in both the p110γ and its binding partners, that are distinct from the other PI3Ks. Since its discovery in myeloid cells in the 90s, a large cohort of studies have revealed crucial insight into the functioning of this enzyme-the ability of PI3Kγ to be directly activated by GPCRs and small GTPases, the association of p110γ with p101 and p84 and the roles of these complexes. However, many knowledge gaps still existed with regards to the regulation of this enzyme which prevented us from understanding how it is capable of translating unique signals from the upstream activators into cellular effects.

The first insight into the molecular details of class I PI3Ks came from the crystal structure of a p110γ fragment solved more than 20 years ago (14). The structure revealed a domain organization that was eventually found to be shared across all other p110s. This was immediately followed by the structure of the same fragment with Ras bound to its RBD, a feature that is also shared by the four p110 isoforms (22). Since these discoveries, extensive structural and biochemical studies on the class IA PI3Ks have revealed molecular details on the complexes of p85 with all three of its p110 partners and their regulation downstream of RTKs (33,211,212). On the other hand, progress on the class IB PI3K front had largely slowed until HDX studies provided the first insight into its regulation by GPCRs (213). Since this study, the work presented in this dissertation provides the first major advancement in our understanding of the molecular basis of PI3Kγ regulation.

As part of this dissertation, I have used a combination of cutting-edge biochemical and structural tools to define regulatory features that distinguish PI3Kγ from its class IA PI3K counterparts. In chapter 2, I described the unique auto-inhibitory C-terminal motif in p110γ and its roles in disease and inhibition. In chapter 3, I described the characterization of molecular tools that can be used to bias activating inputs into the different PI3Kγ complexes and potentially study the cellular effects of regulation. This was followed by studies on the p110γ-p101 complex in chapter 4 which presents the first structural insight into a complete class IB PI3K complex. This revealed a unique mode of assembly between p110γ and its regulatory partners, highlighting how these partners differ from p85. In

this final chapter, I will summarize the findings of this thesis, the implications of these findings and my ideas on future studies into PI3Kγ regulation.

5.2 The regulatory C-terminal motif in p110γ

The PI3Kγ isoform is critical to maintain immune system function, and plays important roles in the regulation of the tumor microenvironment (11,16). Key to the involvement in these physiological roles is the recruitment of the enzyme to the plasma membrane by membrane localized activators such as Ras and the Gβγ subunit of GPCRs (27,40). Upon binding the membrane, a regulatory motif at the C-terminus of p110γ undergoes reorganization leading to an active form of the enzyme. This motif is shared amongst all class I p110s, but in class IA p110s it is maintained in the inactive conformation by inhibitory contacts with p85 (13). p110γ does not have inhibitory partners but still requires activating signals that recruit the enzyme to the membrane. This implied the presence of an autoregulatory mechanism within p110γ to keep the enzyme inactive in the absence of activators. Bi-allelic loss of function mutations in p110γ are a driver of human immunodeficiencies, and multiple inactivating mutations located in the C-terminal regulatory motif of the kinase domain have been described (74,107). There have also been numerous reports of overexpression and single nucleotide variants in *PIK3CG* linked to cancer development in multiple tissues (54,57–60,60,61). Oncogenic mutations in *PIK3CG* are widely distributed, which is distinct from the oncogenic hotspot mutations seen in the helical and kinase domain of *PIK3CA*. However, there has been limited analysis of the functional consequences of oncogenic *PIK3CG* mutants. Inhibiting PI3Kγ has shown promise as an immunomodulatory agent due to the enzyme's role in blocking the recruitment of cytotoxic lymphocytes to the tumor site (214,215).

In chapter 2, I described the characterization of both activating and inactivating disease-linked mutations in R1021 in the regulatory motif of the p110γ kinase domain. R1021 in the kα8 helix is conserved across all class I PI3Ks and makes a number of hydrogen bonds with residues in kα10 and kα11. HDX-MS experiments indicated that the inactivating immunodeficiency-linked mutation R1021P leads to disruption of the secondary structure in the C-terminal regulatory motif while the cancer-linked activating mutation R1021C pre-organizes the motif for membrane binding. This work corroborates the important role of the C-terminal regulatory motif in controlling PI3K lipid kinase activity. The orientation of this motif is critical in the regulation of all class I PI3Ks, although this is regulated by different molecular mechanisms in p110α, p110β, p110δ, and p110γ. In class IA PI3Ks, the nSH2 of p85 interacts

with kα10 (129,139), while the cSH2 contacts kα7, kα8, kα11 and kα12 for p110β and p110δ (110,127). The p110γ isoform is unique in that its C-terminal motif adopts an inhibited conformation through locking interactions such as those made by R1021 and W1080. The importance of the C-terminal regulatory motif in controlling p110γ activity is also underscored by post-translational modifications both in a residue in the motif (T1024) (18) and in an adjacent region of helical domain (S582) (50).

The regulatory C-terminal motif was shown to be manipulated by AZ2, a novel type II-like kinase inhibitor that preferentially targets an active conformation of PI3Kγ (94). This was mediated through a cyclopropyl moiety on the inhibitor, which putatively alters the orientation of the activation loop, leading to disruption of the inhibitory interactions on the C-terminal regulatory motif. Many of the changes observed for this inhibitor were similar to those seen in the R1021C mutant. HDX-MS of multiple clinically relevant inhibitors with PI3Kγ indicated that a number of these molecules were also selective for the active conformation. The crystal structure of p110γ with one such inhibitor, Gedatolisib revealed that the inhibitor reorganized the regulatory motif through extensive interactions with the activation loop, unlike IPI-549, an inhibitor that was not conformationally selective. Given the similarity in HDX-MS differences between the R1021C mutant and p110γ bound to Gedatolisib, we explored if conformationally selective inhibitors could target mutants more potently over the wild type enzyme. In line with this, Gedatolisib showed increased potency with a ~3-fold decrease in IC_{50} values. These results provide a basic framework for designing oncogenic PI3K specific inhibitors through further optimisation of the inhibitor moieties in the activation loop binding region. Further exploration of the dynamic regulation of the C-terminal regulatory motif of other class I PI3Ks may reveal more unique approaches to develop therapeutics for PI3K related human diseases. For instance, PI3Kα is a major therapeutic target in cancer. A major mutation hotspot in p110α is the regulatory C-terminal motif (examples- R992Q, M1043L, H1047R and G1049R). Hence, exploring the effects of mutations and inhibitors on the orientation of the motif would be useful in selectively targeting mutants and reducing off-target effects.

5.3 Nanobodies as tools to modulate PI3Kγ signaling

Small molecule inhibitors of class I PI3Ks are in clinical and pre-clinical development for cancer, immune disorders, developmental disorders, and inflammatory disorders. Partially limiting this approach is the severe side effects associated with pan-PI3K ATP-competitive inhibitors (180). Further development of biomolecules that can

selectively modulate distinct PI3K isoforms and complexes will be critical in fully understanding PI3K signaling, and may prove useful as therapeutics for multiple human diseases. In chapter 3, I described an HDX-MS optimized flow-path for the rapid identification of a panel of class IB binding nanobodies, identifying nanobodies that selectively modulated different PI3Kγ complexes and enabled high resolution structural studies.

Nanobodies are rapidly emerging as therapeutics due to ease of large-scale production, small size and high affinity for specific epitopes. This is highlighted by their utilization as neutralizing agents blocking cellular entry of betacoronaviruses, including SARS CoV-1/2 and MERS CoV (167,168). A complication of generating optimized nanobodies is the extensive screening required to identify the epitopes of these molecules. In chapter 3, I outlined how HDX-MS can be utilized to rapidly identify epitopes for nanobodies and conformational changes induced upon binding. HDX-MS is a well-established technique for efficiently defining antibody binding sites for biopharmaceuticals (183), and has been used to define nanobody binding sites (161,184). The identification of the NB1-PIK3R5 nanobody, which stabilized the dynamic C-terminus of the p101 subunit, allowed us to obtain a high-resolution map of the p110γ-p101 complex by cryo-EM. Overall, this HDX-MS based approach provides a repeatable method to rapidly identify the most suitable nanobodies to optimize structural studies.

In addition, combined HDX-MS and EM studies revealed multiple nanobodies that bound at critical regulatory interfaces involved in the binding of Ras and Gβγ in both p110γ and p101. We identified two nanobodies (NB6-PIK3CG, NB7-PIK3CG) that bound to the RBD in p110γ, which contains the Ras binding interface (93). Kinase activity assays with one such nanobody showed inhibition of Ras-mediated activation. Intriguingly, this nanobody was found to be a biased inhibitor of p110γ-p84 activation over p110γ-p101 in line with Ras being crucial for the activity of this complex *in vivo* (84). We also identified NB1-PIK3R5, a nanobody that could preferentially target activation of the p110γ-p101 complex. This nanobody bound the Gβγ binding site in p101 (85,185) greatly reducing the increased sensitivity of this complex to activation downstream of GPCRs. Selectively inhibiting the p110γ-p101 complex has potential applications and advantages in targeting p110γ in disease. In heart failure, the p110γ-p101 complex is upregulated (71,140) and this complex is proposed to drive TLR-mediated inflammation (48). Overall, the HDX-focused approach presented in chapter 3 identified a wide variety of biomolecules that were useful in both high-resolution structural analysis and as selective modulators of PI3K activity. This approach can be employed for other large multi-component protein complexes, and is uniquely well-suited to develop and identify biomolecules that can allosterically modulate enzyme activity outside of the active site.

5.4 Molecular basis of p110γ-p101 assembly and regulation

The association of p110γ with the p84 or p101 regulatory subunits is absolutely critical to its ability in mediating physiological roles (83,92,185). Understanding the roles of these subunits in regulation is also key in designing novel therapeutics for inflammatory diseases (66,146,202) and immunomodulatory cancer treatment (63,90). Therefore, obtaining the molecular details of PI3Kγ heterodimers constitutes a major advancement in the PI3K field. In chapter 4, I described our collaborative effort to structurally characterize the p110γ-p101 complex.

Our cryo-EM structure of p110γ-p101 revealed important differences in the assembly of catalytic and regulatory subunits between class IA and class IB PI3Ks, and provided novel insight into PI3Kγ regulation. The structure showed an evolutionarily well-conserved binding surface between p101 subunit and p110γ. The interfacial regions on p101 were also conserved in p84 indicating a shared mode of assembly with p110γ. Unlike in class IA p110s, the p110γ ABD does not directly bind p101, but instead coordinates the p101 interaction site on the RBD-C2 linker. The architecture of the p110γ-p101 complex also revealed a novel role for p101 in mediating membrane and Gβγ binding. The structural similarity of the α/β barrel and the GBD of p101 with the lipid binding surfaces of the lipid kinases diacylglycerol kinase and sphingosine kinase (200) further support the idea that the GBD participates in membrane binding. Our p101 structural model also validated at high resolution the presence of a Gβγ binding surface on the GBD of p101 (86). Once recruited to the membrane, the p110γ-p101 complex can engage a second Gβγ binding site located on the helical domain of p110γ, leading to full activation. Further structural analysis of the GBD bound to Gβγ will be required to narrow down the exact molecular details of GPCR activation.

The p101 and p84 regulatory subunits control distinct physiological functions. This has been highlighted by responses in neutrophils and mast cells, where p101 complexes mediate cell migration, and p84 complexes mediate reactive oxide production and degranulation (83,92). The p101 and p84 regulatory subunits confer the ability to be preferentially stimulated by a specific subset of these stimuli. The p110γ-p84 complex is uniquely sensitive to Ras activation (84), and is less responsive to signals downstream of GPCRs relative to the p101 complex (185). Our TIRF microscopy data revealed how p110γ-p101 is uniquely situated to generate varying PIP_3 responses depending on the different Gβγ membrane surface densities. The GBD of p101 is capable of responding to low Gβγ surface densities and allows for distinct p110γ-p101 stimulated PIP_3 responses. On the other hand, the p110γ-p84 complex responds

largely to high membrane densities of Gβγ due to the presence of a singular binding site in p110γ. This potentially explains the requirement of Ras for robust p110γ-p84 activation. At low surface densities of Gβγ, Ras can potentially work in tandem to effectively recruit the complex to the membrane. Hence, p110γ-p84 requires co-stimulation by Ras and GPCR inputs while p110γ-p101 is able to be efficiently activated by signals from GPCRs only.

Activating mutations in the class I PI3K pathway are the most frequent alterations in human cancer(179), with this primarily driven by mutations in the p110α isozyme (98,128). Although, tumor associated mutations in p110γ are rare compared to p110α, multiple studies have found an association of somatic mutations in *PIK3CG* with cancer development and progression (56,59,60,207). We found several oncogenic mutations clustered at the ABD and p101 interfaces in *PIK3CG*. Our preliminary HDX-MS data suggested that these mutants led to increased kinase activity upon Gβγ stimulation, potentially through an altered interaction between p110γ and p101. Further analysis of the effect of these mutations on membrane recruitment, and their effects in cells and model organisms, will be required to understand their complete mechanism of regulation.

The association of p110γ in human disease has driven intense interest in the generation of PI3K selective small molecule inhibitors, however, severe side-effects have limited their efficacy, particularly for pan-PI3K inhibitors (208). We identified the structural basis for how the NB1-PIK3R5 nanobody can selectively inhibit Gβγ activation of the p110γ-p101 complex, which can be used to determine potential advantages of p110γ-p101 specific inhibition in p110γ-linked diseases, and may allow for design of novel therapeutic strategies.

In summary, the detailed biochemical and structural analysis of the p110γ-p101 described in chapter 4 provides unique insight into the assembly and regulation of PI3Kγ complexes. This work will be useful to decipher PI3Kγ signaling roles and for the generation of potential therapeutics in inflammatory diseases and cancer.

5.5 Future Directions

Class I PI3Ks are important signaling proteins with roles in growth, survival, metabolism, cytoskeleton and immunity. All members of this enzyme family are implicated in a host of disease states and it is therefore essential that we understand the regulatory features in order to target them better in therapy. p110γ contains a regulatory C-terminal motif that keeps the activation loop in the inactive conformation in the absence of signals recruiting the enzyme to the membrane. The work described in chapter 2 showed that mutations disrupting these regulatory

interactions without affecting secondary structure can putatively pre-organize the enzyme to adopt an active conformation. Mutations in p110α encoded by the PIK3CA gene represent some of the most frequent drivers of human cancers and many of these mutations cluster to the C-terminal regulatory motif. This underscores the need of a similar approach to study the role of this motif in p110α. The mutations in the C-terminal motif have long been thought to increase membrane binding owing to most of them introducing a positive residue near the end of the protein (H1047R, G1049R). Intriguingly, analysis of existing crystal structures of WT p110α and a mutant showed that the region of the protein corresponding to kα12 in p110γ actually adopts different conformations in the two structures. This could indicate the presence of an autoinhibitory mechanism in the regulatory motif on p110α as well. PI3Kα is the target of numerous inhibitors, both approved (Alpelisib) and in clinical trials. The work presented in this dissertation showed how inhibitors interacting with the activation loop of p110γ were conformationally selective. Using a similar approach, p110α inhibitors can be tested to see if some of these molecules can preferentially target mutants. These studies could facilitate the development of better small molecules targeting this very clinically relevant isoform in disease.

The data presented in chapter 4 represents the first structural model of a complete PI3Kγ complex. This showed a novel mode of assembly between the catalytic and regulatory subunits in addition to elucidating the mechanism of activation by Gβγ. This study also provides exciting new avenues for further understanding PI3Kγ regulation. Gβγ binds to two distinct sites on the p110γ-p101 complex. Binding to p110γ is dependent on the orientation of the C2-helical linker with mutations in this linker inhibiting activation. This mode of binding is conserved with p110β, the only other class I PI3K that is activated by GPCRs (216). On the other hand, the p101 GBD represents a unique regulatory interface that is specific to only the p110γ-p101 complex. Understanding molecular details of how Gβγ binds to the GBD would therefore be useful to understand how this interaction compares with other downstream effectors of the GPCR subunit. Such studies could also potentially drive the development of molecules targeting this interface in disease. Gβγ can only interact with PI3Kγ when localized to a membrane presenting a potential challenge for such a structural study. This could be resolved by bringing Gβγ and p101 together spatially by using fusions of Gβγ either directly with p101 or with the nanobody that binds to the p101 PBD. HDX-MS can then be used to verify binding of Gβγ with the GBD, after which high resolution structural studies can be used to reveal molecular details of this interface.

Given the findings of this thesis and numerous previous studies on class IA PI3Ks, p84 remains the last class I PI3K subunit to be structurally characterized. Sequence alignment of p101 with p84 indicates limited conservation with most of the conserved residues forming the primary interface with p110γ (PBD). A key difference between the two PI3Kγ complexes is the requirement of different activating inputs for physiological functions. Structural and biochemical characterization of the p110γ-p84 complex and its activation by Ras and GPCRs would provide further crucial insight into the regulatory differences from the p110γ-p101 complex. Another difference between p101 and p84 is the C-terminal domain. In p101, this domain is the GBD, responsible for Gβγ binding. Sequence analysis indicates a general lack of conservation in this region between the two regulatory subunits. Hence, structural characterization of p110γ-p84 would also provide novel insight into the role of this domain in p84. Such a structural study could be potentially facilitated by the p84-binding nanobody characterized as part of this dissertation.

5.6. Conclusion

The class IB PI3Kγ complexes are master regulators of immune functions with crucial roles in cell migration and inflammatory response. Studying the molecular basis for the regulation of these complexes is therefore crucial in understanding how diverse regulatory inputs from receptors and membrane associated proteins translate into distinct cellular outputs. Inhibitors targeting PI3Kγ are currently being investigated for use in conjunction with cancer immunotherapy and in inflammatory disease. Elucidating the unique regulatory features in PI3Kγ that are distinct from other class I PI3Ks would be useful in the design of targeted therapies with fewer off-target effects. In line with these goals, this thesis describes regulatory features in p110γ , its assembly with p101 and the regulation of the complex by GPCRs. In addition, characterization of nanobodies that bind novel regulatory interfaces provide novel avenues to investigate missing links between regulation and function *in vivo* and could potentially facilitate development of therapeutics that target specific PI3Kγ complexes in disease.

Bibliography

1. Balla T. Phosphoinositides: Tiny Lipids With Giant Impact on Cell Regulation. Physiol Rev. 2013 Jul;93(3):1019–137.

2. Traynor-Kaplan AE, Harris AL, Thompson BL, Taylor P, Sklar LA. An inositol tetrakisphosphate-containing phospholipid in activated neutrophils. Nature. 1988 Jul;334(6180):353–6.

3. Auger KR, Serunian LA, Soltoff SP, Libby P, Cantley LC. PDGF-dependent tyrosine phosphorylation stimulates production of novel polyphosphoinositides in intact cells. Cell. 1989 Apr 7;57(1):167–75.

4. Whitman M, Downes CP, Keeler M, Keller T, Cantley L. Type I phosphatidylinositol kinase makes a novel inositol phospholipid, phosphatidylinositol-3-phosphate. Nature. 1988 Apr;332(6165):644–6.

5. Damen JE, Liu L, Rosten P, Humphries RK, Jefferson AB, Majerus PW, et al. The 145-kDa protein induced to associate with Shc by multiple cytokines is an inositol tetraphosphate and phosphatidylinositol 3,4,5-triphosphate 5-phosphatase. Proc Natl Acad Sci. 1996 Feb 20;93(4):1689–93.

6. Kisseleva MV, Wilson MP, Majerus PW. The Isolation and Characterization of a cDNA Encoding Phospholipid-specific Inositol Polyphosphate 5-Phosphatase. J Biol Chem. 2000 Jun 30;275(26):20110–6.

7. Bilanges B, Posor Y, Vanhaesebroeck B. PI3K isoforms in cell signaling and vesicle trafficking. Nat Rev Mol Cell Biol. 2019 Sep;20(9):515–34.

8. Alessi DR, James SR, Downes CP, Holmes AB, Gaffney PR, Reese CB, et al. Characterization of a 3-phosphoinositide-dependent protein kinase which phosphorylates and activates protein kinase Balpha. Curr Biol CB. 1997 Apr 1;7(4):261–9.

9. Lučić I, Rathinaswamy MK, Truebestein L, Hamelin DJ, Burke JE, Leonard TA. Conformational sampling of membranes by Akt controls its activation and inactivation. Proc Natl Acad Sci. 2018 Apr 24;115(17):E3940–9.

10. Sarbassov DD. Phosphorylation and Regulation of Akt/PKB by the Rictor-mTOR Complex. Science. 2005 Feb 18;307(5712):1098–101.

11. Fruman DA, Chiu H, Hopkins BD, Bagrodia S, Cantley LC, Abraham RT. The PI3K Pathway in Human Disease. Cell. 2017 Aug;170(4):605–35.

12. Philippon H, Brochier-Armanet C, Perrière G. Evolutionary history of phosphatidylinositol- 3-kinases: ancestral origin in eukaryotes and complex duplication patterns. BMC Evol Biol. 2015 Dec;15(1):226.

13. Burke JE. Structural Basis for Regulation of Phosphoinositide Kinases and Their Involvement in Human Disease. Mol Cell. 2018 Sep;71(5):653–73.

14. Walker EH, Perisic O, Ried C, Stephens L, Williams RL. Structural insights into phosphoinositide 3-kinase catalysis and signaling. Nature. 1999 Nov;402(6759):313–20.

15. Eickholt BJ, Ahmed AI, Davies M, Papakonstanti EA, Pearce W, Starkey ML, et al. Control of Axonal Growth and Regeneration of Sensory Neurons by the p110δ PI 3-Kinase. McCabe B, editor. PLoS ONE. 2007 Sep 12;2(9):e869.

16. Okkenhaug K. Signaling by the Phosphoinositide 3-Kinase Family in Immune Cells. Annu Rev Immunol. 2013 Mar 21;31(1):675–704.

17. Okkenhaug K, Vanhaesebroeck B. PI3K in lymphocyte development, differentiation and activation. Nat Rev Immunol. 2003 Apr;3(4):317–30.

18. Perino A, Ghigo A, Ferrero E, Morello F, Santulli G, Baillie GS, et al. Integrating Cardiac PIP3 and cAMP Signaling through a PKA Anchoring Function of p110γ. Mol Cell. 2011 Apr;42(1):84–95.

19. Burke JE, Williams RL. Synergy in activating class I PI3Ks. Trends Biochem Sci. 2015 Feb;40(2):88–100.

20. Vanhaesebroeck B, Guillermet-Guibert J, Graupera M, Bilanges B. The emerging mechanisms of isoform-specific PI3K signaling. Nat Rev Mol Cell Biol. 2010 May;11(5):329–41.

21. Buckles TC, Ziemba BP, Masson GR, Williams RL, Falke JJ. Single-Molecule Study Reveals How Receptor and Ras Synergistically Activate PI3Kα and PIP3 Signaling. Biophys J. 2017 Dec;113(11):2396–405.

22. Pacold ME, Suire S, Perisic O, Lara-Gonzalez S, Davis CT, Walker EH, et al. Crystal structure and functional analysis of Ras binding to its effector phosphoinositide 3-kinase gamma. Cell. 2000 Dec 8;103(6):931–43.

23. Rodriguez-Viciana P, Warne PH, Dhand R, Vanhaesebroeck B, Gout I, Fry MJ, et al. Phosphatidylinositol-3-OH kinase as a direct target of Ras. Nature. 1994 Aug 18;370(6490):527–32.

24. Siempelkamp BD, Rathinaswamy MK, Jenkins ML, Burke JE. Molecular mechanism of activation of class IA phosphoinositide 3-kinases (PI3Ks) by membrane-localized HRas. J Biol Chem. 2017 Jul;292(29):12256–66.

25. Fritsch R, de Krijger I, Fritsch K, George R, Reason B, Kumar MS, et al. RAS and RHO families of GTPases directly regulate distinct phosphoinositide 3-kinase isoforms. Cell. 2013 May 23;153(5):1050–63.

26. Kurosu H, Maehama T, Okada T, Yamamoto T, Hoshino S, Fukui Y, et al. Heterodimeric phosphoinositide 3-kinase consisting of p85 and p110beta is synergistically activated by the betagamma subunits of G proteins and phosphotyrosyl peptide. J Biol Chem. 1997 Sep 26;272(39):24252–6.

27. Stephens L, Smrcka A, Cooke FT, Jackson TR, Sternweis PC, Hawkins PT. A novel phosphoinositide 3 kinase activity in myeloid-derived cells is activated by G protein beta gamma subunits. Cell. 1994 Apr 8;77(1):83–93.

28. Carpenter CL, Auger KR, Chanudhuri M, Yoakim M, Schaffhausen B, Shoelson S, et al. Phosphoinositide 3-kinase is activated by phosphopeptides that bind to the SH2 domains of the 85-kDa subunit. J Biol Chem. 1993 May 5;268(13):9478–83.

29. Yu J, Zhang Y, McIlroy J, Rordorf-Nikolic T, Orr GA, Backer JM. Regulation of the p85/p110 phosphatidylinositol 3'-kinase: stabilization and inhibition of the p110alpha catalytic subunit by the p85 regulatory subunit. Mol Cell Biol. 1998 Mar;18(3):1379–87.

30. Yu J, Wjasow C, Backer JM. Regulation of the p85/p110α Phosphatidylinositol 3′-Kinase. J Biol Chem. 1998 Nov;273(46):30199–203.

31. Burke JE, Vadas O, Berndt A, Finegan T, Perisic O, Williams RL. Dynamics of the Phosphoinositide 3-Kinase p110δ Interaction with p85α and Membranes Reveals Aspects of Regulation Distinct from p110α. Structure. 2011 Aug;19(8):1127–37.

32. Burke JE, Williams RL. Dynamic steps in receptor tyrosine kinase mediated activation of class IA phosphoinositide 3-kinases (PI3K) captured by H/D exchange (HDX-MS). Adv Biol Regul. 2013 Jan;53(1):97–110.

33. Zhang X, Vadas O, Perisic O, Anderson KE, Clark J, Hawkins PT, et al. Structure of Lipid Kinase p110β/p85β Elucidates an Unusual SH2-Domain-Mediated Inhibitory Mechanism. Mol Cell. 2011 Mar;41(5):567–78.

34. Dbouk HA, Pang H, Fiser A, Backer JM. A biochemical mechanism for the oncogenic potential of the p110 catalytic subunit of phosphoinositide 3-kinase. Proc Natl Acad Sci. 2010 Nov 16;107(46):19897–902.

35. Burke JE, Perisic O, Masson GR, Vadas O, Williams RL. Oncogenic mutations mimic and enhance dynamic events in the natural activation of phosphoinositide 3-kinase p110α (*PIK3CA*). Proc Natl Acad Sci. 2012 Sep 18;109(38):15259–64.

36. Tang X, Downes CP. Purification and Characterization of Gβγ-responsive Phosphoinositide 3-Kinases from Pig Platelet Cytosol. J Biol Chem. 1997 May;272(22):14193–9.

37. Stephens L, Smrcka A, Jackson TR, Stemweis PC, Hawkins PT, Hall B. A Novel Phosphoinositide 3 Kinase Activity in Myeloid-Derived Cells Is Activated by G Protein Subunits. Cell. 1994 Apr 8;77(1):83-93.

38. Gentile DR, Rathinaswamy MK, Jenkins ML, Moss SM, Siempelkamp BD, Renslo AR, et al. Ras Binder Induces a Modified Switch-II Pocket in GTP and GDP States. Cell Chem Biol. 2017 Dec;24(12):1455-1466.e14.

39. Deladeriere A, Gambardella L, Pan D, Anderson KE, Hawkins PT, Stephens LR. The regulatory subunits of PI3Kγ control distinct neutrophil responses. Sci Signal. 2015 Jan 20;8(360):ra8.

40. Suire S, Condliffe AM, Ferguson GJ, Ellson CD, Guillou H, Davidson K, et al. Gβγs and the Ras binding domain of p110γ are both important regulators of PI3Kγ signaling in neutrophils. Nat Cell Biol. 2006 Nov;8(11):1303–9.

41. Luo L, Wall AA, Yeo JC, Condon ND, Norwood SJ, Schoenwaelder S, et al. Rab8a interacts directly with PI3Kγ to modulate TLR4-driven PI3K and mTOR signaling. Nat Commun. 2014 Dec;5(1):4407.

42. Hilger D, Masureel M, Kobilka BK. Structure and dynamics of GPCR signaling complexes. Nat Struct Mol Biol. 2018 Jan;25(1):4–12.

43. Vadas O, Dbouk HA, Shymanets A, Perisic O, Burke JE, Abi Saab WF, et al. Molecular determinants of PI3K -mediated activation downstream of G-protein-coupled receptors (GPCRs). Proc Natl Acad Sci. 2013 Nov 19;110(47):18862–7.

44. Rynkiewicz NK, Anderson KE, Suire S, Collins DM, Karanasios E, Vadas O, et al. Gβγ is a direct regulator of endogenous p101/p110γ and p84/p110γ PI3Kγ complexes in mouse neutrophils. Sci Signal. 2020 Nov 3;13(656).

45. Shymanets A, Prajwal null, Bucher K, Beer-Hammer S, Harteneck C, Nürnberg B. p87 and p101 subunits are distinct regulators determining class IB phosphoinositide 3-kinase (PI3K) specificity. J Biol Chem. 2013 Oct 25;288(43):31059–68.

46. Stephens LR, Eguinoa A, Erdjument-Bromage H, Lui M, Cooke F, Coadwell J, et al. The G beta gamma sensitivity of a PI3K is dependent upon a tightly associated adaptor, p101. Cell. 1997 Apr 4;89(1):105–14.

47. Schmid MC, Avraamides CJ, Dippold HC, Franco I, Foubert P, Ellies LG, et al. Receptor tyrosine kinases and TLR/IL1Rs unexpectedly activate myeloid cell PI3kγ, a single convergent point promoting tumor inflammation and progression. Cancer Cell. 2011 Jun 14;19(6):715–27.

48. Luo L, Wall AA, Tong SJ, Hung Y, Xiao Z, Tarique AA, et al. TLR Crosstalk Activates LRP1 to Recruit Rab8a and PI3Kγ for Suppression of Inflammatory Responses. Cell Rep. 2018 Sep 11;24(11):3033–44.

49. Suire S, Coadwell J, Ferguson GJ, Davidson K, Hawkins P, Stephens L. p84, a new Gbetagamma-activated regulatory subunit of the type IB phosphoinositide 3-kinase p110gamma. Curr Biol CB. 2005 Mar 29;15(6):566–70.

50. Walser R, Burke JE, Gogvadze E, Bohnacker T, Zhang X, Hess D, et al. PKCβ phosphorylates PI3Kγ to activate it and release it from GPCR control. PLoS Biol. 2013;11(6):e1001587.

51. Kurig B, Shymanets A, Bohnacker T, Prajwal null, Brock C, Ahmadian MR, et al. Ras is an indispensable coregulator of the class IB phosphoinositide 3-kinase p87/p110gamma. Proc Natl Acad Sci U S A. 2009 Dec 1;106(48):20312–7.

52. Bohnacker T, Marone R, Collmann E, Calvez R, Hirsch E, Wymann MP. PI3Kgamma adaptor subunits define coupling to degranulation and cell motility by distinct PtdIns(3,4,5)P3 pools in mast cells. Sci Signal. 2009 Jun 9;2(74):ra27.

53. Wilson LS, Baillie GS, Pritchard LM, Umana B, Terrin A, Zaccolo M, et al. A phosphodiesterase 3B-based signaling complex integrates exchange protein activated by cAMP 1 and phosphatidylinositol 3-kinase signals in human arterial endothelial cells. J Biol Chem. 2011 May 6;286(18):16285–96.

54. Edling CE, Selvaggi F, Buus R, Maffucci T, Di Sebastiano P, Friess H, et al. Key role of phosphoinositide 3-kinase class IB in pancreatic cancer. Clin Cancer Res Off J Am Assoc Cancer Res. 2010 Oct 15;16(20):4928–37.

55. Falasca M, Maffucci T. Targeting p110gamma in gastrointestinal cancers: attack on multiple fronts. Front Physiol. 2014;5:391.

56. Torres C, Mancinelli G, Cordoba-Chacon J, Viswakarma N, Castellanos K, Grimaldo S, et al. p110γ deficiency protects against pancreatic carcinogenesis yet predisposes to diet-induced hepatotoxicity. Proc Natl Acad Sci U S A. 2019 Jul 16;116(29):14724–33.

57. Dituri F, Mazzocca A, Lupo L, Edling CE, Azzariti A, Antonaci S, et al. PI3K class IB controls the cell cycle checkpoint promoting cell proliferation in hepatocellular carcinoma. Int J Cancer. 2012 Jun 1;130(11):2505–13.

58. Wang J, Li M, Han X, Wang H, Wang X, Ma G, et al. MiR-1976 knockdown promotes epithelial-mesenchymal transition and cancer stem cell properties inducing triple-negative breast cancer metastasis. Cell Death Dis. 2020 Jul 3;11(7):500.

59. Ge Y, He Z, Xiang Y, Wang D, Yang Y, Qiu J, et al. The identification of key genes in nasopharyngeal carcinoma by bioinformatics analysis of high-throughput data. Mol Biol Rep. 2019 Jun;46(3):2829–40.

60. Rodrigues DN, Rescigno P, Liu D, Yuan W, Carreira S, Lambros MB, et al. Immunogenomic analyzes associate immunological alterations with mismatch repair defects in prostate cancer. J Clin Invest. 2018 Nov 1;128(11):5185.

61. Shu X, Gu J, Huang M, Tannir NM, Matin SF, Karam JA, et al. Germline genetic variants in somatically significantly mutated genes in tumors are associated with renal cell carcinoma risk and outcome. Carcinogenesis. 2018 May 28;39(6):752–7.

62. Carter H, Samayoa J, Hruban RH, Karchin R. Prioritization of driver mutations in pancreatic cancer using cancer-specific high-throughput annotation of somatic mutations (CHASM). Cancer Biol Ther. 2010 Sep 15;10(6):582–7.

63. Kaneda MM, Messer KS, Ralainirina N, Li H, Leem CJ, Gorjestani S, et al. PI3Kγ is a molecular switch that controls immune suppression. Nature. 2016 Nov 17;539(7629):437–42.

64. Xie Y, Abel PW, Kirui JK, Deng C, Sharma P, Wolff DW, et al. Identification of upregulated phosphoinositide 3-kinase γ as a target to suppress breast cancer cell migration and invasion. Biochem Pharmacol. 2013 May 15;85(10):1454–62.

65. Heller R, Chang Q, Ehrlich G, Hsieh SN, Schoenwaelder SM, Kuhlencordt PJ, et al. Overlapping and distinct roles for PI3Kbeta and gamma isoforms in S1P-induced migration of human and mouse endothelial cells. Cardiovasc Res. 2008 Oct 1;80(1):96–105.

66. Camps M, Rückle T, Ji H, Ardissone V, Rintelen F, Shaw J, et al. Blockade of PI3Kgamma suppresses joint inflammation and damage in mouse models of rheumatoid arthritis. Nat Med. 2005 Sep;11(9):936–43.

67. Breasson L, Becattini B, Sardi C, Molinaro A, Zani F, Marone R, et al. PI3Kγ activity in leukocytes promotes adipose tissue inflammation and early-onset insulin resistance during obesity. Sci Signal. 2017 Jul 18;10(488).

68. Barber DF, Bartolomé A, Hernandez C, Flores JM, Redondo C, Fernandez-Arias C, et al. PI3Kgamma inhibition blocks glomerulonephritis and extends lifespan in a mouse model of systemic lupus. Nat Med. 2005 Sep;11(9):933–5.

69. Collmann E, Bohnacker T, Marone R, Dawson J, Rehberg M, Stringer R, et al. Transient targeting of phosphoinositide 3-kinase acts as a roadblock in mast cells' route to allergy. J Allergy Clin Immunol. 2013 Oct;132(4):959–68.

70. Sala V, Della Sala A, Ghigo A, Hirsch E. Roles of phosphatidyl inositol 3 kinase gamma (PI3Kγ) in respiratory diseases. Cell Stress. 2021 Mar 8;5(4):40–51.

71. Patrucco E, Notte A, Barberis L, Selvetella G, Maffei A, Brancaccio M, et al. PI3Kgamma modulates the cardiac response to chronic pressure overload by distinct kinase-dependent and -independent effects. Cell. 2004 Aug 6;118(3):375–87.

72. Evans CA, Liu T, Lescarbeau A, Nair SJ, Grenier L, Pradeilles JA, et al. Discovery of a Selective Phosphoinositide-3-Kinase (PI3K)-γ Inhibitor (IPI-549) as an Immuno-Oncology Clinical Candidate. ACS Med Chem Lett. 2016 Sep 8;7(9):862–7.

73. Dwyer CJ, Arhontoulis DC, Rangel Rivera GO, Knochelmann HM, Smith AS, Wyatt MM, et al. Ex vivo blockade of PI3K gamma or delta signaling enhances the antitumor potency of adoptively transferred CD8+ T cells. Eur J Immunol. 2020 Sep;50(9):1386–99.

74. Takeda AJ, Maher TJ, Zhang Y, Lanahan SM, Bucklin ML, Compton SR, et al. Human PI3Kγ deficiency and its microbiota-dependent mouse model reveal immunodeficiency and tissue immunopathology. Nat Commun. 2019 Sep 25;10(1):4364.

75. Hirsch E, Katanaev VL, Garlanda C, Azzolino O, Pirola L, Silengo L, et al. Central role for G protein-coupled phosphoinositide 3-kinase gamma in inflammation. Science. 2000 Feb 11;287(5455):1049–53.

76. Li Z, Jiang H, Xie W, Zhang Z, Smrcka AV, Wu D. Roles of PLC-beta2 and -beta3 and PI3Kgamma in chemoattractant-mediated signal transduction. Science. 2000 Feb 11;287(5455):1046–9.

77. Sasaki T, Irie-Sasaki J, Jones RG, Oliveira-dos-Santos AJ, Stanford WL, Bolon B, et al. Function of PI3Kgamma in thymocyte development, T cell activation, and neutrophil migration. Science. 2000 Feb 11;287(5455):1040–6.

78. Laffargue M, Calvez R, Finan P, Trifilieff A, Barbier M, Altruda F, et al. Phosphoinositide 3-kinase gamma is an essential amplifier of mast cell function. Immunity. 2002 Mar;16(3):441–51.

79. Stoyanov B, Volinia S, Hanck T, Rubio I, Loubtchenkov M, Malek D, et al. Cloning and characterization of a G protein-activated human phosphoinositide-3 kinase. Science. 1995 Aug 4;269(5224):690–3.

80. Schmid MC, Avraamides CJ, Dippold HC, Franco I, Foubert P, Ellies LG, et al. Receptor tyrosine kinases and TLR/IL1Rs unexpectedly activate myeloid cell PI3kγ, a single convergent point promoting tumor inflammation and progression. Cancer Cell. 2011 Jun 14;19(6):715–27.

81. Luo L, Wall AA, Yeo JC, Condon ND, Norwood SJ, Schoenwaelder S, et al. Rab8a interacts directly with PI3Kγ to modulate TLR4-driven PI3K and mTOR signaling. Nat Commun. 2014 Jul 15;5:4407.

82. Luo L, Wall AA, Tong SJ, Hung Y, Xiao Z, Tarique AA, et al. TLR Crosstalk Activates LRP1 to Recruit Rab8a and PI3Kγ for Suppression of Inflammatory Responses. Cell Rep. 2018 Sep 11;24(11):3033–44.

83. Bohnacker T, Marone R, Collmann E, Calvez R, Hirsch E, Wymann MP. PI3Kgamma adaptor subunits define coupling to degranulation and cell motility by distinct PtdIns(3,4,5)P3 pools in mast cells. Sci Signal. 2009 Jun 9;2(74):ra27.

84. Kurig B, Shymanets A, Bohnacker T, Prajwal null, Brock C, Ahmadian MR, et al. Ras is an indispensable coregulator of the class IB phosphoinositide 3-kinase p87/p110gamma. Proc Natl Acad Sci U S A. 2009 Dec 1;106(48):20312–7.

85. Stephens LR, Eguinoa A, Erdjument-Bromage H, Lui M, Cooke F, Coadwell J, et al. The G beta gamma sensitivity of a PI3K is dependent upon a tightly associated adaptor, p101. Cell. 1997 Apr 4;89(1):105–14.

86. Vadas O, Dbouk HA, Shymanets A, Perisic O, Burke JE, Abi Saab WF, et al. Molecular determinants of PI3Kγ-mediated activation downstream of G-protein-coupled receptors (GPCRs). Proc Natl Acad Sci U S A. 2013 Nov 19;110(47):18862–7.

87. Campa CC, Silva RL, Margaria JP, Pirali T, Mattos MS, Kraemer LR, et al. Inhalation of the prodrug PI3K inhibitor CL27c improves lung function in asthma and fibrosis. Nat Commun. 2018 Dec 12;9(1):5232.

88. Thomas M, Edwards MJ, Sawicka E, Duggan N, Hirsch E, Wymann MP, et al. Essential role of phosphoinositide 3-kinase gamma in eosinophil chemotaxis within acute pulmonary inflammation. Immunology. 2009 Mar;126(3):413–22.

89. Kaneda MM, Cappello P, Nguyen AV, Ralainirina N, Hardamon CR, Foubert P, et al. Macrophage PI3Kγ Drives Pancreatic Ductal Adenocarcinoma Progression. Cancer Discov. 2016 Aug;6(8):870–85.

90. De Henau O, Rausch M, Winkler D, Campesato LF, Liu C, Cymerman DH, et al. Overcoming resistance to checkpoint blockade therapy by targeting PI3Kγ in myeloid cells. Nature. 2016 Nov 17;539(7629):443–7.

91. Walker EH, Perisic O, Ried C, Stephens L, Williams RL. Structural insights into phosphoinositide 3-kinase catalysis and signaling. Nature. 1999 Nov 18;402(6759):313–20.

92. Deladeriere A, Gambardella L, Pan D, Anderson KE, Hawkins PT, Stephens LR. The regulatory subunits of PI3Kγ control distinct neutrophil responses. Sci Signal. 2015 Jan 20;8(360):ra8.

93. Pacold ME, Suire S, Perisic O, Lara-Gonzalez S, Davis CT, Walker EH, et al. Crystal structure and functional analysis of Ras binding to its effector phosphoinositide 3-kinase gamma. Cell. 2000 Dec 8;103(6):931–43.

94. Gangadhara G, Dahl G, Bohnacker T, Rae R, Gunnarsson J, Blaho S, et al. A class of highly selective inhibitors bind to an active state of PI3Kγ. Nat Chem Biol. 2019 Apr;15(4):348–57.

95. Vadas O, Burke JE, Zhang X, Berndt A, Williams RL. Structural basis for activation and inhibition of class I phosphoinositide 3-kinases. Sci Signal. 2011 Oct 18;4(195):re2.

96. Burke JE. Structural Basis for Regulation of Phosphoinositide Kinases and Their Involvement in Human Disease. Mol Cell. 2018 Sep;71(5):653–73.

97. Kang S, Denley A, Vanhaesebroeck B, Vogt PK. Oncogenic transformation induced by the p110beta, -gamma, and -delta isoforms of class I phosphoinositide 3-kinase. Proc Natl Acad Sci U S A. 2006 Jan 31;103(5):1289–94.

98. Samuels Y, Velculescu VE. Oncogenic mutations of PIK3CA in human cancers. Cell Cycle Georget Tex. 2004 Oct;3(10):1221–4.

99. Vasan N, Razavi P, Johnson JL, Shao H, Shah H, Antoine A, et al. Double PIK3CA mutations in cis increase oncogenicity and sensitivity to PI3Kα inhibitors. Science. 2019 Nov 8;366(6466):714–23.

100. Lindhurst MJ, Parker VER, Payne F, Sapp JC, Rudge S, Harris J, et al. Mosaic overgrowth with fibroadipose hyperplasia is caused by somatic activating mutations in PIK3CA. Nat Genet. 2012 Jun 24;44(8):928–33.

101. Angulo I, Vadas O, Garçon F, Banham-Hall E, Plagnol V, Leahy TR, et al. Phosphoinositide 3-kinase δ gene mutation predisposes to respiratory infection and airway damage. Science. 2013 Nov 15;342(6160):866–71.

102. Dornan GL, Siempelkamp BD, Jenkins ML, Vadas O, Lucas CL, Burke JE. Conformational disruption of PI3Kδ regulation by immunodeficiency mutations in PIK3CD and PIK3R1. Proc Natl Acad Sci U S A. 2017 Feb 21;114(8):1982–7.

103. Lucas CL, Chandra A, Nejentsev S, Condliffe AM, Okkenhaug K. PI3Kδ and primary immunodeficiencies. Nat Rev Immunol. 2016 Nov;16(11):702–14.

104. AACR Project GENIE Consortium. AACR Project GENIE: Powering Precision Medicine through an International Consortium. Cancer Discov. 2017 Aug;7(8):818–31.

105. Lowery MA, Bradley M, Chou JF, Capanu M, Gerst S, Harding JJ, et al. Binimetinib plus Gemcitabine and Cisplatin Phase I/II Trial in Patients with Advanced Biliary Cancers. Clin Cancer Res Off J Am Assoc Cancer Res. 2019 Feb 1;25(3):937–45.

106. Tate JG, Bamford S, Jubb HC, Sondka Z, Beare DM, Bindal N, et al. COSMIC: the Catalogue Of Somatic Mutations In Cancer. Nucleic Acids Res. 2019 Jan 8;47(D1):D941–7.

107. Thian M, Hoeger B, Kamnev A, Poyer F, Köstel Bal S, Caldera M, et al. Germline biallelic PIK3CG mutations in a multifaceted immunodeficiency with immune dysregulation. Haematologica. 2020 Oct 1;105(10):e488.

108. Safina BS, Elliott RL, Forrest AK, Heald RA, Murray JM, Nonomiya J, et al. Design of Selective Benzoxazepin PI3Kδ Inhibitors Through Control of Dihedral Angles. ACS Med Chem Lett. 2017 Sep 14;8(9):936–40.

109. Furet P, Guagnano V, Fairhurst RA, Imbach-Weese P, Bruce I, Knapp M, et al. Discovery of NVP-BYL719 a potent and selective phosphatidylinositol-3 kinase alpha inhibitor selected for clinical evaluation. Bioorg Med Chem Lett. 2013 Jul 1;23(13):3741–8.

110. Zhang X, Vadas O, Perisic O, Anderson KE, Clark J, Hawkins PT, et al. Structure of lipid kinase p110β/p85β elucidates an unusual SH2-domain-mediated inhibitory mechanism. Mol Cell. 2011 Mar 4;41(5):567–78.

111. Fruman DA, Rommel C. PI3K and cancer: lessons, challenges and opportunities. Nat Rev Drug Discov. 2014 Feb;13(2):140–56.

112. André F, Ciruelos E, Rubovszky G, Campone M, Loibl S, Rugo HS, et al. Alpelisib for PIK3CA-Mutated, Hormone Receptor-Positive Advanced Breast Cancer. N Engl J Med. 2019 May 16;380(20):1929–40.

113. Brown JR, Byrd JC, Coutre SE, Benson DM, Flinn IW, Wagner-Johnston ND, et al. Idelalisib, an inhibitor of phosphatidylinositol 3-kinase p110δ, for relapsed/refractory chronic lymphocytic leukemia. Blood. 2014 May 29;123(22):3390–7.

114. Flinn IW, Kahl BS, Leonard JP, Furman RR, Brown JR, Byrd JC, et al. Idelalisib, a selective inhibitor of phosphatidylinositol 3-kinase-δ, as therapy for previously treated indolent non-Hodgkin lymphoma. Blood. 2014 May 29;123(22):3406–13.

115. Collier PN, Martinez-Botella G, Cornebise M, Cottrell KM, Doran JD, Griffith JP, et al. Structural basis for isoform selectivity in a class of benzothiazole inhibitors of phosphoinositide 3-kinase γ. J Med Chem. 2015 Jan 8;58(1):517–21.

116. Berger I, Fitzgerald DJ, Richmond TJ. Baculovirus expression system for heterologous multiprotein complexes. Nat Biotechnol. 2004 Dec;22(12):1583–7.

117. Kozasa T. Purification of G protein subunits from Sf9 insect cells using hexahistidine-tagged alpha and beta gamma subunits. Methods Mol Biol Clifton NJ. 2004;237:21–38.

118. Perez-Riverol Y, Csordas A, Bai J, Bernal-Llinares M, Hewapathirana S, Kundu DJ, et al. The PRIDE database and related tools and resources in 2019: improving support for quantification data. Nucleic Acids Res. 2019 Jan 8;47(D1):D442–50.

119. Kabsch W. XDS. Acta Crystallogr D Biol Crystallogr. 2010 Feb;66(Pt 2):125–32.

120. McCoy AJ, Grosse-Kunstleve RW, Adams PD, Winn MD, Storoni LC, Read RJ. Phaser crystallographic software. J Appl Crystallogr. 2007 Aug 1;40(Pt 4):658–74.

121. Knight ZA, Gonzalez B, Feldman ME, Zunder ER, Goldenberg DD, Williams O, et al. A pharmacological map of the PI3-K family defines a role for p110alpha in insulin signaling. Cell. 2006 May 19;125(4):733–47.

122. Bohnacker T, Prota AE, Beaufils F, Burke JE, Melone A, Inglis AJ, et al. Deconvolution of Buparlisib's mechanism of action defines specific PI3K and tubulin inhibitors for therapeutic intervention. Nat Commun. 2017 Mar 9;8:14683.

123. Emsley P, Lohkamp B, Scott WG, Cowtan K. Features and development of Coot. Acta Crystallogr D Biol Crystallogr. 2010 Apr;66(Pt 4):486–501.

124. Afonine PV, Grosse-Kunstleve RW, Echols N, Headd JJ, Moriarty NW, Mustyakimov M, et al. Towards automated crystallographic structure refinement with phenix.refine. Acta Crystallogr D Biol Crystallogr. 2012 Apr;68(Pt 4):352–67.

125. Chen VB, Arendall WB, Headd JJ, Keedy DA, Immormino RM, Kapral GJ, et al. MolProbity: all-atom structure validation for macromolecular crystallography. Acta Crystallogr D Biol Crystallogr. 2010 Jan;66(Pt 1):12–21.

126. Vadas O, Jenkins ML, Dornan GL, Burke JE. Using Hydrogen-Deuterium Exchange Mass Spectrometry to Examine Protein-Membrane Interactions. Methods Enzymol. 2017;583:143–72.

127. Burke JE, Vadas O, Berndt A, Finegan T, Perisic O, Williams RL. Dynamics of the phosphoinositide 3-kinase p110δ interaction with p85α and membranes reveals aspects of regulation distinct from p110α. Struct Lond Engl 1993. 2011 Aug 10;19(8):1127–37.

128. Burke JE, Perisic O, Masson GR, Vadas O, Williams RL. Oncogenic mutations mimic and enhance dynamic events in the natural activation of phosphoinositide 3-kinase p110α (PIK3CA). Proc Natl Acad Sci U S A. 2012 Sep 18;109(38):15259–64.

129. Burke JE, Williams RL. Dynamic steps in receptor tyrosine kinase mediated activation of class IA phosphoinositide 3-kinases (PI3K) captured by H/D exchange (HDX-MS). Adv Biol Regul. 2013 Jan;53(1):97–110.

130. Bruce I, Akhlaq M, Bloomfield GC, Budd E, Cox B, Cuenoud B, et al. Development of isoform selective PI3-kinase inhibitors as pharmacological tools for elucidating the PI3K pathway. Bioorg Med Chem Lett. 2012 Sep 1;22(17):5445–50.

131. Knight SD, Adams ND, Burgess JL, Chaudhari AM, Darcy MG, Donatelli CA, et al. Discovery of GSK2126458, a Highly Potent Inhibitor of PI3K and the Mammalian Target of Rapamycin. ACS Med Chem Lett. 2010 Apr 8;1(1):39–43.

132. Venkatesan AM, Dehnhardt CM, Delos Santos E, Chen Z, Dos Santos O, Ayral-Kaloustian S, et al. Bis(morpholino-1,3,5-triazine) derivatives: potent adenosine 5'-triphosphate competitive phosphatidylinositol-3-kinase/mammalian target of rapamycin inhibitors: discovery of compound 26 (PKI-587), a highly efficacious dual inhibitor. J Med Chem. 2010 Mar 25;53(6):2636–45.

133. Berndt A, Miller S, Williams O, Le DD, Houseman BT, Pacold JI, et al. The p110 delta structure: mechanisms for selectivity and potency of new PI(3)K inhibitors. Nat Chem Biol. 2010 Feb;6(2):117–24.

134. Somoza JR, Koditek D, Villaseñor AG, Novikov N, Wong MH, Liclican A, et al. Structural, biochemical, and biophysical characterization of idelalisib binding to phosphoinositide 3-kinase δ. J Biol Chem. 2015 Mar 27;290(13):8439–46.

135. Heffron TP, Heald RA, Ndubaku C, Wei B, Augistin M, Do S, et al. The Rational Design of Selective Benzoxazepin Inhibitors of the α-Isoform of Phosphoinositide 3-Kinase Culminating in the Identification of (S)-2-((2-(1-Isopropyl-1H-1,2,4-triazol-5-yl)-5,6-dihydrobenzo[f]imidazo[1,2-d][1,4]oxazepin-9-yl)oxy)propanamide (GDC-0326). J Med Chem. 2016 Feb 11;59(3):985–1002.

136. Fruman DA, Chiu H, Hopkins BD, Bagrodia S, Cantley LC, Abraham RT. The PI3K Pathway in Human Disease. Cell. 2017 Aug;170(4):605–35.

137. Okkenhaug K. Signaling by the phosphoinositide 3-kinase family in immune cells. Annu Rev Immunol. 2013;31:675–704.

138. Barbier M, Attoub S, Calvez R, Laffargue M, Jarry A, Mareel M, et al. Tumor biology. Weakening link to colorectal cancer? Nature. 2001 Oct 25;413(6858):796.

139. Mandelker D, Gabelli SB, Schmidt-Kittler O, Zhu J, Cheong I, Huang C-H, et al. A frequent kinase domain mutation that changes the interaction between PI3Kalpha and the membrane. Proc Natl Acad Sci U S A. 2009 Oct 6;106(40):16996–7001.

140. Perino A, Ghigo A, Ferrero E, Morello F, Santulli G, Baillie GS, et al. Integrating cardiac PIP3 and cAMP signaling through a PKA anchoring function of p110γ. Mol Cell. 2011 Apr 8;42(1):84–95.

141. Walser R, Burke JE, Gogvadze E, Bohnacker T, Zhang X, Hess D, et al. PKCβ phosphorylates PI3Kγ to activate it and release it from GPCR control. PLoS Biol. 2013;11(6):e1001587.

142. Miller MS, Maheshwari S, McRobb FM, Kinzler KW, Amzel LM, Vogelstein B, et al. Identification of allosteric binding sites for PI3Kα oncogenic mutant specific inhibitor design. Bioorg Med Chem. 2017 Feb 15;25(4):1481–6.

143. Drew SL, Thomas-Tran R, Beatty JW, Fournier J, Lawson KV, Miles DH, et al. Discovery of Potent and Selective PI3Kγ Inhibitors. J Med Chem. 2020 Oct 8;63(19):11235–57.

144. Madsen RR, Vanhaesebroeck B. Cracking the context-specific PI3K signaling code. Sci Signal. 2020 Jan 7;13(613).

145. Burke JE, Williams RL. Synergy in activating class I PI3Ks. Trends Biochem Sci. 2015 Feb;40(2):88–100.

146. Hawkins PT, Stephens LR. PI3K signaling in inflammation. Biochim Biophys Acta. 2015 Jun;1851(6):882–97.

147. Maier U, Babich A, Nürnberg B. Roles of Non-catalytic Subunits in Gβγ-induced Activation of Class I Phosphoinositide 3-Kinase Isoforms β and γ. J Biol Chem. 1999 Oct;274(41):29311–7.

148. Vadas O, Dbouk HA, Shymanets A, Perisic O, Burke JE, Abi Saab WF, et al. Molecular determinants of PI3K -mediated activation downstream of G-protein-coupled receptors (GPCRs). Proc Natl Acad Sci. 2013 Nov 19;110(47):18862–7.

149. Hamers-Casterman C, Atarhouch T, Muyldermans S, Robinson G, Hammers C, Songa EB, et al. Naturally occurring antibodies devoid of light chains. Nature. 1993 Jun;363(6428):446–8.

150. Muyldermans S. Nanobodies: Natural Single-Domain Antibodies. Annu Rev Biochem. 2013 Jun 2;82(1):775–97.

151. Desmyter A, Transue TR, Ghahroudi MA, Thi MH, Poortmans F, Hamers R, et al. Crystal structure of a camel single-domain VH antibody fragment in complex with lysozyme. Nat Struct Biol. 1996 Sep;3(9):803–11.

152. Uchański T, Pardon E, Steyaert J. Nanobodies to study protein conformational states. Curr Opin Struct Biol. 2020 Feb;60:117–23.

153. Baranova E, Fronzes R, Garcia-Pino A, Van Gerven N, Papapostolou D, Péhau-Arnaudet G, et al. SbsB structure and lattice reconstruction unveil Ca2+ triggered S-layer assembly. Nature. 2012 Jul;487(7405):119–22.

154. Domanska K, Vanderhaegen S, Srinivasan V, Pardon E, Dupeux F, Marquez JA, et al. Atomic structure of a nanobody-trapped domain-swapped dimer of an amyloidogenic 2-microglobulin variant. Proc Natl Acad Sci. 2011 Jan 25;108(4):1314–9.

155. Korotkov KV, Pardon E, Steyaert J, Hol WGJ. Crystal structure of the N-terminal domain of the secretin GspD from ETEC determined with the assistance of a nanobody. Struct Lond Engl 1993. 2009 Feb 13;17(2):255–65.

156. Schubert AF, Gladkova C, Pardon E, Wagstaff JL, Freund SMV, Steyaert J, et al. Structure of PINK1 in complex with its substrate ubiquitin. Nature. 2017 Dec 7;552(7683):51–6.

157. Huang W, Manglik A, Venkatakrishnan AJ, Laeremans T, Feinberg EN, Sanborn AL, et al. Structural insights into μ-opioid receptor activation. Nature. 2015 Aug;524(7565):315–21.

158. Rasmussen SGF, Choi H-J, Fung JJ, Pardon E, Casarosa P, Chae PS, et al. Structure of a nanobody-stabilized active state of the β2 adrenoceptor. Nature. 2011 Jan;469(7329):175–80.

159. Rasmussen SGF, DeVree BT, Zou Y, Kruse AC, Chung KY, Kobilka TS, et al. Crystal structure of the β2 adrenergic receptor-Gs protein complex. Nature. 2011 Jul 19;477(7366):549–55.

160. Ruprecht JJ, King MS, Zögg T, Aleksandrova AA, Pardon E, Crichton PG, et al. The Molecular Mechanism of Transport by the Mitochondrial ADP/ATP Carrier. Cell. 2019 Jan;176(3):435-447.e15.

161. Rostislavleva K, Soler N, Ohashi Y, Zhang L, Pardon E, Burke JE, et al. Structure and flexibility of the endosomal Vps34 complex reveals the basis of its function on membranes. Science. 2015 Oct 9;350(6257):aac7365.

162. García-Nafría J, Lee Y, Bai X, Carpenter B, Tate CG. Cryo-EM structure of the adenosine A2A receptor coupled to an engineered heterotrimeric G protein. eLife. 2018 May 4;7:e35946.

163. Laverty D, Desai R, Uchański T, Masiulis S, Stec WJ, Malinauskas T, et al. Cryo-EM structure of the human α1β3γ2 GABAA receptor in a lipid bilayer. Nature. 2019 Jan;565(7740):516–20.

164. Westfield GH, Rasmussen SGF, Su M, Dutta S, DeVree BT, Chung KY, et al. Structural flexibility of the G s -helical domain in the 2-adrenoceptor Gs complex. Proc Natl Acad Sci. 2011 Sep 20;108(38):16086–91.

165. Bannas P, Hambach J, Koch-Nolte F. Nanobodies and Nanobody-Based Human Heavy Chain Antibodies As Antitumor Therapeutics. Front Immunol. 2017 Nov 22;8:1603.

166. Beghein E, Gettemans J. Nanobody Technology: A Versatile Toolkit for Microscopic Imaging, Protein–Protein Interaction Analysis, and Protein Function Exploration. Front Immunol. 2017 Jul 4;8:771.

167. Huo J, Le Bas A, Ruza RR, Duyvesteyn HME, Mikolajek H, Malinauskas T, et al. Neutralizing nanobodies bind SARS-CoV-2 spike RBD and block interaction with ACE2. Nat Struct Mol Biol. 2020 Sep;27(9):846–54.

168. Wrapp D, De Vlieger D, Corbett KS, Torres GM, Wang N, Van Breedam W, et al. Structural Basis for Potent Neutralization of Betacoronaviruses by Single-Domain Camelid Antibodies. Cell. 2020 Jun 11;181(6):1436–41.

169. Manglik A, Kobilka BK, Steyaert J. Nanobodies to Study G Protein-Coupled Receptor Structure and Function. Annu Rev Pharmacol Toxicol. 2017 Jan 6;57:19–37.

170. Pardon E, Laeremans T, Triest S, Rasmussen SGF, Wohlkönig A, Ruf A, et al. A general protocol for the generation of Nanobodies for structural biology. Nat Protoc. 2014 Mar;9(3):674–93.

171. McMahon C, Staus DP, Wingler LM, Wang J, Skiba MA, Elgeti M, et al. Synthetic nanobodies as angiotensin receptor blockers. Proc Natl Acad Sci U S A. 2020 Aug 18;117(33):20284–91.

172. Staus DP, Strachan RT, Manglik A, Pani B, Kahsai AW, Kim TH, et al. Allosteric nanobodies reveal the dynamic range and diverse mechanisms of G-protein-coupled receptor activation. Nature. 2016 Jul 21;535(7612):448–52.

173. Wingler LM, McMahon C, Staus DP, Lefkowitz RJ, Kruse AC. Distinctive Activation Mechanism for Angiotensin Receptor Revealed by a Synthetic Nanobody. Cell. 2019 Jan;176(3):479-490.e12.

174. Gulati S, Jin H, Masuho I, Orban T, Cai Y, Pardon E, et al. Targeting G protein-coupled receptor signaling at the G protein level with a selective nanobody inhibitor. Nat Commun. 2018 May 18;9(1):1996.

175. Dobbs JM, Jenkins ML, Burke JE. Escherichia coli and Sf9 Contaminant Databases to Increase Efficiency of Tandem Mass Spectrometry Peptide Identification in Structural Mass Spectrometry Experiments. J Am Soc Mass Spectrom. 2020 Oct 7;31(10):2202–9.

176. Masson GR, Jenkins ML, Burke JE. An overview of hydrogen deuterium exchange mass spectrometry (HDX-MS) in drug discovery. Expert Opin Drug Discov. 2017 Oct;12(10):981–94.

177. Rathinaswamy MK, Gaieb Z, Fleming KD, Borsari C, Harris NJ, Moeller BE, et al. Disease-related mutations in PI3Kγ disrupt regulatory C-terminal dynamics and reveal a path to selective inhibitors. eLife. 2021 Mar 4;10.

178. Shymanets A, Prajwal, Vadas O, Czupalla C, LoPiccolo J, Brenowitz M, et al. Different inhibition of Gβγ-stimulated class IB phosphoinositide 3-kinase (PI3K) variants by a monoclonal antibody. Specific function of p101 as a Gβγ-dependent regulator of PI3Kγ enzymatic activity. Biochem J. 2015 Jul 1;469(1):59–69.

179. Lawrence MS, Stojanov P, Mermel CH, Robinson JT, Garraway LA, Golub TR, et al. Discovery and saturation analysis of cancer genes across 21 tumor types. Nature. 2014 Jan 23;505(7484):495–501.

180. McPhail JA, Burke JE. Drugging the Phosphoinositide 3-Kinase (PI3K) and Phosphatidylinositol 4-Kinase (PI4K) Family of Enzymes for Treatment of Cancer, Immune Disorders, and Viral/Parasitic Infections. Adv Exp Med Biol. 2020;1274:203–22.

181. Steeland S, Vandenbroucke RE, Libert C. Nanobodies as therapeutics: big opportunities for small antibodies. Drug Discov Today. 2016 Jul;21(7):1076–113.

182. Muyldermans S. Applications of Nanobodies. Annu Rev Anim Biosci. 2021 Feb 16;9:401–21.

183. Berkowitz SA, Engen JR, Mazzeo JR, Jones GB. Analytical tools for characterizing biopharmaceuticals and the implications for biosimilars. Nat Rev Drug Discov. 2012 Jun 29;11(7):527–40.

184. Buckles TC, Ohashi Y, Tremel S, McLaughlin SH, Pardon E, Steyaert J, et al. The G-Protein Rab5A Activates VPS34 Complex II, a Class III PI3K, by a Dual Regulatory Mechanism. Biophys J. 2020 Dec 1;119(11):2205–18.

185. Rynkiewicz NK, Anderson KE, Suire S, Collins DM, Karanasios E, Vadas O, et al. Gβγ is a direct regulator of endogenous p101/p110γ and p84/p110γ PI3Kγ complexes in mouse neutrophils. Sci Signal. 2020 Nov 3;13(656).

186. Shymanets A, Prajwal null, Bucher K, Beer-Hammer S, Harteneck C, Nürnberg B. p87 and p101 subunits are distinct regulators determining class IB phosphoinositide 3-kinase (PI3K) specificity. J Biol Chem. 2013 Oct 25;288(43):31059–68.

187. De Groof TWM, Bobkov V, Heukers R, Smit MJ. Nanobodies: New avenues for imaging, stabilizing and modulating GPCRs. Mol Cell Endocrinol. 2019 Mar 15;484:15–24.

188. Scholler P, Nevoltris D, de Bundel D, Bossi S, Moreno-Delgado D, Rovira X, et al. Allosteric nanobodies uncover a role of hippocampal mGlu2 receptor homodimers in contextual fear consolidation. Nat Commun. 2017 Dec 6;8(1):1967.

189. Irannejad R, Tomshine JC, Tomshine JR, Chevalier M, Mahoney JP, Steyaert J, et al. Conformational biosensors reveal GPCR signaling from endosomes. Nature. 2013 Mar 28;495(7442):534–8.

190. Fougerat A, Gayral S, Gourdy P, Schambourg A, Rückle T, Schwarz MK, et al. Genetic and pharmacological targeting of phosphoinositide 3-kinase-gamma reduces atherosclerosis and favors plaque stability by modulating inflammatory processes. Circulation. 2008 Mar 11;117(10):1310–7.

191. Yu J, Zhang Y, McIlroy J, Rordorf-Nikolic T, Orr GA, Backer JM. Regulation of the p85/p110 phosphatidylinositol 3'-kinase: stabilization and inhibition of the p110alpha catalytic subunit by the p85 regulatory subunit. Mol Cell Biol. 1998 Mar;18(3):1379–87.

192. Dornan GL, Burke JE. Molecular Mechanisms of Human Disease Mediated by Oncogenic and Primary Immunodeficiency Mutations in Class IA Phosphoinositide 3-Kinases. Front Immunol. 2018;9:575.

193. Zhang S, Chung W-C, Wu G, Egan SE, Miele L, Xu K. Manic fringe promotes a claudin-low breast cancer phenotype through notch-mediated PIK3CG induction. Cancer Res. 2015 May 15;75(10):1936–43.

194. Masson GR, Burke JE, Ahn NG, Anand GS, Borchers C, Brier S, et al. Recommendations for performing, interpreting and reporting hydrogen deuterium exchange mass spectrometry (HDX-MS) experiments. Nat Methods. 2019 Jul;16(7):595–602.

195. Walker EH, Pacold ME, Perisic O, Stephens L, Hawkins PT, Wymann MP, et al. Structural determinants of phosphoinositide 3-kinase inhibition by wortmannin, LY294002, quercetin, myricetin, and staurosporine. Mol Cell. 2000 Oct;6(4):909–19.

196. Holm L. DALI and the persistence of protein shape. Protein Sci Publ Protein Soc. 2020 Jan;29(1):128–40.

197. Miller DJ, Jerga A, Rock CO, White SW. Analysis of the Staphylococcus aureus DgkB structure reveals a common catalytic mechanism for the soluble diacylglycerol kinases. Struct Lond Engl 1993. 2008 Jul;16(7):1036–46.

198. Nichols CE, Lamb HK, Lockyer M, Charles IG, Pyne S, Hawkins AR, et al. Characterization of Salmonella typhimurium YegS, a putative lipid kinase homologous to eukaryotic sphingosine and diacylglycerol kinases. Proteins. 2007 Jul 1;68(1):13–25.

199. Wang Z, Min X, Xiao S-H, Johnstone S, Romanow W, Meininger D, et al. Molecular basis of sphingosine kinase 1 substrate recognition and catalysis. Struct Lond Engl 1993. 2013 May 7;21(5):798–809.

200. Pulkoski-Gross MJ, Jenkins ML, Truman J-P, Salama MF, Clarke CJ, Burke JE, et al. An intrinsic lipid-binding interface controls sphingosine kinase 1 function. J Lipid Res. 2018 Mar;59(3):462–74.

201. Chung JK, Nocka LM, Decker A, Wang Q, Kadlecek TA, Weiss A, et al. Switch-like activation of Bruton's tyrosine kinase by membrane-mediated dimerization. Proc Natl Acad Sci U S A. 2019 May 28;116(22):10798–803.

202. Stark A-K, Sriskantharajah S, Hessel EM, Okkenhaug K. PI3K inhibitors in inflammation, autoimmunity and cancer. Curr Opin Pharmacol. 2015 Aug;23:82–91.

203. Huang C-H, Mandelker D, Schmidt-Kittler O, Samuels Y, Velculescu VE, Kinzler KW, et al. The structure of a human p110alpha/p85alpha complex elucidates the effects of oncogenic PI3Kalpha mutations. Science. 2007 Dec 14;318(5857):1744–8.

204. Miled N, Yan Y, Hon W-C, Perisic O, Zvelebil M, Inbar Y, et al. Mechanism of two classes of cancer mutations in the phosphoinositide 3-kinase catalytic subunit. Science. 2007 Jul 13;317(5835):239–42.

205. Brock C, Schaefer M, Reusch HP, Czupalla C, Michalke M, Spicher K, et al. Roles of G beta gamma in membrane recruitment and activation of p110 gamma/p101 phosphoinositide 3-kinase gamma. J Cell Biol. 2003 Jan 6;160(1):89–99.

206. Wall AA, Luo L, Hung Y, Tong SJ, Condon ND, Blumenthal A, et al. Small GTPase Rab8a-recruited Phosphatidylinositol 3-Kinase γ Regulates Signaling and Cytokine Outputs from Endosomal Toll-like Receptors. J Biol Chem. 2017 Mar 17;292(11):4411–22.

207. Zhang P, Kang B, Xie G, Li S, Gu Y, Shen Y, et al. Genomic sequencing and editing revealed the GRM8 signaling pathway as potential therapeutic targets of squamous cell lung cancer. Cancer Lett. 2019 Feb 1;442:53–67.

208. Hanker AB, Kaklamani V, Arteaga CL. Challenges for the Clinical Development of PI3K Inhibitors: Strategies to Improve Their Impact in Solid Tumors. Cancer Discov. 2019 Apr;9(4):482–91.

209. Li M, Sala V, De Santis MC, Cimino J, Cappello P, Pianca N, et al. Phosphoinositide 3-Kinase Gamma Inhibition Protects From Anthracycline Cardiotoxicity and Reduces Tumor Growth. Circulation. 2018 Aug 14;138(7):696–711.

210. Lima BHF, Marques PE, Gomides LF, Mattos MS, Kraemer L, Queiroz-Junior CM, et al. Converging TLR9 and PI3Kgamma signaling induces sterile inflammation and organ damage. Sci Rep. 2019 Dec 13;9(1):19085.

211. Berndt A, Miller S, Williams O, Le DD, Houseman BT, Pacold JI, et al. The p110 delta structure: mechanisms for selectivity and potency of new PI(3)K inhibitors. Nat Chem Biol. 2010 Feb;6(2):117–24.

212. Miled N, Yan Y, Hon W-C, Perisic O, Zvelebil M, Inbar Y, et al. Mechanism of two classes of cancer mutations in the phosphoinositide 3-kinase catalytic subunit. Science. 2007 Jul 13;317(5835):239–42.

213. Vadas O, Dbouk HA, Shymanets A, Perisic O, Burke JE, Abi Saab WF, et al. Molecular determinants of PI3Kγ-mediated activation downstream of G-protein-coupled receptors (GPCRs). Proc Natl Acad Sci U S A. 2013 Nov 19;110(47):18862–7.

214. De Henau O, Rausch M, Winkler D, Campesato LF, Liu C, Cymerman DH, et al. Overcoming resistance to checkpoint blockade therapy by targeting PI3Kγ in myeloid cells. Nature. 2016 Nov 17;539(7629):443–7.

215. Kaneda MM, Messer KS, Ralainirina N, Li H, Leem CJ, Gorjestani S, et al. PI3Kγ is a molecular switch that controls immune suppression. Nature. 2016 Nov 17;539(7629):437–42.

216. Dbouk HA, Vadas O, Shymanets A, Burke JE, Salamon RS, Khalil BD, et al. G protein-coupled receptor-mediated activation of p110β by Gβγ is required for cellular transformation and invasiveness. Sci Signal. 2012 Dec 4;5(253):ra89.

Appendix

Chapter 2

Appendix A. Full statistics on all hydrogen deuterium exchange experiments according to the guidelines from the International Conference on HDX-MS (194) (refers to Figure 2.2)

Data set – Figure 2	**p110γ / p101**	**R1021C p110γ /p101**	**R1021P p110γ /p101**
HDX reaction details	$\%D_2O$=62.0% $pH_{(read)}$=7.5 Temp=18ºC	$\%D_2O$=62.0% $pH_{(read)}$=7.5 Temp=18ºC	$\%D_2O$=62.0% $pH_{(read)}$=7.5 Temp=18ºC
HDX time course (seconds)	3, 30, 300, 3000	3, 30, 300, 3000	3, 30, 300, 3000
HDX controls	N/A	N/A	N/A
Back-exchange	No correction	No correction	No correction
Number of peptides	153	153	152
Sequence coverage	92.7%	92.7%	91.7%
Average peptide /redundancy	Length=14.8 Redundancy= 2.0	Length=14.8 Redundancy= 2.0	Length=14.8 Redundancy= 2.0
Replicates	3	3	3
Repeatability	Average StDev=0.6%	Average StDev=0.6%	Average StDev=0.6%
Significant differences in HDX	>5% and >0.4 Da and unpaired t-test ≤0.01	>5% and >0.4 Da and unpaired t-test ≤0.01	>5% and >0.4 Da and unpaired t-test ≤0.01

Appendix B. List of all compounds analyzed by HDX-MS with potency towards all class I PI3K isoforms. N.D is not determined.

	Compound	Structure	PDB ID	IC_{50} PI3Kα (nM)	IC_{50} PI3Kβ (nM)	IC_{50} PI3Kδ (nM)	IC_{50} PI3Kγ (nM)
1	IPI-549	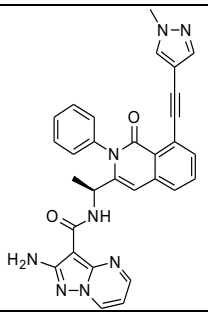	7JWZ	3,200	3,500	>8,400	16
2	PIK-90	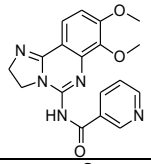	2CHX	11	350	58	18
3	AS-604850	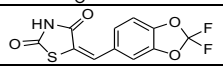	2A4Z	4,500	>20,000	>20,000	250
4	Gedatolisib	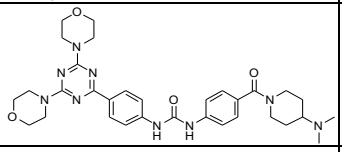	7JWE	0.4	-	-	5.4
5	Omipalisib	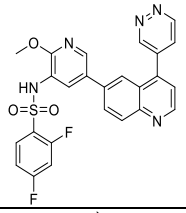	3L08	0.0019 (K_i)	0.13 (K_i)	0.024 (K_i)	0.06 (K_i)
6	NVS-PI3-4	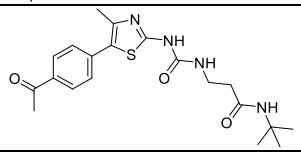	7JX0	1,800	250	750	90
7	AZ2	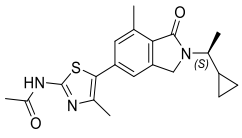	N.D.	3,981	31,622	200	0.3

Appendix C. Full statistics on all hydrogen deuterium exchange experiments according to the guidelines from the International Conference on HDX-MS (194) (refers to Figure 2.4)

Data set – Figure 2.4	**Apo p110γ**	**+ IPI-549**	**+ AZg1/AZ**	**+ AS-605240**
HDX reaction details	%D_2O=75.5% $pH_{(read)}$=7.5 Temp=18ºC	%D_2O=75.5% $pH_{(read)}$=7.5 Temp=18ºC	%D_2O=75.5% $pH_{(read)}$=7.5 Temp=18ºC	%D_2O=75.5% $pH_{(read)}$=7.5 Temp=18ºC
HDX time course (seconds)	3, 30, 300, 3000	3, 30, 300, 3000	3, 30, 300, 3000	3, 30, 300, 3000
HDX controls	N/A	N/A	N/A	N/A
Back-exchange	Corrected based on %D_2O	Corrected based on %D_2O	Corrected based on %D_2O	Corrected based on %D_2O
Number of peptides	180	180	180	180
Sequence coverage	88.6%	88.6%	88.6%	88.6%
Average peptide /redundancy	Length= 13.4 Redundancy= 2.2	Length= 13.4 Redundancy= 2.2	Length= 13.4 Redundancy= 2.2	Length= 13.4 Redundancy= 2.2
Replicates	3	3	3	3
Repeatability	Average StDev=0.9%	Average StDev=0.9%	Average StDev=0.9%	Average StDev=0.9%
Significant differences in HDX	>5% and >0.4 Da and unpaired t-test ≤0.01	>5% and >0.4 Da and unpaired t-test ≤0.01	>5% and >0.4 Da and unpaired t-test ≤0.01	>5% and >0.4 Da and unpaired t-test ≤0.01
Data set – Figure 2.4	**+ Gedatolisib**	**+ Omipalisib**	**+ RD-HBC 520**	**+ PIK-90**
HDX reaction details	%D_2O=75.5% $pH_{(read)}$=7.5 Temp=18ºC	%D_2O=75.5% $pH_{(read)}$=7.5 Temp=18ºC	%D_2O=75.5% $pH_{(read)}$=7.5 Temp=18ºC	%D_2O=75.5% $pH_{(read)}$=7.5 Temp=18ºC
HDX time course (seconds)	3, 30, 300, 3000	3, 30, 300, 3000	3, 30, 300, 3000	3, 30, 300, 3000
HDX controls	N/A	N/A	N/A	N/A
Back-exchange	No correction	No correction	No correction	No correction
Number of peptides	180	180	180	180
Sequence coverage	88.6%	88.6%	88.6%	88.6%
Average peptide /redundancy	Length= 13.4 Redundancy= 2.2	Length= 13.4 Redundancy= 2.2	Length= 13.4 Redundancy= 2.2	Length= 13.4 Redundancy= 2.2
Replicates	3	3	3	3
Repeatability	Average StDev=0.9%	Average StDev=0.9%	Average StDev=0.9%	Average StDev=0.9%
Significant differences in HDX	>5% and >0.4 Da and unpaired t-test ≤0.01	>5% and >0.4 Da and unpaired t-test ≤0.01	>5% and >0.4 Da and unpaired t-test ≤0.01	>5% and >0.4 Da and unpaired t-test ≤0.01

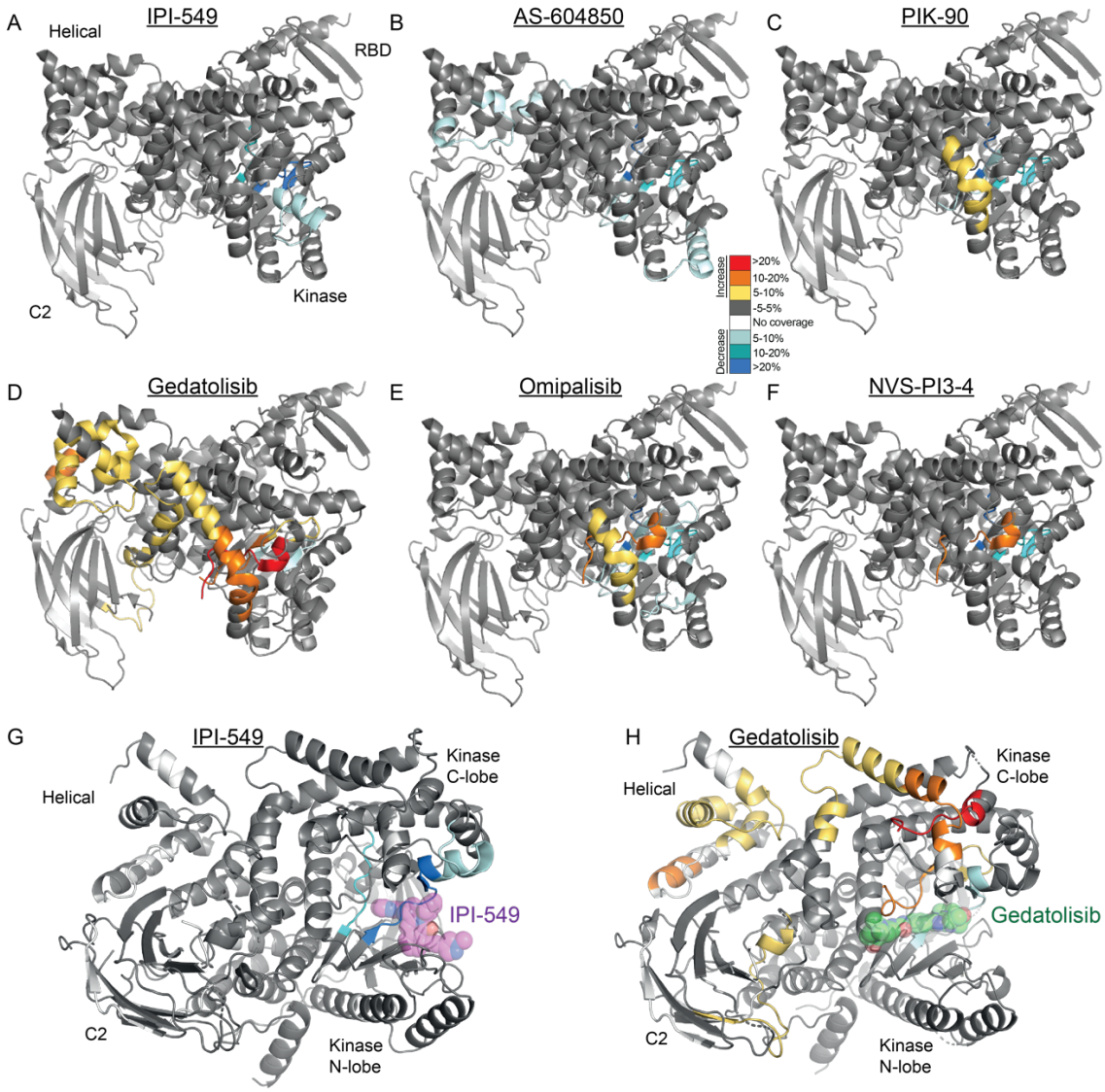

Appendix D. HDX-MS reveals that different classes of PI3K inhibitors lead to unique allosteric conformational changes. (A-F) Peptides showing significant deuterium exchange differences (>5 %, >0.4 kDa and $p<0.01$ in an unpaired two-tailed t-test) between wild-type and six different inhibitors are colored on a model of p110γ (PDB: 6AUD). Differences in exchange are mapped according to the legend. **(G-H)** The same HDX-MS differences in exchange mapped in panel **A+D** are shown on the crystal structure of p110γ bound to IPI-549 (**G**) and Gedatolisib (**H**). Both IPI-549 and Gedatolisib inhibitors are shown as spheres.

Appendix E. X-ray data collection and refinement statistics

	PI3Kγ IPI-549 PDB:7JWZ	PI3Kγ Gedatolisib PDB:7JWE	PI3Kγ NVS-PI3-4 PDB:7JX0
Data collection			
Wavelength	0.97949	0.97949	0.97949
Space group	C121	C121	C121
Cell dimensions			
a, *b*, *c* (Å)	144.3, 67.9, 106.4	143.5, 67.6, 106.3	143.6 67.6 106.8
α, β, γ(°)	90, 94.5, 90	90, 95.4, 90	90, 95.4, 90
Resolution (Å)	44.4-2.65 (2.74-2.65)*	40.72-2.55 (2.64-2.55)	40.93-3.15 (3.26-3.15)
R_{merge}	0.125 (1.919)	0.061 (1.349)	0.119 (1.118)
$I / \sigma I$	7.1 (0.69)	11.91 (0.87)	7.92 (0.84)
CC1/2	0.992 (0.407)	0.999 (0.385)	0.994 (0.425)
Completeness (%)	98.9 (98.23)	99.41 (99.40)	98.08 (99.04)
Redundancy	3.3 (3.4)	3.3 (3.4)	3.0 (3.0)
Refinement			
Resolution (Å)	44.4-2.65 (2.74 - 2.65)	40.72-2.55(2.64-2.55)	40.93-3.15 (3.26-3.15)
No. unique reflections	29,722 (2941)	33,183 (3303)	17,573 (1761)
R_{work} / R_{free}	22.7/26.8	20.9/25.3	22.9/27.4
No. atoms			
Protein	6,752	6,612	6,506
Ligand/ion	40	45	28
Water	0	9	0
B-factors			
Protein	100.4	88.9	108.2
Ligand/ion	88.3	78.7	117.2
Water		65.5	
Ramachandran favored	94.47	95.21	96.51
Ramachandran outliers	0.61	0.0	0.13
Rotamer outliers	0.53	0.41	0.0
R.m.s. deviations			
Bond lengths (Å)	0.003	0.003	0.004
Bond angles (°)	0.53	0.59	0.56

*Values in parentheses are for highest-resolution shell.

Number of crystals used for each of the above structures=1

Chapter 3

Appendix F. Table summarizing nanobody protein specificity determined by pulldown assays, ΔTm induced by nanobody binding as determined by DSF and peptides stabilized in HDX-MS.

Nanobody	Protein Specificity	DSF stabilization (Δ Tm °C)	Regions with significant protection in HDX
NB1-PIK3R5	p101	0	176-193, 279-288, 605-623, 650-654
NB2-PIK3R5	p101	1	165-193, 289-298, 304-317, 378-389, 537-546
NB3-PIK3R5	p101	0	677-726, 816-830
NB4-PIK3R6	p84	-0.5	650,655, 656-673
NB5-PIK3CG	p110γ	0.5	125-157, 623-630
NB6-PIK3CG	p110γ	3	196-221, 574-607, 611-630, 636-654, 849-861
NB7-PIK3CG	p110γ	3.3	196-211, 578-607, 611-630, 643-657, 816-838, 853-861, 1035-1050
NB8-PIK3CG	p110γ	0.3	138-164, 316-339, 593-607, 611-622, 748-782
NB9-PIK3CG	p110γ	0.3	557-578, 579-607, 611-635
NB10-PIK3CG	p110γ	0.2	593-607, 611-630
NB11-PIK3CG	p110γ	1.2	579-607, 611-630, 768-782, 849-861
NB12-PIK3CG	p110γ	1.1	138-164, 593-607, 748-782
NB13-PIK3CG	p110γ	0.6	138-164, 593-607, 748-782
NB14-PIK3CG	p110γ	0.1	593-607, 623-630, 748-782
NB15-PIK3CG	p110γ	0.4	623-630
NB16-PIK3CG	p110γ	0	593-607, 623-630, 888-907, 1072-1084, 1088-1092
NB17-PIK3CG	p110γ	0.2	593-607, 816-838, 888-910, 1072-1084, 1088-1092
NB18-PIK3CG	p110γ	1.5	557-601, 954-975, 961-992, 1035-1050
NB19-PIK3CG	p110γ	0.2	593-607, 623-630, 954-992, 1035-1050, 1072-1084

Appendix G. Full statistics on hydrogen deuterium exchange experiments with nanobodies binding to the regulatory subunits according to the guidelines from the International Conference on HDX-MS (194) (refers to Figure 3.2)

Data set	**Apo p110γ-p101**	**NB1-PIK3R5**	**NB2-PIK3R5**	**NB3-PIK3R5**
HDX reaction details	%D_2O=81.7% $pH_{(read)}$=7.5 Temp=18ºC	%D_2O=81.7% $pH_{(read)}$=7.5 Temp=18ºC	%D_2O=81.7% $pH_{(read)}$=7.5 Temp=18ºC	%D_2O=81.7% $pH_{(read)}$=7.5 Temp=18ºC
HDX time course (seconds)	3 and 300s	3 and 300s	3 and 300s	3 and 300s
HDX controls	N/A	N/A	N/A	N/A
Back-exchange	No correction	No correction	No correction	No correction
Number of peptides	p110γ: 118 p101: 105	p110γ: 118 p101: 105	p110γ: 118 p101: 105	p110γ: 118 p101: 105
Sequence coverage	p110γ: 79.3% p101: 71.2%	p110γ: 79.3% p101: 71.2%	p110γ: 79.3% p101: 71.2%	p110γ: 79.3% p101: 71.2%
Average peptide /redundancy	p110γ: Length=12.7 Redund.= 1.4 p101: length=11.6 Redund.=1.4	p110γ: Length=12.7 Redund.= 1.4 p101: length=11.6 Redund.=1.4	p110γ: Length=12.7 Redund.= 1.4 p101: length=11.6 Redund.=1.4	p110γ: Length=12.7 Redund.= 1.4 p101: length=11.6 Redund.=1.4
Replicates	1	1	1	1
Repeatability	N/A	N/A	N/A	N/A
Significant differences in HDX	>5% and >0.4 Da	>5% and >0.4 Da	>5% and >0.4 Da	>5% and >0.4 Da

Data set	**Apo p110γ-p84**	**NB4-PIK3R6**
HDX reaction details	%D_2O=86.8% $pH_{(read)}$=7.5 Temp=18ºC	%D_2O=86.8% $pH_{(read)}$=7.5 Temp=18ºC
HDX time course (seconds)	3 and 300s	3 and 300s
HDX controls	N/A	N/A
Back-exchange	No correction	No correction
Number of peptides	p110γ: 156 p84: 154	p110γ: 156 p84: 154
Sequence coverage	p110γ: 86.0% p84: 90.5%	p110γ: 86.0% p84: 90.5%
Average peptide /redundancy	p110γ: Length=13.0 Redund.= 1.8 P84: length=13.1 Redund.=2.7	p110γ: Length=13.0 Redund.= 1.8 P84: length=13.1 Redund.=2.7
Replicates	1	1
Repeatability	N/A	N/A
Significant differences in HDX	>5% and >0.4 Da	>5% and >0.4 Da

Appendix H. Full statistics on hydrogen deuterium exchange experiments with a set of nanobodies binding to p110γ according to the guidelines from the International Conference on HDX-MS (194) (refers to Figure 3.2)

Data set	**Apo p110γ-p84**	**NB5-PIK3CG**	**NB6-PIK3CG**	**NB9-PIK3CG**	**NB10-PIK3CG**	**NB11-PIK3CG**
HDX reaction details	%D_2O=83.8% $pH_{(read)}$=7.5 Temp=18ºC	%D_2O=83.8% $pH_{(read)}$=7.5 Temp=18ºC	%D_2O=83.8% $pH_{(read)}$=7.5 Temp=18ºC	%D_2O=83.8% $pH_{(read)}$=7.5 Temp=18ºC	%D_2O=83.8% $pH_{(read)}$=7.5 Temp=18ºC	%D_2O=83.8% $pH_{(read)}$=7.5 Temp=18ºC
HDX time course (seconds)	3 and 300s	3 and 300s	3 and 300s	3 and 300s	3 and 300s	3 and 300s
HDX controls	N/A	N/A	N/A	N/A	N/A	N/A
Back-exchange	No correction	No correction	No correction	No correction	No correction	No correction
Number of peptides	p110γ: 174 p84: 121	p110γ: 174 p84: 121	p110γ: 174 p84: 121	p110γ: 174 p84: 121	p110γ: 174 p84: 121	p110γ: 174 p84: 121
Sequence coverage	p110γ: 87.9% p84: 86.6%	p110γ: 87.9% p84: 86.6%	p110γ: 87.9% p84: 86.6%	p110γ: 87.9% p84: 86.6%	p110γ: 87.9% p84: 86.6%	p110γ: 87.9% p84: 86.6%
Average peptide /redundancy	p110γ: Length=13.2 Redund.= 2.1 p84: Length=12.9 Redund.= 2.1	p110γ: Length=13.2 Redund.= 2.1 p84: Length=12.9 Redund.= 2.1	p110γ: Length=13.2 Redund.= 2.1 p84: Length=12.9 Redund.= 2.1	p110γ: Length=13.2 Redund.= 2.1 p84: Length=12.9 Redund.= 2.1	p110γ: Length=13.2 Redund.= 2.1 p84: Length=12.9 Redund.= 2.1	p110γ: Length=13.2 Redund.= 2.1 p84: Length=12.9 Redund.= 2.1
Replicates	1	1	1	1	1	1
Repeatability	N/A	N/A	N/A	N/A	N/A	N/A
Significant differences in HDX	>5% and >0.4 Da	>5% and >0.4 Da	>5% and >0.4 Da	>5% and >0.4 Da	>5% and >0.4 Da	>5% and >0.4 Da
Data set	**NB12-PIK3CG**	**NB13-PIK3CG**	**NB14-PIK3CG**	**NB15-PIK3CG**	**NB16-PIK3CG**	**NB19-PIK3CG**
HDX reaction details	%D_2O=83.8% $pH_{(read)}$=7.5 Temp=18ºC	%D_2O=83.8% $pH_{(read)}$=7.5 Temp=18ºC	%D_2O=83.8% $pH_{(read)}$=7.5 Temp=18ºC	%D_2O=83.8% $pH_{(read)}$=7.5 Temp=18ºC	%D_2O=83.8% $pH_{(read)}$=7.5 Temp=18ºC	%D_2O=83.8% $pH_{(read)}$=7.5 Temp=18ºC
HDX time course (seconds)	3 and 300s	3 and 300s	3 and 300s	3 and 300s	3 and 300s	3 and 300s
HDX controls	N/A	N/A	N/A	N/A	N/A	N/A
Back-exchange	No correction	No correction	No correction	No correction	No correction	No correction
Number of peptides	p110γ: 174 p84: 121	p110γ: 174 p84: 121	p110γ: 174 p84: 121	p110γ: 174 p84: 121	p110γ: 174 p84: 121	p110γ: 174 p84: 121
Sequence coverage	p110γ: 87.9% p84: 86.6%	p110γ: 87.9% p84: 86.6%	p110γ: 87.9% p84: 86.6%	p110γ: 87.9% p84: 86.6%	p110γ: 87.9% p84: 86.6%	p110γ: 87.9% p84: 86.6%
Average peptide /redundancy	p110γ: Length=13.2 Redund.= 2.1 p84: Length=12.9 Redund.= 2.1	p110γ: Length=13.2 Redund.= 2.1 p84: Length=12.9 Redund.= 2.1	p110γ: Length=13.2 Redund.= 2.1 p84: Length=12.9 Redund.= 2.1	p110γ: Length=13.2 Redund.= 2.1 p84: Length=12.9 Redund.= 2.1	p110γ: Length=13.2 Redund.= 2.1 p84: Length=12.9 Redund.= 2.1	p110γ: Length=13.2 Redund.= 2.1 p84: Length=12.9 Redund.= 2.1
Replicates	1	1	1	1	1	1
Repeatability	N/A	N/A	N/A	N/A	N/A	N/A
Significant differences in HDX	>5% and >0.4 Da	>5% and >0.4 Da	>5% and >0.4 Da	>5% and >0.4 Da	>5% and >0.4 Da	>5% and >0.4 Da

Appendix I. Full statistics on hydrogen deuterium exchange experiments with a set of nanobodies binding to p110γ according to the guidelines from the International Conference on HDX-MS (194) (refers to Figure 3.2)

Data set	**Apo p110γ-p84**	**NB7-PIK3CG**	**NB8-PIK3CG**	**NB17-PIK3CG**	**NB18-PIK3CG**
HDX reaction details	%D_2O=84.5% $pH_{(read)}$=7.5 Temp=18ºC	%D_2O=84.5% $pH_{(read)}$=7.5 Temp=18ºC	%D_2O=84.5% $pH_{(read)}$=7.5 Temp=18ºC	%D_2O=84.5% $pH_{(read)}$=7.5 Temp=18ºC	%D_2O=84.5% $pH_{(read)}$=7.5 Temp=18ºC
HDX time course (seconds)	3 and 300s	3 and 300s	3 and 300s	3 and 300s	3 and 300s
HDX controls	N/A	N/A	N/A	N/A	N/A
Back-exchange	No correction	No correction	No correction	No correction	No correction
Number of peptides	p110γ: 151 p84: 123	p110γ: 151 p84: 123	p110γ: 151 p84: 123	p110γ: 151 p84: 123	p110γ: 151 p84: 123
Sequence coverage	p110γ: 84.6% p84: 88.2%	p110γ: 84.6% p84: 88.2%	p110γ: 84.6% p84: 88.2%	p110γ: 84.6% p84: 88.2%	p110γ: 84.6% p84: 88.2%
Average peptide /redundancy	p110γ: Length=13.4 Redund.= 1.8 p84: Length=13.7 Redund.= 2.2	p110γ: Length=13.4 Redund.= 1.8 p84: Length=13.7 Redund.= 2.2	p110γ: Length=13.4 Redund.= 1.8 p84: Length=13.7 Redund.= 2.2	p110γ: Length=13.4 Redund.= 1.8 p84: Length=13.7 Redund.= 2.2	p110γ: Length=13.4 Redund.= 1.8 p84: Length=13.7 Redund.= 2.2
Replicates	1	1	1	1	1
Repeatability	N/A	N/A	N/A	N/A	N/A
Significant differences in HDX	>5% and >0.4 Da	>5% and >0.4 Da	>5% and >0.4 Da	>5% and >0.4 Da	>5% and >0.4 Da

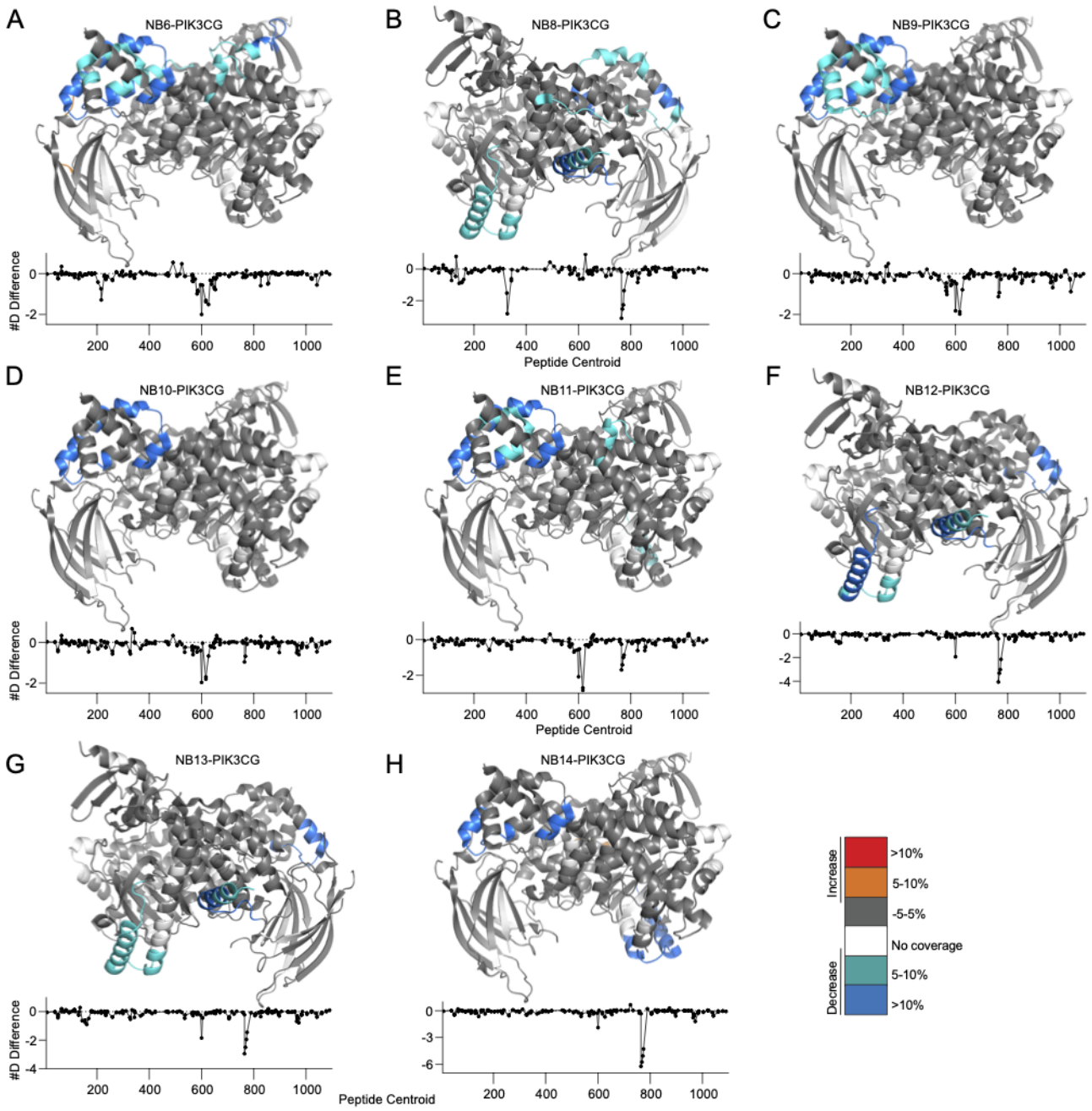

Appendix J. HDX-MS differences in p110γ on nanobody binding. (A) HDX-MS differences in p110γ-p84 with the addition of NB6-PIK3CG mapped on a model of p110γ. The number of deuteron difference for all peptides analyzed over the entire deuterium exchange time course is shown for p110γ. In panels **A-H**, peptides showing significant difference in deuterium exchange (>5%,>0.4 kDa) between conditions with and without nanobody are colored on the cartoon model. **(B)** HDX-MS differences in p110γ-p84 with the addition of NB8-PIK3CG mapped on a model of p110γ. The number of deuteron difference for all peptides analyzed over the entire deuterium exchange time course is shown for p110γ. **(C)** HDX-MS differences in p110γ-p84 with the addition of NB9-PIK3CG mapped on a model of p110γ. The number of deuteron difference for all peptides analyzed over the entire deuterium exchange time course is shown for p110γ. **(D)** HDX-MS differences in p110γ-p84 with the addition of NB10-PIK3CG mapped on a model of p110γ. The number of deuteron difference for all peptides analyzed over the entire deuterium exchange time course is shown for p110γ. **(E)** HDX-MS differences in p110γ-p84 with the addition of NB11-PIK3CG mapped on a model of p110γ. The number of deuteron difference for all peptides analyzed over the

entire deuterium exchange time course is shown for p110γ. **(F)** HDX-MS differences in p110γ-p84 with the addition of NB12-PIK3CG mapped on a model of p110γ. The number of deuteron difference for all peptides analyzed over the entire deuterium exchange time course is shown for p110γ. **(G)** HDX-MS differences in p110γ-p84 with the addition of NB13-PIK3CG mapped on a model of p110γ. The number of deuteron difference for all peptides analyzed over the entire deuterium exchange time course is shown for p110γ. **(H)** HDX-MS differences in p110γ-p84 with the addition of NB14-PIK3CG mapped on a model of p110γ. The number of deuteron difference for all peptides analyzed over the entire deuterium exchange time course is shown for p110γ.

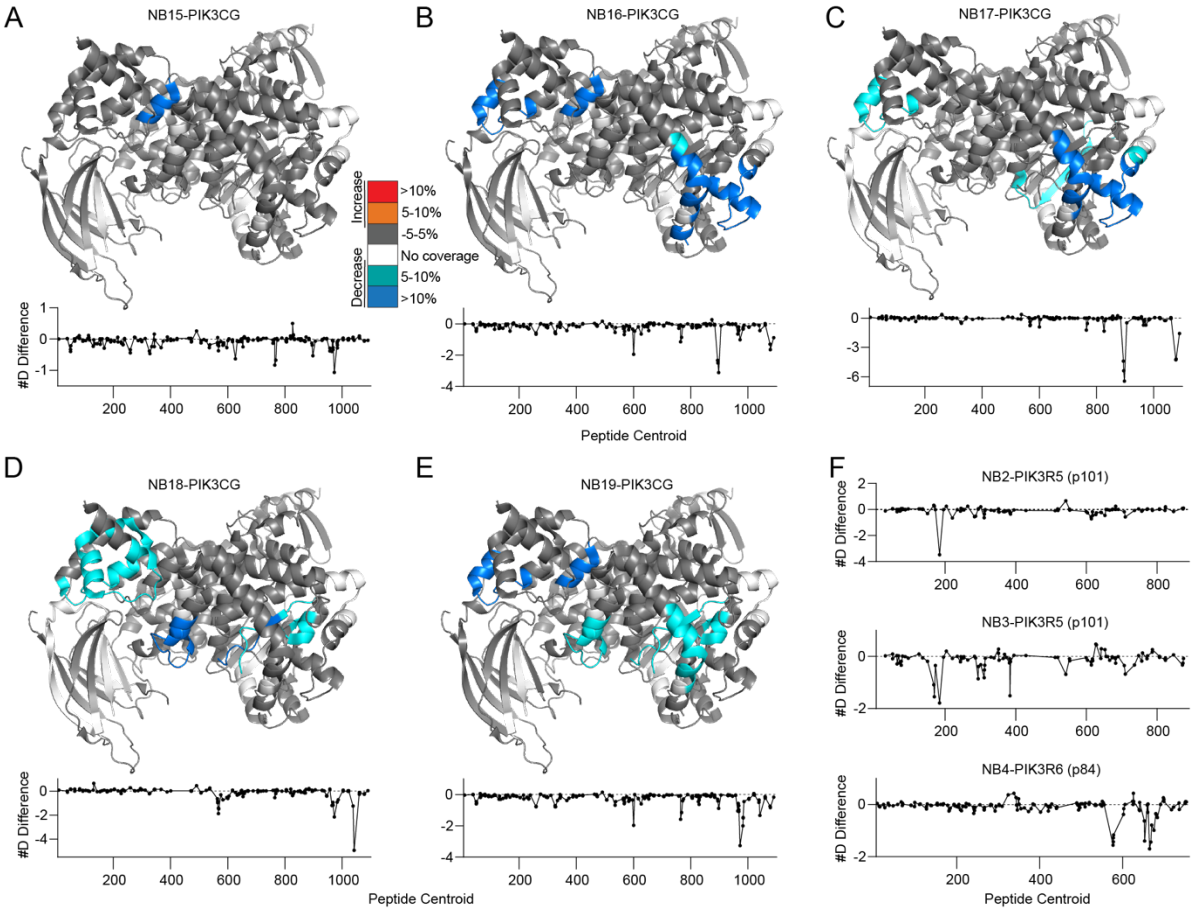

Appendix K. HDX-MS differences in p110γ, p101 and p84 on nanobody binding (A) HDX-MS differences in p110γ-p84 with the addition of NB15-PIK3CG mapped on a model of p110γ. The number of deuteron difference for all peptides analyzed over the entire deuterium exchange time course is shown for p110γ. For panels **A-E**, peptides showing significant difference in deuterium exchange (>5%,>0.4 kDa) between conditions with and without nanobody are colored on the cartoon model. **(B)** HDX-MS differences in p110γ-p84 with the addition of NB16-PIK3CG mapped on a model of p110γ. The number of deuteron difference for all peptides analyzed over the entire deuterium exchange time course is shown for p110γ. **(C)** HDX-MS differences in p110γ-p84 with the addition of NB17-PIK3CG mapped on a model of p110γ. The number of deuteron difference for all peptides analyzed over the entire deuterium exchange time course is shown for p110γ. **(D)** HDX-MS differences in p110γ-p84 with the addition of NB18-PIK3CG mapped on a model of p110γ. The number of deuteron difference for all peptides analyzed over the entire deuterium exchange time course is shown for p110γ. **(E)** HDX-MS differences in p110γ-p84 with the addition of NB19-PIK3CG mapped on a model of p110γ. The number of deuteron difference for all peptides analyzed over the entire deuterium exchange time course is shown for p110γ. **(F)** The number of deuteron difference between conditions with and without nanobody for all peptides analyzed over the entire deuterium exchange time course is shown for p101 (NB2-PIK3R5 and NB3-PIK3R5) and p84 (NB4-PIK3R6).

Chapter 4

Appendix L. Cryo-EM data collection, refinement and validation statistics

	p110γ-p101-NB1-PIK3R5 EMD- 23808 PDB:7MEZ	p110γ-p101 EMD- 23812
Data collection and processing		
Magnification	75,000	75,000
Voltage (kV)	300	300
Electron exposure (e/ Å^2)	36	50
Defocus range (μM)	1.0-2.4	0.8-2.0
Pixel size (Å)	1.079	1.059
Symmetry imposed	C1	C1
Initial particle images (no.)	952,702	1,285,510
Final particle images (no.)	320,179	196,390
Map resolution (Å)	2.89	3.36
FSC threshold	0.143	0.143
Map resolution range (Å)	2.34-8	2.5-8
Refinement		
Initial model used (PDB)	1E8Y	
Model Resolution (Å)	3.1	
FSC threshold	0.5	
Map sharpening B factor	Sharpened locally	
Model composition		
Non-hydrogen atoms	12,369	
Protein residues	1,536	
Ligands	0	
B-factors		
Protein	67.6	
Validation		
Mol probability score	1.70	
Clashscore	8.87	
Poor rotamers (%)	0.0	
Ramachandran		
Favored	96.56	
Allowed	3.24	
Outliers	0.20	
R.m.s. deviations		
Bond lengths (Å)	0.003	
Bond angles (°)	0.563	

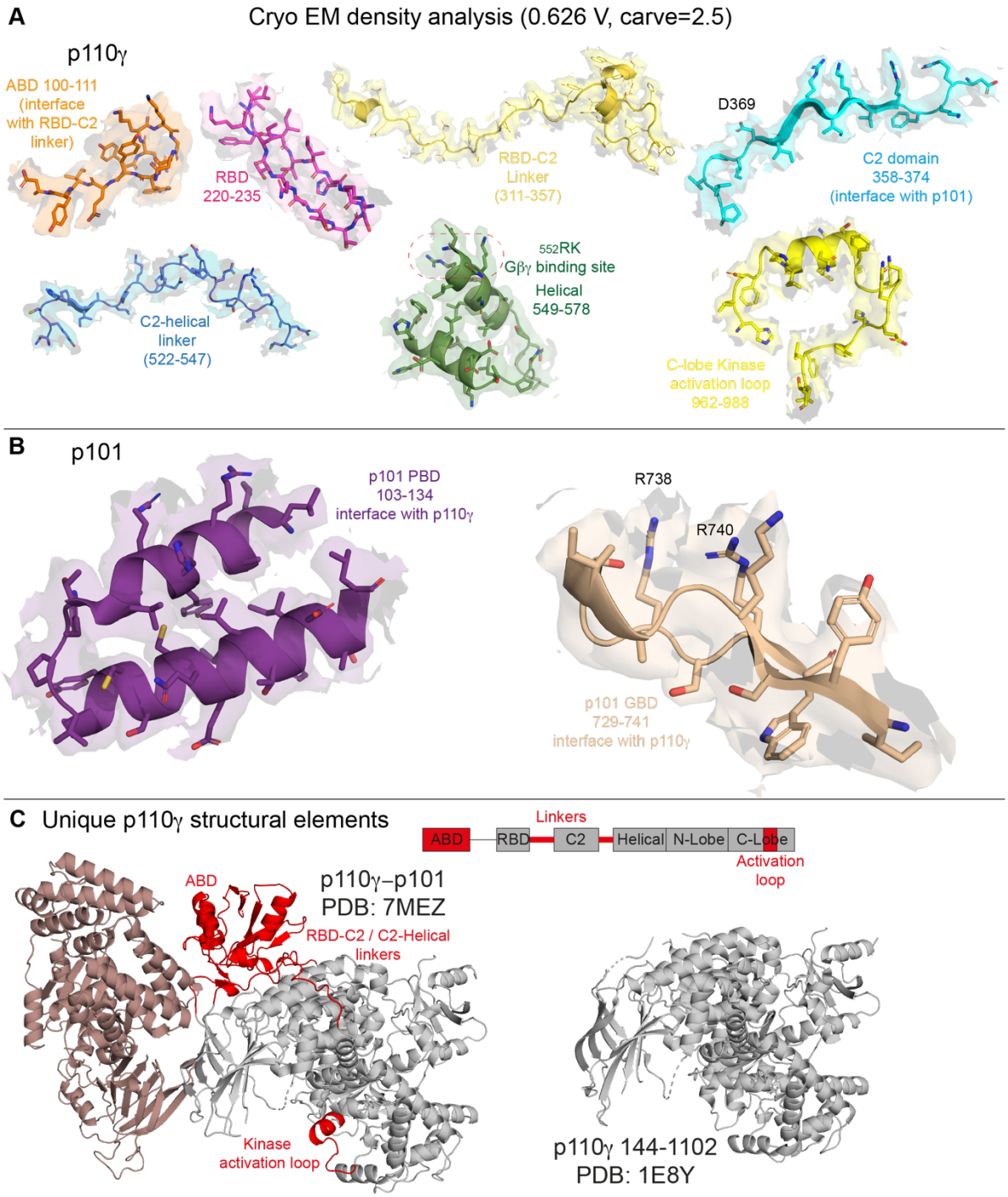

Appendix M. Structural analysis of the p110γ-p101 model. (A) Electron density in select regions covering all five domains of p110γ. **(B)** Electron density in select regions of the PBD and GBD of p101**. (C)** Novel structural features in the p110 subunit (in red) that were previously absent in the structure of p110γ (aas 144-1102).

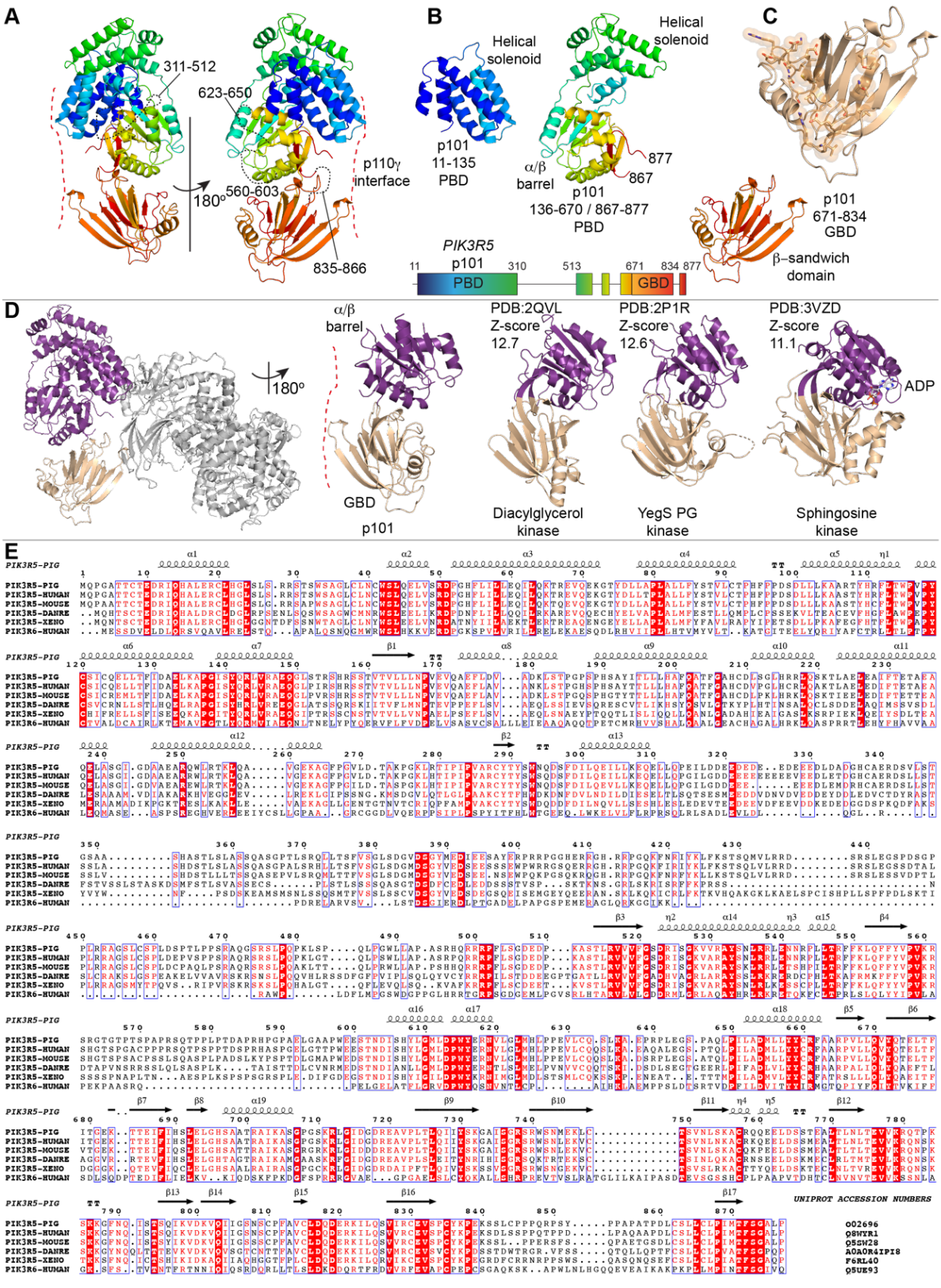

Appendix N. p101 (PIK3R5) protein: Structure, structural conservation with DGKs, evolutionary conservation of p101, and comparison with p84 (*PIK3R6*) (A) Domain map and model of p101 coloured from N- to C-terminus in the rainbow spectrum from blue through red.**(B)** Representation of different regions of the model in panel A showing

various protein folds in the PBD and GBD domains of p101.**(C)** Zoom in on the GBD, showing residues identified as important in Gβγ activation of p110γ-p101 as sticks/spheres. **(D)** Structural comparison of the α/β barrel and β-sandwich in p101 compared to the corresponding regions in diacylglycerol kinase, sphingosine kinase 1, and the *Salmonella* phosphatidylglycerol kinase YegS. **(E)** Alignment (generated with ESPript 3.0) showing evolutionary conservation of residues in porcine p101 with p101 sequences from human, mouse, Xenopus and zebrafish and p84 sequence from human. The secondary structure elements of porcine p101 are shown above the alignment.

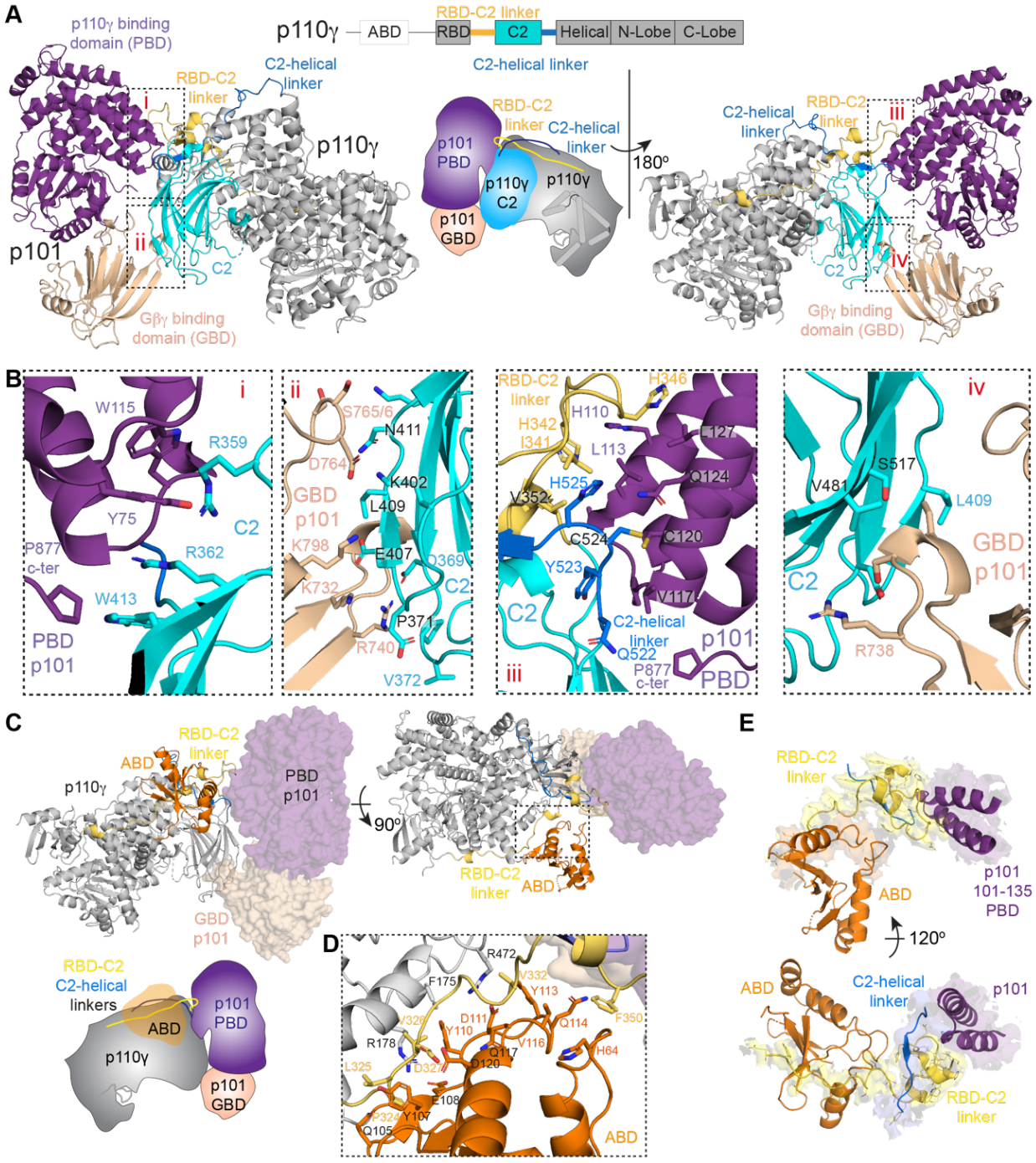

Appendix O. Interface details for p110γ with p101 and ABD. (A) Cartoon representation of the p110γ-p101 complex, with p101 colored as in Figure 1, and p110γ colored according to the attached schematic, with p101 interacting regions (RBD-C2 linker, C2, and the C2-helical linker) indicated. Important features are shown in a cartoon schematic. Interacting regions are indicated in the boxes, and are labeled i-iv. **(B)** Residues that mediate the interaction between p110γ and p101. Residues that have more than 20 Å of buried surface area are labelled and shown in a stick representation. **(C)** The structure of p110γ-p101 complex, with p110γ shown as cartoon, and p101 as a transparent surface. The different domains are colored as indicated according to the cartoon schematic. **(D)** Residues that mediate the interaction between the p110γ ABD and the rest of p110γ. Residues that have more than 20 Å of buried surface area are labelled and shown in a stick representation. **(E)** The ABD of p110γ coordinates the RBD-C2 linker of p110γ

to interact with p101. The RBD-C2 linker, ABD, and the region of p101 that binds the RBD-C2 linker are shown in a cartoon representation. The electron density of the RBD-C2 linker and region of p101 that binds the RBD-C2 linker are visible (both views), with the ABD interface with the RBD-C2 linker (top view) and the N-terminus of the C2-helical linker domain (bottom view) are shown.

Appendix P. Full statistics on all HDX experiments in Chapter 4 according to IC HDX-MS guidelines (194)

Data set	**Apo p110γ**	**p110γ/p101**	**p110γ/p84**	**Apo p110γ/p101**	**p110γ/p101 + nanobody**
HDX reaction details	%D_2O=91.7% $pH_{(read)}$=7.5 Temp=18ºC	%D_2O=91.7% $pH_{(read)}$=7.5 Temp=18ºC	%D_2O=91.7% $pH_{(read)}$=7.5 Temp=18ºC	%D_2O=86.8% $pH_{(read)}$=7.5 Temp=18ºC	%D_2O=86.8% $pH_{(read)}$=7.5 Temp=18ºC
HDX time course (seconds)	3, 30, 300, 3000	3, 30, 300, 3000	3, 30, 300, 3000	3, 300	3, 300
HDX controls	N/A	N/A	N/A	N/A	N/A
Back-exchange	Corrected based on %D_2O	Corrected based on %D_2O	Corrected based on %D_2O	Corrected based on %D_2O	Corrected based on %D_2O
Number of peptides	165	165	165	p110γ: 181 p101: 130	p110γ: 181 p101: 130
Sequence coverage	93.4%	93.4%	93.4%	p110γ: 89.6% p101: 80.6%	p110γ: 89.6% p101: 80.6%
Average peptide /redundancy	Length=12.9 Redundancy= 1.9	Length= 14.4 Redundancy= 1.9	Length= 14.4 Redundancy= 1.9	p110γ: Length= 14.2 Redundancy= 2.3 p101: Length= 13.9 Redundancy= 2.1	p110γ: Length= 14.2 Redundancy= 2.3 p101: Length= 13.9 Redundancy= 2.1
Replicates	3	3	3 (2 300s, 2 3000s)	3	3
Repeatability	Average StDev=0.6%	Average StDev=0.6%	Average StDev=0.6%	Average StDev p110γ=0.5% p101=0.7%	Average StDev p110γ=0.7% p101=0.8%
Significant differences in HDX	>5% and >0.4 Da and unpaired t-test ≤0.01	>5% and >0.4 Da and unpaired t-test ≤0.01	>5% and >0.4 Da and unpaired t-test ≤0.01	>5% and >0.4 Da and unpaired t-test ≤0.01	>5% and >0.4 Da and unpaired t-test ≤0.01

Data set	**Apo p110γ**	**p110γ ABD deletion**	**Apo p110γ/p101**	**p110γ/p101 R472C**	**p110γ/p101 E347K**
HDX reaction details	%D_2O=92.0% $pH_{(read)}$=7.5 Temp=18ºC	%D_2O=92.0% $pH_{(read)}$=7.5 Temp=18ºC	%D_2O=90.5% $pH_{(read)}$=7.5 Temp=18ºC	%D_2O=90.5% $pH_{(read)}$=7.5 Temp=18ºC	%D_2O=90.5% $pH_{(read)}$=7.5 Temp=18ºC
HDX time course (seconds)	3, 30, 300, 3000	3, 30, 300, 3000	0.3, 3, 30, 300, 3000	0.3, 3, 30, 300, 3000	0.3, 3, 30, 300, 3000
HDX controls	N/A	N/A	N/A	N/A	N/A
Back-exchange	Corrected based on %D_2O	Corrected based on %D_2O	Corrected based on %D_2O	Corrected based on %D_2O	Corrected based on %D_2O
Number of peptides	150	150	p110γ: 194 p101: 122	p110γ: 194 p101: 122	p110γ: 194 p101: 122
Sequence coverage	91.0%	91.0%	p110γ: 92.1% p101: 87.5%	p110γ: 92.1% p101: 87.5%	p110γ: 92.1% p101: 87.5%
Average peptide /redundancy	Length= 14.4 Redundancy= 2.0	Length= 14.4 Redundancy= 2.0	p110γ: Length= 14.3 Redundancy= 2.5 p101: Length= 14.0 Redundancy= 1.9	p110γ: Length= 14.3 Redundancy= 2.5 p101: Length= 14.0 Redundancy= 1.9	p110γ: Length= 14.3 Redundancy= 2.5 p101: Length= 14.0 Redundancy= 1.9
Replicates	3	3	3	3	3
Repeatability	Average StDev=0.4%	Average StDev=0.4%	Average StDev p110γ=0.6% p101=0.9%	Average StDev p110γ=0.6% p101=0.8%	Average StDev p110γ=0.6% p101=0.9%
Significant differences in HDX	>5% and >0.4 Da and unpaired t-test ≤0.01	>5% and >0.4 Da and unpaired t-test ≤0.01	>4% and >0.4 Da and unpaired t-test ≤0.01	>4% and >0.4 Da and unpaired t-test ≤0.01	>4% and >0.4 Da and unpaired t-test ≤0.01

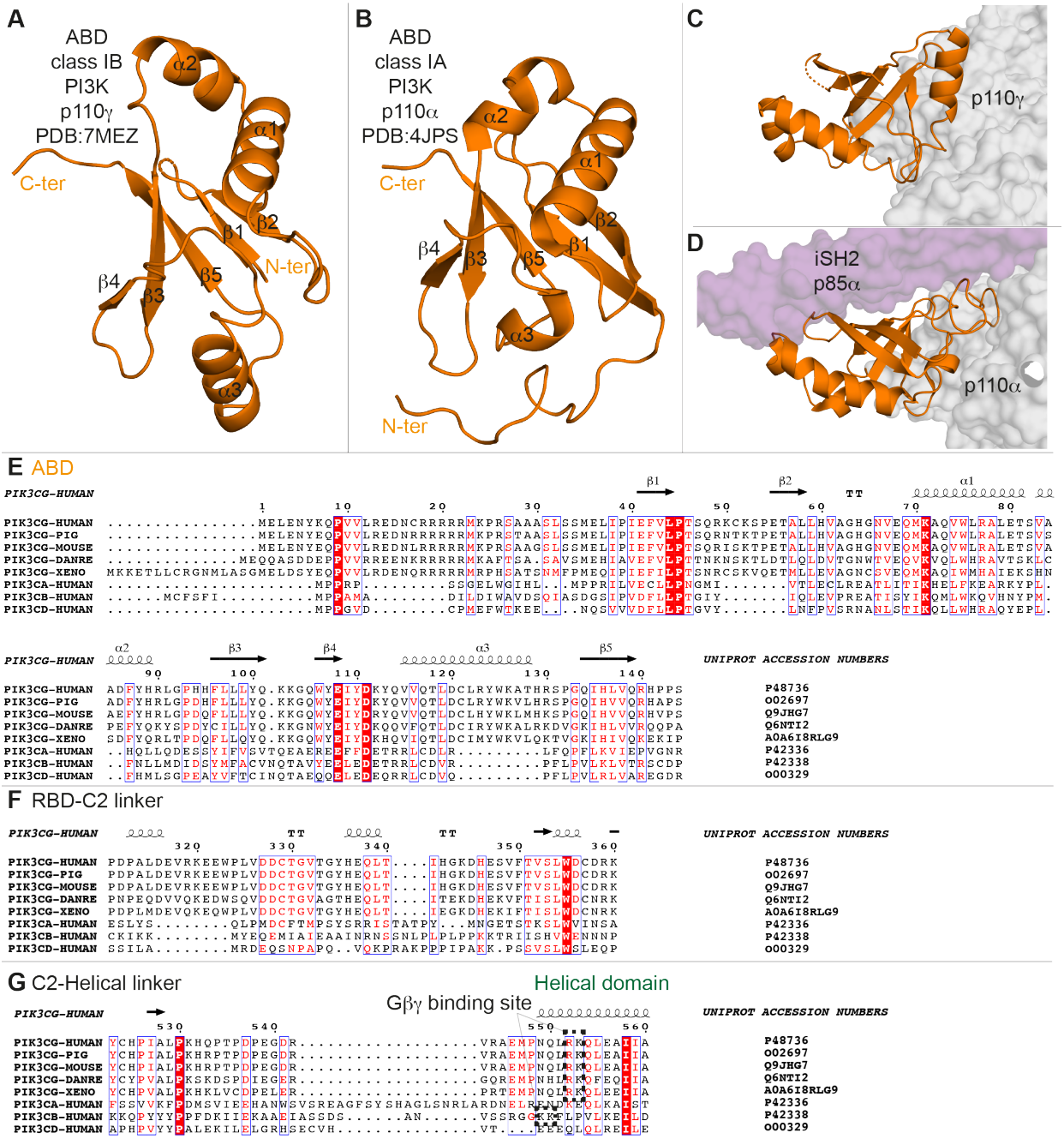

Appendix Q. Key structural differences between p110γ and Class IA p110s. (A) Structural model of p110γ ABD with secondary structure elements. **(B)** Structural model of p110α ABD with secondary structure elements. **(C)** Contacts made by p110γ ABD (orange) with the rest of p110γ (grey surface). **(D)** Contacts made by p110α ABD (orange) with the rest of p110α (grey surface) and the p85α iSH2 domain (purple surface). **(E)** Alignment showing evolutionary conservation of residues in the ABD of human p110γ with corresponding p110γ sequences from pig, mouse, Xenopus and zebrafish and corresponding class IA p110 sequences from human. The secondary structure elements of human p110γ are shown above the alignment. **(F)** Alignment showing evolutionary conservation of residues in the RBD-C2 of human p110γ with corresponding p110γ sequences from pig, mouse, Xenopus and zebrafish and corresponding class IA p110 sequences from human. The secondary structure elements of human p110γ are shown above the alignment. **(G)** Alignment showing evolutionary conservation of residues in the C2-helical linker of human p110γ with corresponding p110γ sequences from pig, mouse, Xenopus and zebrafish and corresponding class IA p110

sequences from human. The secondary structure elements of human p110γ are shown above the alignment. All alignments generated using ESPript 3.0.

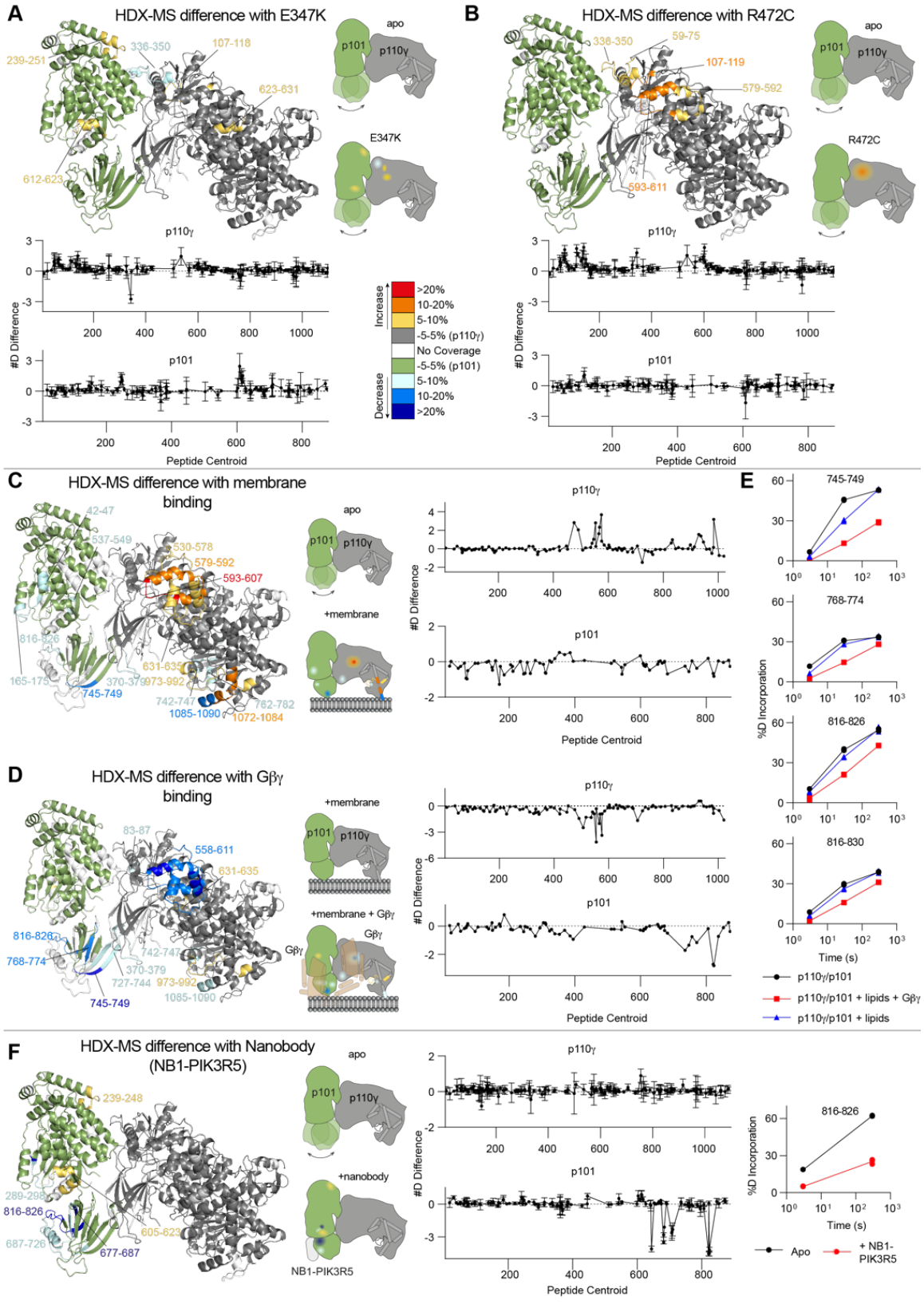

Appendix R. HDX-MS differences of p110γ oncogenic mutants and p110γ binding to lipids, Gβγ, and nanobody
(A) HDX-MS differences in p110γ-p101 between wild-type p110γ-p101 and E347K. For panels **A-D+F,** peptides

showing significant deuterium exchange differences (>5%,>0.4 kDa and p<0.01 in an unpaired two-tailed t-test) between conditions are colored on a cartoon model of p110γ-p101. A cartoon schematic is shown indicating the two conditions compared using HDX-MS. The number of deuteron difference for E357K for all peptides analyzed over the entire deuterium exchange time course is shown for p110γ and p101. For all #D graphs, every point represents the central residue of an individual peptide, with error shown as standard deviation (n = 3). **(B)** HDX-MS differences in p110γ-p101 between wild-type p110γ-p101 and R472C mapped on a model of p110γ-p101. The number of deuteron difference for R472C for all peptides over the full time course of exchange is shown for p110γ and p101. **(C)** HDX-MS differences in p110γ-p101 upon binding to membrane mapped on a model of p110γ-p101. The number of deuteron difference for all peptides analyzed over the full time course of exchange is shown for p110γ and p101. **(D)** HDX-MS differences in p110γ-p101 upon binding to Gβγ mapped on a model of p110γ-p101. The number of deuteron difference for all peptides analyzed over the full time course of exchange is shown for p110γ and p101. **(E)** Selected p101 peptides that showed decreases and increases in exchange between p110γ-p101 alone, p110γ-p101 with membrane, and p110γ-p101 with membrane and Gβγ. The individual data points are shown on the graph (n=2). **(F)** HDX-MS differences in p110γ-p101 bound to NB1-PIK3R5 mapped on a model of p110γ-p101. The number of deuteron difference for all peptides analyzed over the entire deuterium exchange time course is shown for p110γ and p101. A single p101 peptide showing H/D exchange data is shown. The individual data points are shown on the graph (n=3).